Oil & Natural Gas Technology

DOE Award No.: DE-FC26-06NT43067

Quarterly Progress Report
(July - September 2008)

Mechanisms Leading to Co-Existence of Gas and Hydrate in Ocean Sediments

Submitted by:
The University of Texas at Austin
1 University Station C0300
Austin, TX 78712-0228

Prepared for:
United States Department of Energy
National Energy Technology Laboratory

October 26, 2008

Office of Fossil Energy

MECHANISMS LEADING TO CO-EXISTENCE OF GAS AND HYDRATE IN OCEAN SEDIMENTS

CONTRACT NO. DE-FC26-06NT43067

Deliverable 5.3:
Report on Task 5.3: Compute gas/water interface geometry within fracture

October 30, 2008

Prepared by

Steven L. Bryant
Maša Prodanović
Department of Petroleum and Geosystems Engineering
The University of Texas at Austin
1 University Station C0300
Austin, TX 78712-0228
Phone: (512) 471 3250
Email: steven_bryant@mail.utexas.edu

Prepared for
U.S. Department of Energy - NETL
3610 Collins Ferry Road
P.O. Box 880
Morgantown, WV 26508

Objective of Task 5.3

In the conceptual model to be examined in this project, hydrate formation depends upon the location and geometry of the gas/water interface. The gas/water interface in turn depends on the competition between capillarity-controlled meniscus movement (drainage and imbibition) and grain-mechanics-controlled sediment displacement (sediment fracturing). To study this competition, we have computed gas/water interface geometry within a fracture for representative stages of fracture propagation from Task 4. We have also applied the level set method to compute the capillary-controlled configuration of gas and water in rough-walled fractures. We also applied the model of capillarity-controlled displacement in a fracture domain that is bounded by model sediments. This yields insight into the magnitude of drainage of methane from the fracture into different model sediments.

Description of Findings in Task 5.3

Gas/water Interface Movement in Rough-walled Fractures

We have investigated of the capillary-controlled configuration of gas and water in the rough-walled fractures using progressive quasi-static (PQS) algorithm. Compared to our earlier efforts, we validated the model using available pore scale experiments and extended the method to account for trapping of gas (non-wetting) phase. We summarize main results on two examples of three-dimensional fractures (see below).

1) **Fractured Berea sandstone.** This fracture comes from the experiment done by Dr. Zuleima Karpyn of Pennsylvania State University and enables us to visually compare the level set method drainage and imbibition results with an actual experiment.
2) **Simulation in fractured sediment model.** We artificially created a fracture in mono-disperse sphere packing (resembling a fracture opened by methane gas) and observed very different residual fluid configurations for different directions of the displacement.

Fractured Berea Sandstone

We used an upscaled version of 389 × 116 × 25 elements of the original CT image from Z. Karpyn in order to compare our simulations with experiments. The computational domain thus corresponds to a 101 × 25 × 5.5 mm^3 physical domain.

The LSMPQS simulations agree generally with the experiment. Fig. 1 shows the fracture aperture field (Fig. 1a) and the experimentally determined drainage endpoint (Fig 1b). The nonwetting phase (oil) accessed the fracture from one end (bottom of image), displacing wetting phase (brine) from the other end (top of image). As seen in Fig. 1c, oil (non-wetting phase) at the LSMPQS simulation drainage endpoint occupies wider spaces and cannot enter regions of small aperture.

There are discrepancies in some details of the configuration. One reason is likely to be the upscaling of the aperture field for the simulation. Some of the detailed structure that

controls meniscus movement was averaged out in the simulation domain. Another is that the simulation uses a contact angle of zero, but the contact angle of the experimental fluids was estimated to be 15° for drainage and 25° for imbibition. Finally, the oil configuration in Fig. 1b is the result of segmentation of a multiphase image. Segmentation of such images is prone to misidentification errors: a subjective choice must be made regarding the range of gray scale values corresponding to each phase; different choices for the endpoints of these ranges can affect the interpreted location of the phases.

Selected fluid configurations for drainage simulation are shown in Figs. 2. Bottom (inlet) and top (outlet) are the only boundaries open to flow. Figures 2b and 2c show both oil and water configuration for the same capillary pressure. Water surrounds asperities (visible as white breaks in the green water surface), and is mostly in blobs disconnected from the inlet and outlet but is assumed to flow via water films. We used oil-water interfacial tension value $\sigma_{ow} = 41.2 \cdot 10^{-3}\ N/m$ in order to scale the curvatures from LSMPQS simulation to capillary pressure values. Figure 3b shows the predicted capillary pressure – saturation relationship during drainage and imbibition. Unfortunately no experimental data on capillary pressure curve are available.

Figure 4 shows oil configuration for various imbibition stages. We identify and record the trapped oil blobs (i.e. disconnected from both the main oil phase and the open flow boundaries). Pressure typically needs to be substantially reduced before the trapped phase is observed. The first instance we observe is at $P_{23} = 236.1\ Pa$ (subscript 23 denotes the discrete simulation step) and Fig. 4b shows a slightly later configuration that already has seven trapped oil blobs (in blue). Figure 4c shows one more step until the last imbibition stage shown in Fig. 4d where all oil present is trapped (and thus the imbibition simulation stops).

We conclude that the LSMPQS algorithm successfully captures the physics of capillarity-controlled displacements in rough-walled fractures. This constitutes a significant advance over previously available aperture-scale simulations. Several authors have reported network models of displacement within fractures, but most required *ad hoc* assumptions to construct the network and none accounted rigorously for the in-plane radius of curvature of the meniscus. The results shown above are the first to make no simplifications of the physics of displacement. The simulated disconnection and trapping of the nonwetting phase is especially noteworthy, as it occurs spontaneously within the simulation. The behavior is consistent with our earlier results using this method to study imbibition in granular materials, which agree well with experiments.

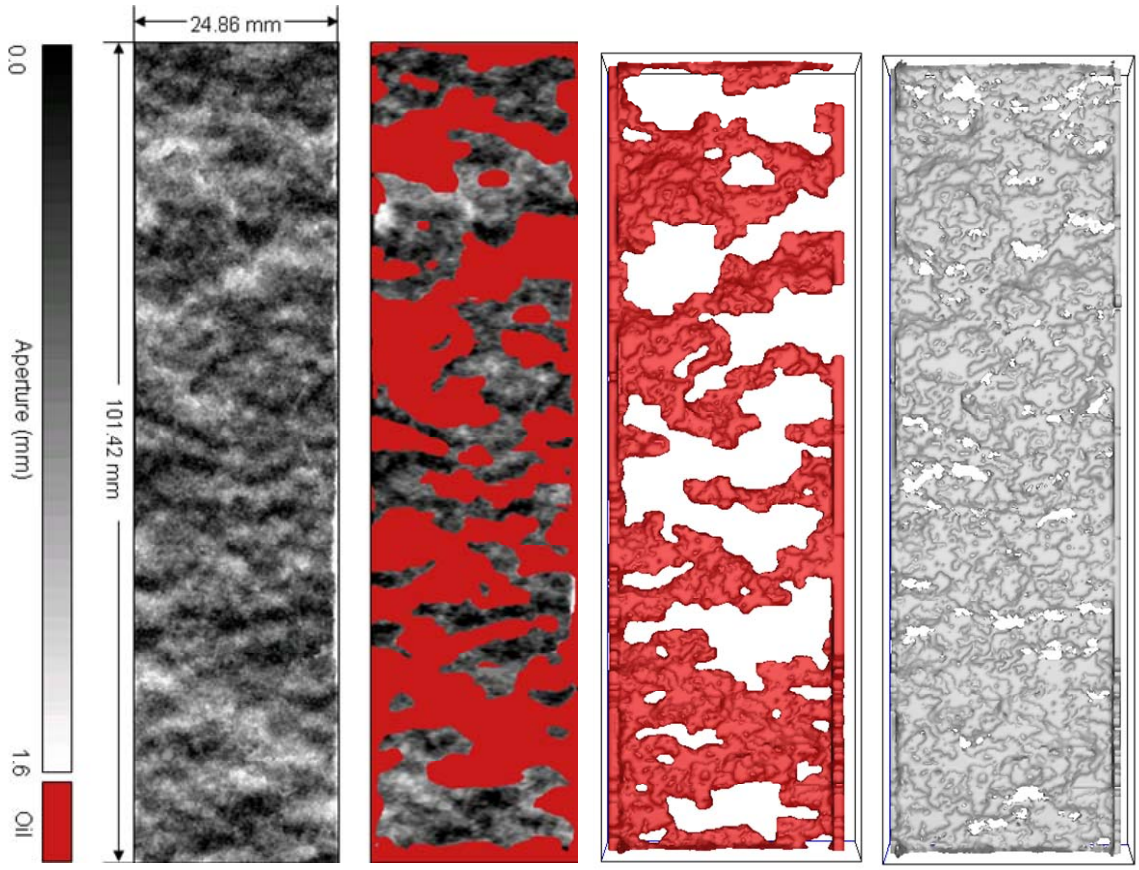

(a) (b) (c) (d)

Fig. 1—Visual comparison of the Berea fracture experimental data (from Z. Karpyn) and LSMPQS simulation. (a) Fracture aperture field shown in shades of gray. Asperities (contact points) are where the aperture field is black and wide parts are where the aperture data is white/light gray. (b) Oil configuration (green) inferred from CT image at the drainage endpoint (S_w=0.35) overlaid upon the aperture field information (grayscale). (c) Top view of the oil configuration from LSMPQS drainage simulation at S_w=0.28. (d) Top view of the pore-grain interface used in LSMPQS simulation. White breaks correspond to asperities.

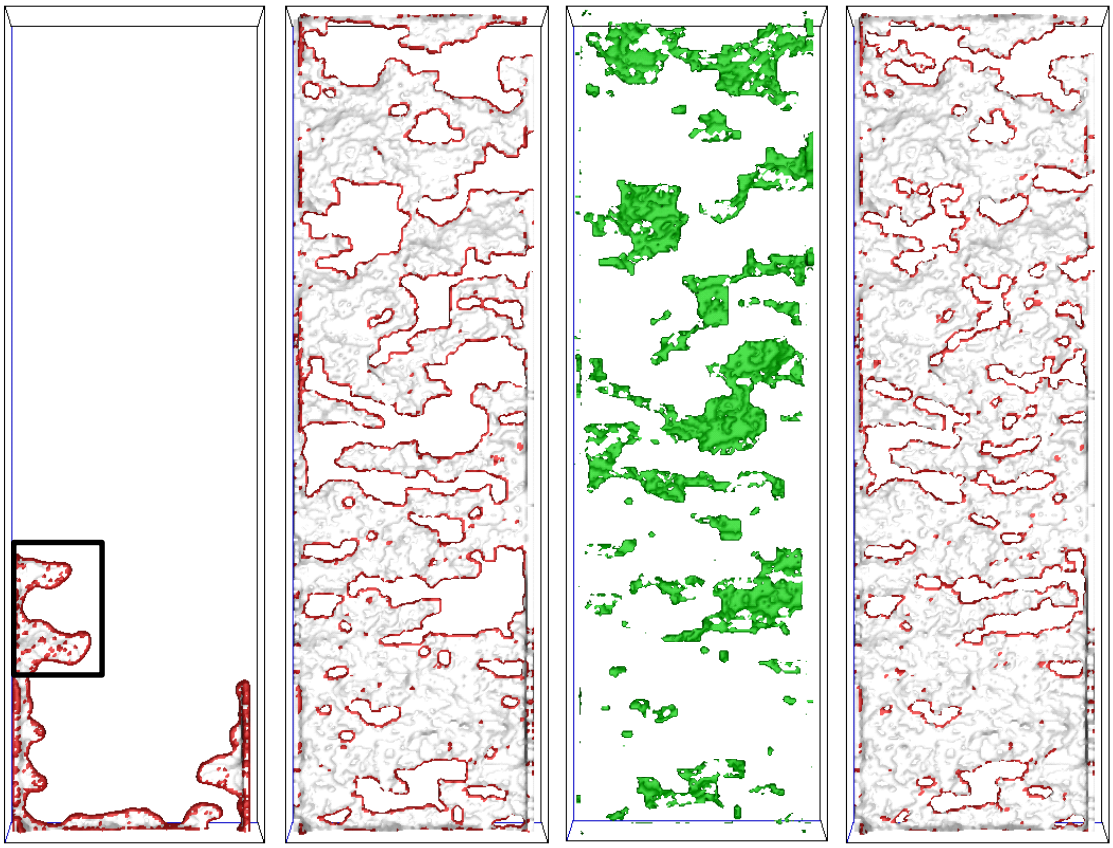

(a) (b) (c) (d)

Fig. 2—(a) Non-wetting phase surface at drainage capillary pressure $P_2 = 153.7\ Pa$. The fluid-fluid interface is shown in red, and the non-wetting phase/grain interface is shown in gray. Long red strip in fracture plane is the main meniscus, small red patches represent the meniscus trying to get into nooks in the grain surface. See Fig 3a for an enlarged view of the region within the black rectangle. (b) Non-wetting phase interface at drainage capillary pressure $P_{13} = 606.9\ Pa$. (c) Wetting fluid interface (in green) at the same pressure stage as in b. (d) Non-wetting phase interface at the end of simulation, $P_{26} = 1142.5\ Pa$.

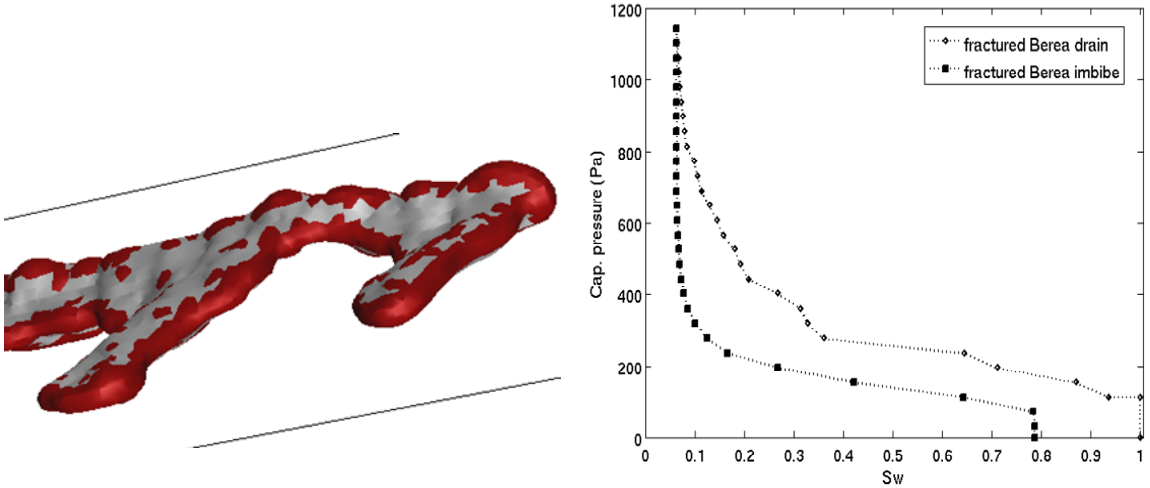

(a) (b)

Fig. 3—(a) Non-wetting phase interface detail corresponding to outlined area from Fig 2a. Long red strip in fracture plane is the main meniscus, small red patches represent the meniscus trying to get into nooks in the grain surface. (b) Simulated capillary pressure – saturation curve for drainage and imbibition in fractured Berea.

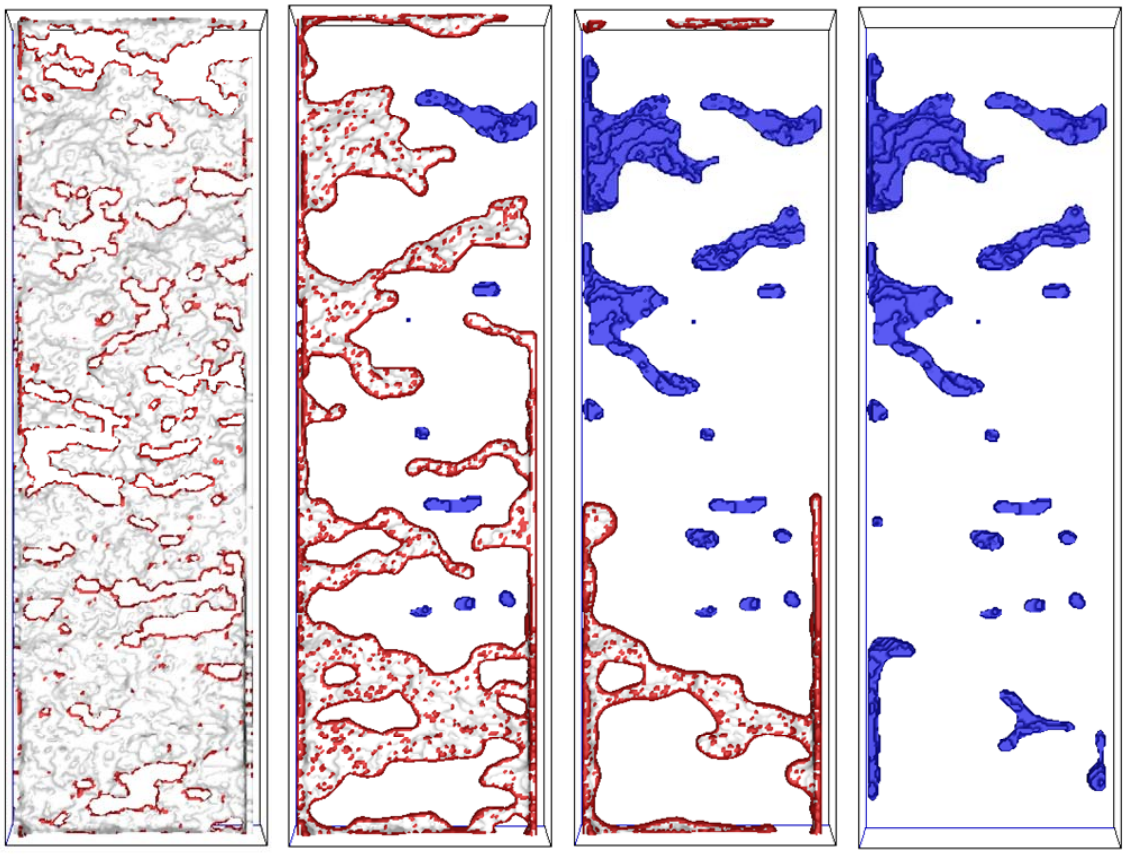

Fig. 4—Oil surface for various imbibition stages. Gray is oil-grain surface, red is oil-water interface for the main connected component of oil and disconnected (residual) oil interface is shown in blue. (a) $P_9^{imb} = 812.9\ Pa$. (b) $P_{25}^{imb} = 153.7\ Pa$. (c) $P_{26}^{imb} = 112.5\ Pa$. (d) Final imbibition configuration for $P_{28}^{imb} = 30.1\ Pa$ consists only of residual oil blobs (volume fraction of 0.214).

Fractured Sediment Model

A subset of a dense, random packing of equal spheres (radius $R = 1$) measured by Finney (1970) was artificially fractured by moving spheres away from and perpendicular to a z-plane. We kept ten randomly chosen pairs of spheres in contact (see Fig. 5a) since the contact points play important role in final fluid configurations. We then performed drainage and imbibition with two different boundary conditions. In one case, the invading (gas) phase entered the domain in the direction parallel to the z-plane of the fracture. It thus had access to fracture and matrix simultaneously. In the other, the gas phase entered the domain in the direction perpendicular to the fracture plane. It had access only to the matrix initially. Invasion of the fracture could occur only from the matrix. The fracture and associated matrix occupied a volume of $[-8R, 8R]^3$ discretized into a mesh of 160^3 numerical cells.

Figure 5b shows gas configuration at a stage that essentially occupied entire fracture opening. At a later drainage step shown in Fig. 6a, drainage of the adjoining matrix has begun. We plot drainage and imbibition curvature-saturation curves in two ways: one measuring saturation in the entire volume and the other set measuring saturation in the matrix adjoining the fracture only (Fig 6b). The “matrix only” drainage curve does not show a sharp percolation threshold (the threshold is at $\kappa = 6$ for monodisperse spheres (Behseresht *et al*. 2007)) because the gas accesses the volume from the entire fracture face. The fracture volume was inferred from the non-wetting fluid configuration shown in Fig. 5b, and subtracted from the overall volume to get the matrix pore space. Imbibition configurations are shown in Figs. 10. Note the disconnected blobs of non-wetting phase result from specifically checking for and recording trapped (disconnected) phase during imbibition simulation.

We repeat the simulation sequence for rotated geometry where the displacement direction is perpendicular to the fracture plane. That is, the fluids access the fracture only from the matrix. This proves to have a major influence. The capillary pressure curve is different for each displacement direction, but more significantly, the saturation and location of the residual nonwetting phase is very different (see Fig. 8). All the nonwetting phase occupying the fracture is trapped.

We conclude that the LSMPQS method successfully captures the physics of capillarity-controlled displacements within a fracture bounded by a granular matrix. This situation is of immediate relevance to gas/water displacements within the hydrate stability zone. The method correctly identifies a two-scale pressure-saturation curve when gas can access both the fracture and the matrix simultaneously: the fracture drains at small pressures, with subsequent invasion of the matrix at large pressures. Trapping of gas in the fracture depends entirely on whether the fracture is connected to a large reservoir of gas. If that connection is lost, then large saturations of gas will be trapped in the fracture. This is likely to affect the growth habit of hydrate.

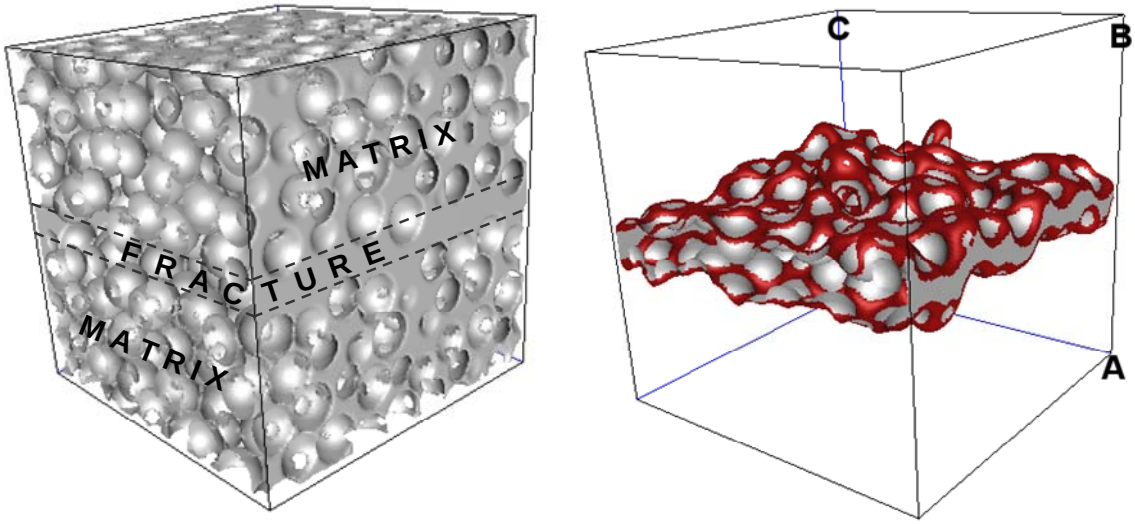

(a) (b)

Fig. 5—(a) Grain surface for fractured sphere pack. Fracture position can be inferred from the flat portion of sealed volume on the side. (b) Drainage simulatioin starts from the face marked ABC. Non-wetting fluid (gas) surface is shown in red at curvature $C_3 = 2.9$ at the drainage step where the entire fracture opening is filled with gas (and capillary invasion into the matrix has just started).

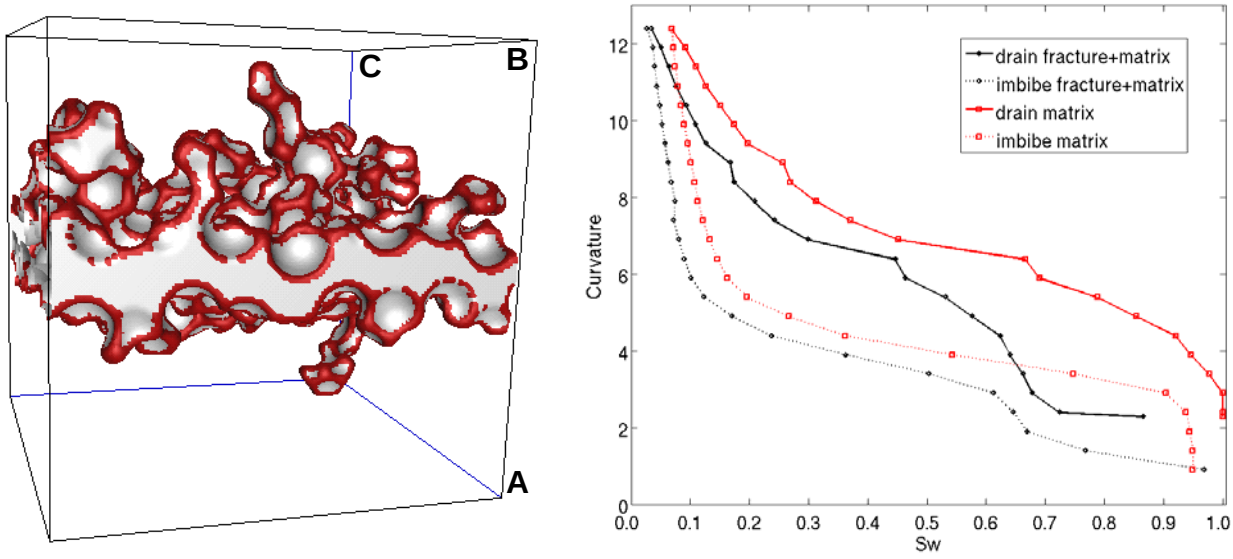

(a) (b)

Fig. 6—(a) Side view of gas (non-wetting fluid) at drainage for $C_7 = 4.9$ when the gas phase started moving from the fracture into the matrix. It entered the domain from the face marked ABC, so the fracture drains first at a curvature of about 2.2. (b) Curvature vs. wetting fluid saturation plots for drainage and imbibition in fractured sphere pack. Curves labeled 'fracture+matrix' show saturation in entire volume, whereas curves labeled 'matrix' show saturation in the matrix adjoining the fracture only.

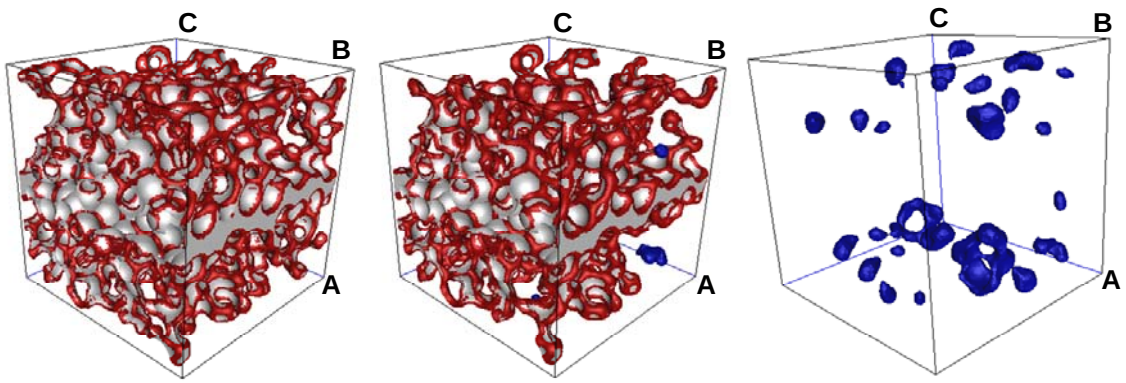

(a) (b) (c)

Fig. 7—NW phase (gas) imbibition configurations for fractured sphere pack. The wetting phase (brine) enters the domain in the direction parallel to the fracture from from the face marked ABC, and gas can exit through the face directly across from the entry face. Disconnected gas blobs are shown in blue and the gas connected to the inlet/outlet is shown in red/gray (red is fluid meniscus, gray is contact with grain). From left to right are shown imbibition steps at curvatures $C_{17}^i = 4.4$, $C_{18}^i = 3.4$, and $C_{24}^i = 0.4$ (final, all of the gas is in disconnected form).

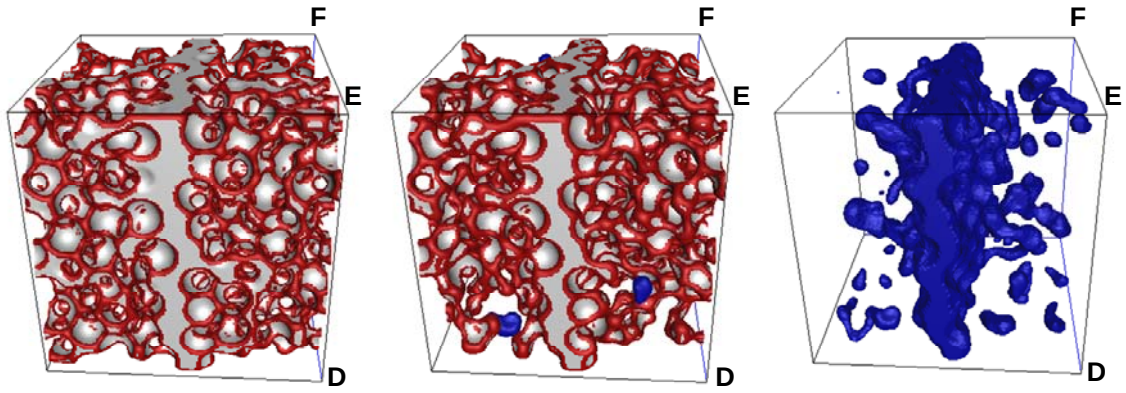

(a) (b) (c)

Fig. 8—NW fluid (gas) imbibition configurations for steps (a) $C_8^i = 5.15$, (b) $C_9^i = 4.15$ and (c) $C_8^i = 2.15$ (final) for rotated geometry. The image is oriented so that the gas in fracture is viewed properly (during drainage the nonwetting phase went from the face marked DEF on the right to the left – the two opposite faces are the only ones open to flow). At the final imbibition step the entire fracture is filled with trapped gas.

MECHANISMS LEADING TO CO-EXISTENCE OF GAS AND HYDRATE IN OCEAN SEDIMENTS

CONTRACT NO. DE-FC26-06NT43067

Deliverable 5.2:
Report on Task 5.2 "Compute gas/water interface geometry during drainage and imbibition in model sediments"

October 30, 2008

Prepared by

Steven L. Bryant
Department of Petroleum and Geosystems Engineering
The University of Texas at Austin
1 University Station C0300
Austin, TX 78712-0228
Phone: (512) 471 3250
Email: steven_bryant@mail.utexas.edu

Prepared for
U.S. Department of Energy - NETL
3610 Collins Ferry Road
P.O. Box 880
Morgantown, WV 26508

Objective of Task 5.2

In the conceptual model to be examined in this project, hydrate formation depends upon the location and geometry of the gas/water interface. In previous tasks we have extracted physically representative networks of pore throats and pore bodies in a large set of model sediments (dense, disordered packings of spheres of different sorting). We also determined the critical curvatures for pore-level events during drainage (gas phase invasion of water-saturated sediment) and imbibition (water invasion of sediment partially filled with gas phase).

In this task we use the previous results to carry out a standard invasion percolation simulation of drainage, then of imbibition in the model sediments. The simulations provide the detailed geometry of the gas/water interface at each step of drainage or imbibition. This will be used in future tasks to model the growth of methane hydrate at these interfaces. The simulations are conveniently summarized with capillary pressure curves, appended to this report; we also report the interfacial area during drainage as this is expected to be the primary mode of hydrate growth.

Summary of Findings in Task 5.2

We extended our earlier investigation of the **critical curvature** for drainage in a pore throat in a model sediment. We generalized the Mayer-Stowe-Princen method to converging/diverging pore throats defined by grains of three different sizes. The results improve the estimate of critical curvature for throats that have larger-than-average cross-section. This in turn improves the consistency of predicted drainage curves in model sediments that are not well sorted.

The simulations of **drainage** yield a systematic decrease in the percolation threshold (capillary pressure when most of the water drains from the pore space) as the sorting of the model sediment becomes poorer. This observation is consistent with the shift of the frequency distribution of critical curvatures toward smaller values. The number fraction of pores containing irreducible wetting phase increases as the sorting becomes poorer. However the volume fraction, and hence the phase saturation, does not necessarily increase because the pores containing water are proportionately smaller than average in the poorly sorted sediments. Hence the irreducible wetting phase saturation does not change significantly as sorting changes.

The simulations of **imbibition** yield consistent hysteresis (the water invades at a smaller capillary pressure than that at which the gas invades) for all the sediments. A remarkable observation is that infinite-acting networks yield larger residual gas saturations than are commonly observed in laboratory experiments in sediments. By way of explanation we note that simulations in finite networks (i.e. having a set of exit pores for gas to leave the domain) yield smaller residual gas saturations that are comparable to laboratory data. The difference is the criterion for trapping the gas phase in the infinite-acting networks: gas phase which occupies a percolating cluster of pores can be displaced by water, but gas phase which occupies a finite cluster of pores is deemed disconnected from the bulk gas phase. Disconnected gas cannot be displaced and is therefore part of the residual phase. In the finite network simulations, gas in a pore can be displaced if that pore is part of a cluster of gas-filled pores that are connected to an exit pore.

Clearly the **percolating-cluster criterion** is more stringent than the finite-network criterion. As a result, larger residual gas saturations occur in the simulations. We argue that the larger residual saturations are the physically relevant ones in the field, where the "exit pores" that characterize the laboratory experiment do not exist. We remark that measurements of residual saturation in the field (obtained by conducting single well partitioning tracer tests) typically yield larger values than observed in the laboratory. This supports the applicability of the infinite-acting network simulations reported here. The literature contains no such simulations in physically realistic networks, so this constitutes an important advance in understanding the behavior of imbibition.

For completeness and for reference we include here the results of the network model approach for the **poorly sorted** sediments. For poorly sorted model sediments, our approach for identifying pore throats (the Delaunay tessellation) is not well suited for capturing the essential geometry. In the Delaunay tessellation every throat is comprised of three nearest-neighbor grains. But the gas/water interface is frequently supported by more than three grains when small grains are mixed in with larger grains. Accounting for this phenomenon would require substantial modification of the network-based approach for simulating gas or water invasion (e.g. the "fourth sphere correction" by Thane [2006]). While this is possible, it is not within the scope of the original program of work. Regardless of that we believe a technically superior alternative exists. This would be to apply the level set method directly to simulate drainage and imbibition in poorly sorted sediments. We think this is feasible based on our progress on other tasks in this project with the level set method. While this too is beyond the scope of the original program of work, it may be possible to demonstrate the idea during Phase 2 of the project.

Results of Task 5.2

The full set of simulations are reported in Appendix B. Here we review the approach.

5.2.1 Drainage Simulation in Model Sediments with Different Sorting

Previously we reported on the application of the Mason and Mellor estimate of critical curvature estimate

$$C^*_{drain} = \frac{2R_{avg}}{r_{inscribed}} - 1.6 \qquad (1)$$

where $r_{inscribed}$ is the radius of a circle inscribed in the pore throat. This estimate is good for very well sorted packings. During the execution of Task 5.2 we found that this estimate yields drainage curves that are not physically realistic when applied to packings with broader distributions of grain sizes. A more rigorous estimate can be obtained from the Mayer-Stowe-Princen (MSP) theory. That theory was developed for equal-size grains. It agrees very well with the Mason/Mellor estimate, which in turn yields drainage curves that agree with experiments. We therefore generalized the MSP theory in two ways: first to account for the 3D nature of the pore throats (original MSP assumes that a throat has constant cross section for arbitrary distance) and second to apply to spheres of different sizes. To our knowledge this is the first time the theory has been so generalized. The methodology is described in the following section. We then used the MSP values to compute drainage curves.

Mayer–Stowe–Princen theory for unequal spheres

MSP calculation is essentially two-dimensional and is valid for constant-cross-section throats. Here we rather present a 3D calculation of MSP theory for pore throat critical curvature. We thus present formulas for throats formed by three spheres of arbitrary sizes R_1, R_2, and R_3.

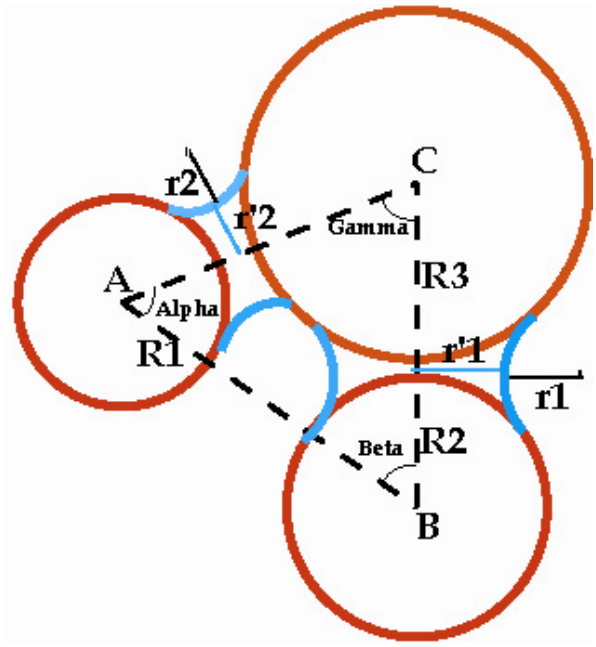

Assume that the non-wetting fluid (gas) fills cross-sectional area A_{eff} at capillary pressure P_c. The work involved in moving the meniscus configuration by a small distance dx along the perpendicular walls is equal to $P_c A_{\text{eff}}$ dx and has to overcome the surface tension. Thus the energy balance reads:

$$P_c A_{eff} dx = \sigma P_L dx + (\sigma_{SG} - \sigma_{SL}) P_S dx$$

where P_L is the total perimeter between the non-wetting and wetting fluids (gas and liquid), P_S is the total perimeter between non-wetting fluid (gas) and solid, and σ, σ_{SG}, and σ_{SL} are the liquid–gas, solid–gas and solid–liquid surface tensions.

From the Young–Dupre equation we know that $\sigma_{SG} - \sigma_{SL} = \sigma \cos(\theta)$ where θ is the contact angle so we obtain:

$$P_c A_{eff} dx = \sigma (P_L + P_S \cos\theta) dx$$

We introduce effective perimeter,

$$P_{eff} = P_L + P_S \cos\theta$$

Then from $P_c = \sigma C$ and the above equation we get the relation $C = \dfrac{P_{eff}}{A_{eff}}$. We have:

$$\begin{cases} A' = A_\Delta - \dfrac{\alpha R_1^2}{2} - \dfrac{\beta R_2^2}{2} - \dfrac{\gamma R_3^2}{2} \\ P' = \alpha R_1 + \beta R_2 + \gamma R_3 \end{cases}$$

$$\begin{cases}\Delta A = \Delta A_{AB} + \Delta A_{AC} + \Delta A_{BC} \\ \Delta P = \Delta P_{AB} + \Delta P_{AC} + \Delta P_{BC}\end{cases}$$

and

$$\begin{matrix} P_{eff} = P' - \Delta P \\ A_{eff} = A' - \Delta A \end{matrix} \quad \text{Therefore, } C = \frac{P' - \Delta P}{A' - \Delta A}$$

For the pendular ring between the spheres A and C which is shown in the following figure we would have:

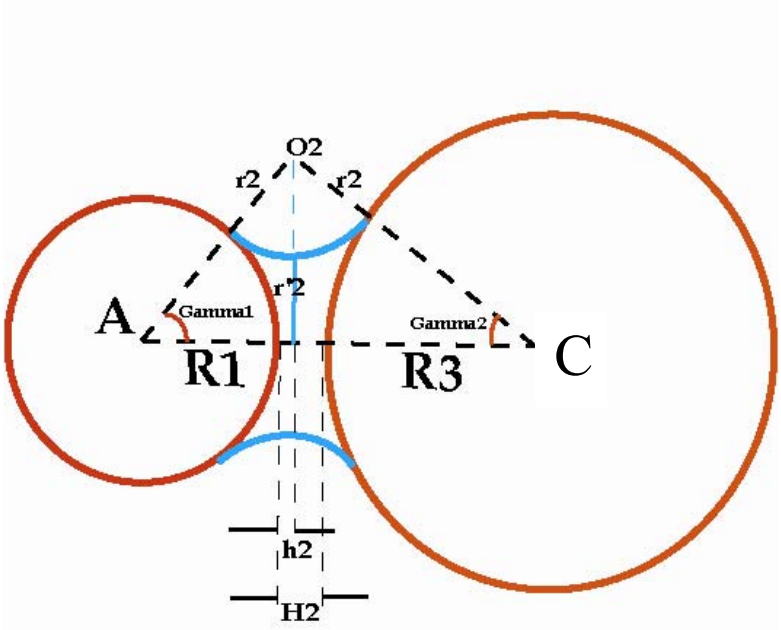

$$\begin{cases}\gamma_1 = \arctan(\frac{r_2 + r_2'}{R_1 + h_2}) \\ \gamma_2 = \arctan(\frac{r_2 + r_2'}{R_3 + H_2 - h_2})\end{cases}$$

$$A_1 = \frac{1}{2}(R_1 + h_2)^2 \tan\gamma_1 + \frac{1}{2}(R_3 + H_2 - h_2)^2 \tan\gamma_2 =$$

$$= \frac{1}{2}b(r_2 + r_2') = \frac{1}{2}b(r_2 + \frac{r_2}{1 - Cr_2})$$

$$\boxed{\Delta P_{AC} = \gamma_1 R_1 + \gamma_2 R_3 - (\pi - \gamma_1 - \gamma_2)r_2}$$

$$\boxed{\Delta A_{AC} = A_1 - \frac{1}{2}\gamma_1 R_1^2 - \frac{1}{2}\gamma_2 R_3^2 - \frac{1}{2}(\pi - \gamma_1 - \gamma_2)r_2^2}$$

$$\begin{cases}\frac{r_2 - h_2}{r_2 - H_2 + h_2} = \frac{2R_3 + r_2 + H_2 - h_2}{2R_1 + r_2 + h_2} \\ (r_2 + \frac{r_2}{1 - Cr_2})^2 = (2R_1 + r_2 + h_2)(r_2 - h_2)\end{cases}$$

Similarly for the pendular ring between the spheres A and B we would have:

$$\begin{cases} \alpha_1 = \arctan(\dfrac{r_3 + r_3'}{R_1 + h_3}) \\ \alpha_2 = \arctan(\dfrac{r_3 + r_3'}{R_2 + H_3 - h_3}) \end{cases}$$

$$A_3 = \frac{1}{2}(R_1 + h_3)^2 \tan\alpha_1 + \frac{1}{2}(R_2 + H_3 - h_3)^2 \tan\alpha_2 =$$

$$= \frac{1}{2}c(r_3 + r_3') = \frac{1}{2}c(r_3 + \frac{r_3}{1 - Cr_3})$$

$$\boxed{\Delta A_{AB} = A_3 - \frac{1}{2}\alpha_1 R_1^2 - \frac{1}{2}\alpha_2 R_2^2 - \frac{1}{2}(\pi - \alpha_1 - \alpha_2)r_3^2}$$

$$\boxed{\Delta P_{AB} = \alpha_1 R_1 + \alpha_2 R_2 - (\pi - \alpha_1 - \alpha_2)r_3}$$

$$\begin{cases} \dfrac{r_3 - h_3}{r_3 - H_3 + h_3} = \dfrac{2R_2 + r_3 + H_3 - h_3}{2R_1 + r_3 + h_3} \\ (r_3 + \dfrac{r_3}{1 - Cr_3})^2 = (2R_1 + r_3 + h_3)(r_3 - h_3) \end{cases}$$

And for the spheres B and C we would have the following relationships:

$$\begin{cases} \beta_1 = \arctan(\dfrac{r_1 + r_1'}{R_2 + h_1}) \\ \beta_2 = \arctan(\dfrac{r_1 + r_1'}{R_3 + H_1 - h_1}) \end{cases}$$

$$A_2 = \frac{1}{2}(R_2 + h_1)^2 \tan\beta_1 + \frac{1}{2}(R_3 + H_1 - h_1)^2 \tan\beta_2 =$$

$$= \frac{1}{2}a(r_1 + r_1') = \frac{1}{2}a(r_1 + \frac{r_1}{1 - Cr_1})$$

$$\boxed{\Delta P_{BC} = \beta_1 R_2 + \beta_2 R_3 - (\pi - \beta_1 - \beta_2)r_1}$$

$$\boxed{\Delta A_{BC} = A_2 - \frac{1}{2}\beta_1 R_2^2 - \frac{1}{2}\beta_2 R_3^2 - \frac{1}{2}(\pi - \beta_1 - \beta_2)r_1^2}$$

$$\begin{cases} \dfrac{r_1 - h_1}{r_1 - H_1 + h_1} = \dfrac{2R_3 + r_1 + H_1 - h_1}{2R_2 + r_1 + h_1} \\ (r_1 + \dfrac{r_1}{1 - Cr_1})^2 = (2R_2 + r_1 + h_1)(r_1 - h_1) \end{cases}$$

Solving the system all above equations the MSP critical values of the pore throats are calculated.

In the following we have compared the MSP critical values and the Mason and Mellor approximation (which we used to use in drainage simulations before) for some sample packings (#11, #41, #49 and #53_reduced, which is #53 with grains smaller that 0.1 R_{mean} removed to avoid spurious throats.) For each packing we show (i) the drainage capillary pressure vs. saturation curve using the MSP critical curvatures; (ii) histogram of MSP and Mason/Mellor critical curvatures for all throats in the model sediment; (iii) cumulative distribution of MSP and Mason/Mellor critical curvatures; and (iv) a cross-plot of the MSP and Mason/Mellor estimate for each throat. The Mason/Mellor estimate is labeled as "Haines – 1.6" in the latter plot, indicating its origin. The drainage curves are reported in two ways, as number fraction of pores still containing water and as volume fraction of pores still containing water. The volume of water held in pendular rings at grain contacts is included in all the drainage curves.

An important improvement afforded by the MSP calculation is that it eliminates the need for the empirical correction of -1.6, introduced by Mason and Mellor for very well sorted packings. This value works very well for those packings, but it results in negative critical curvatures for a few of the Delaunay throats in the poorly sorted packings. This is evident in the histograms. Clearly negative critical curvatures are nonphysical, since the grains are water-wet. The negative values occur partly because these throats do not correspond to the full set of grains that support the gas/water interface in that region of pore space. But it is also true that the correction should vary with the size of the grains comprising the throat. This matters in a poorly sorted packing, because throats can be made of several large grains or several small grains. But with the generalized MSP method, it is not possible to obtain negative critical curvatures.

Example of generalized MSP calculation: Pack 11

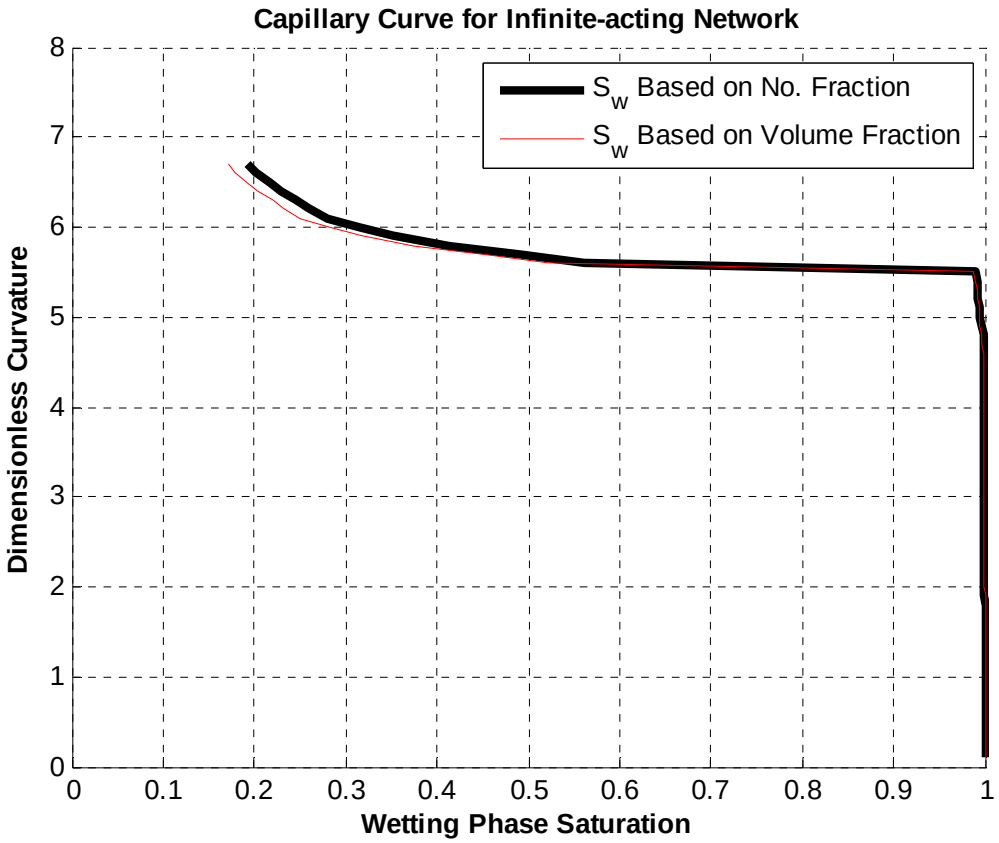

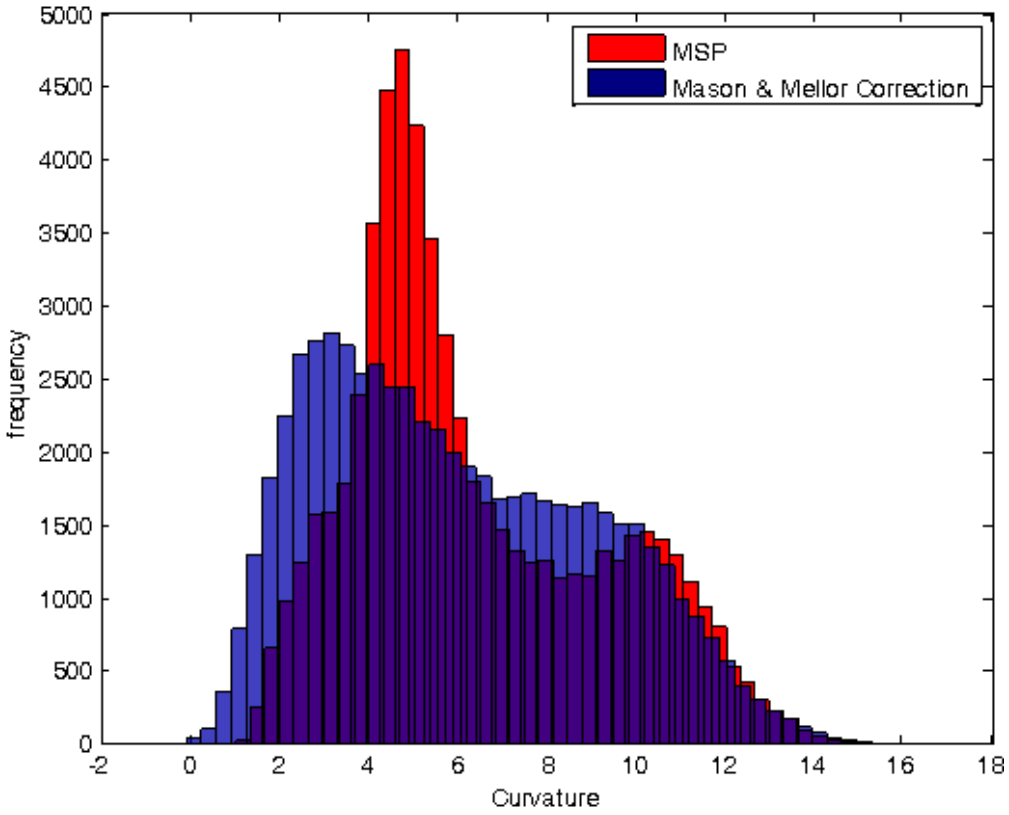

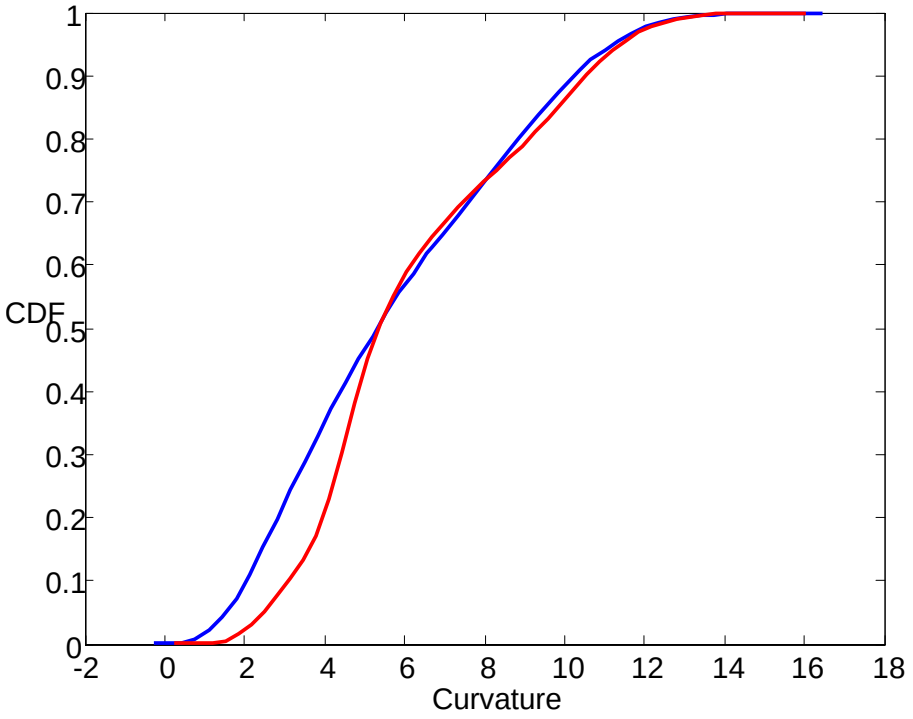
CDF
Curvature
0
0.1
0.2
0.3
0.4
0.5
0.6
0.7
0.8
0.9
1
-2
0
2
4
6
8
10
12
14
16
18

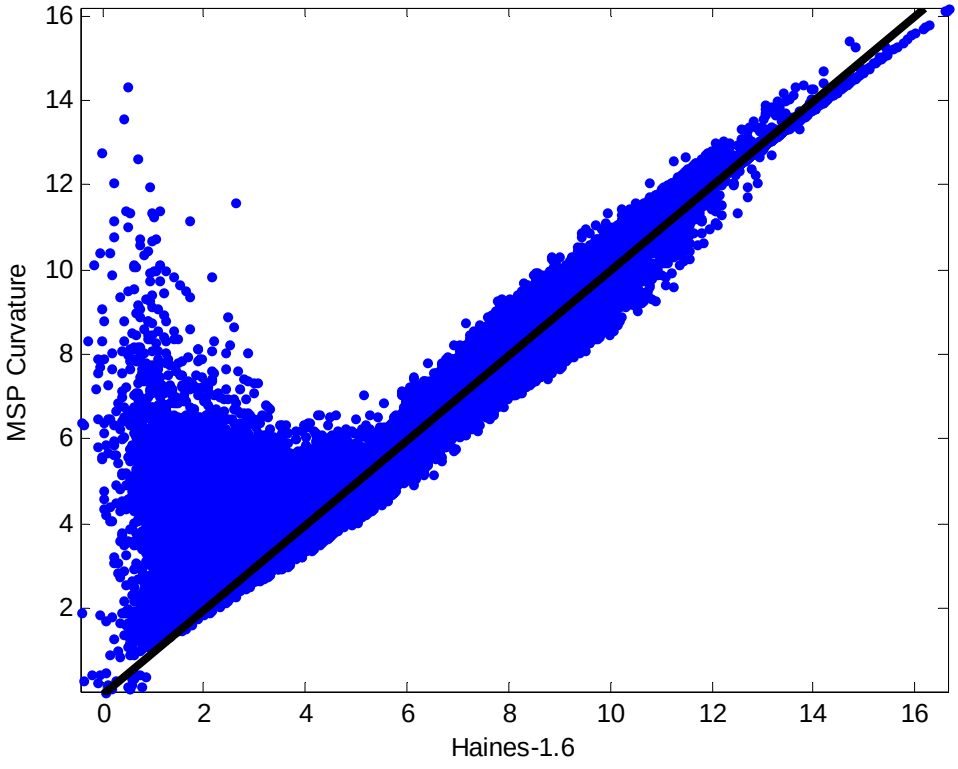
MSP Curvature
Haines-1.6
2
4
6
8
10
12
14
16
0
2
4
6
8
10
12
14
16

Example of generalized MSP calculation: Pack 41

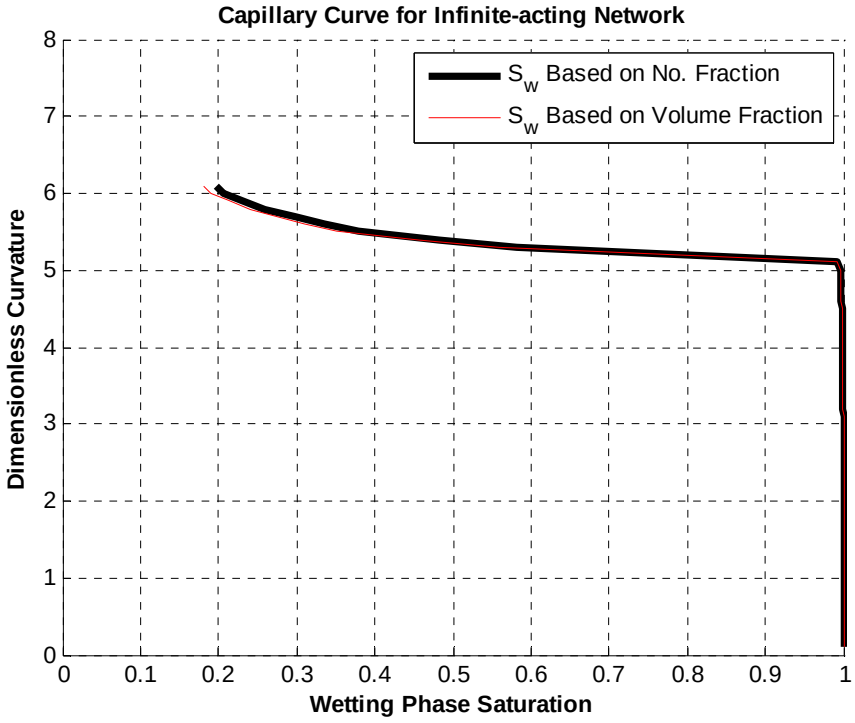

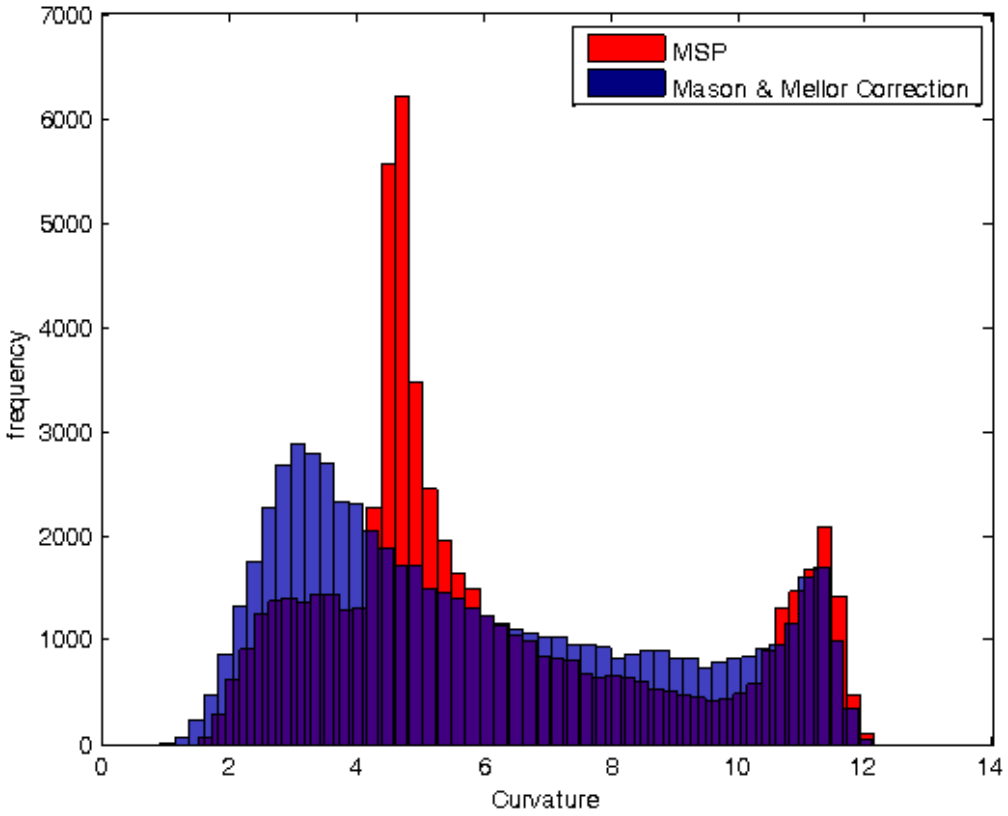

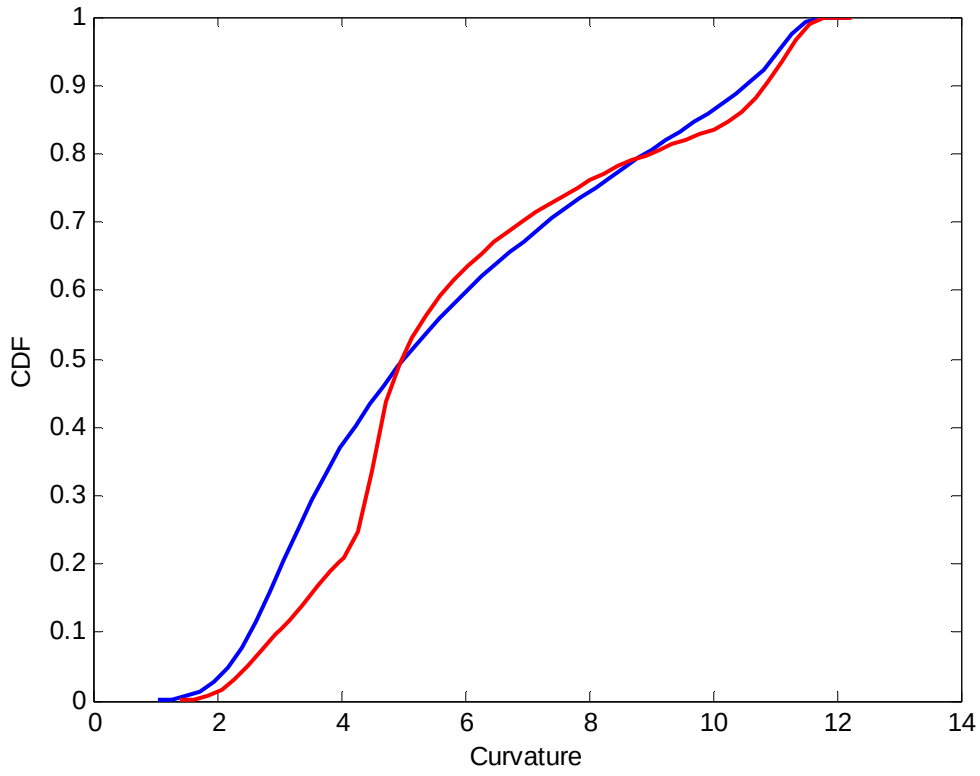
CDF
Curvature
0
0.1
0.2
0.3
0.4
0.5
0.6
0.7
0.8
0.9
1
0
2
4
6
8
10
12
14

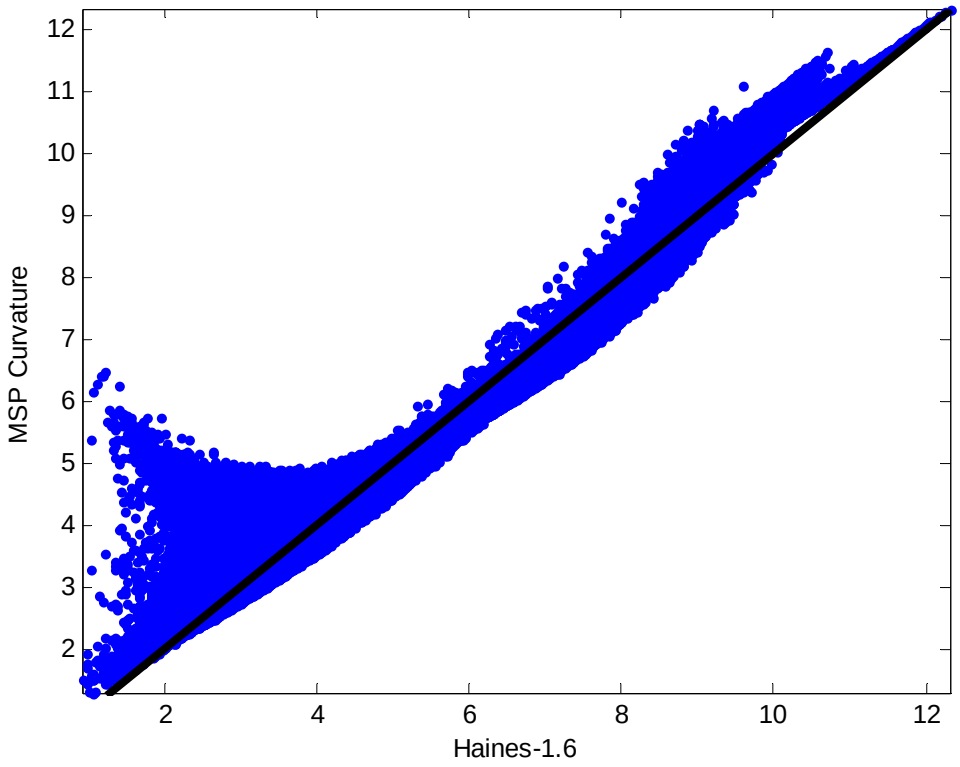
MSP Curvature
Haines-1.6
2
3
4
5
6
7
8
9
10
11
12
2
4
6
8
10
12

Example of generalized MSP calculation: Pack 49

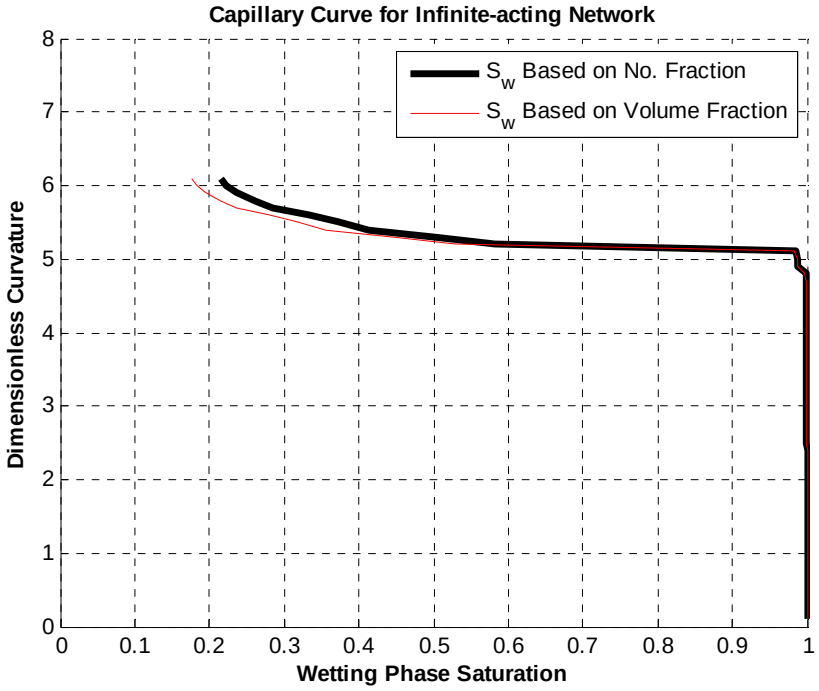

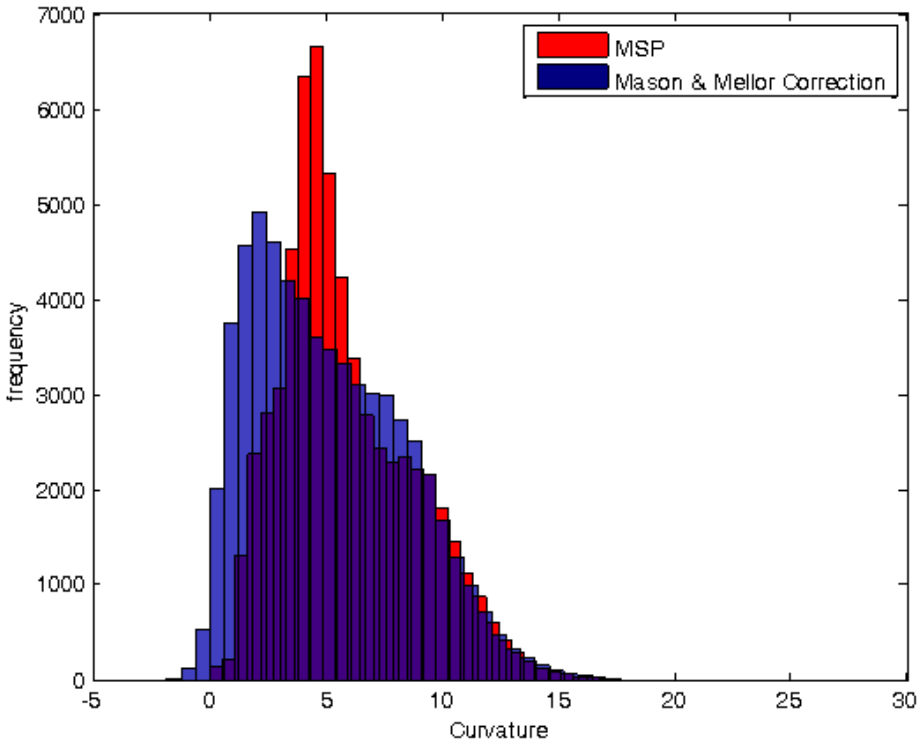

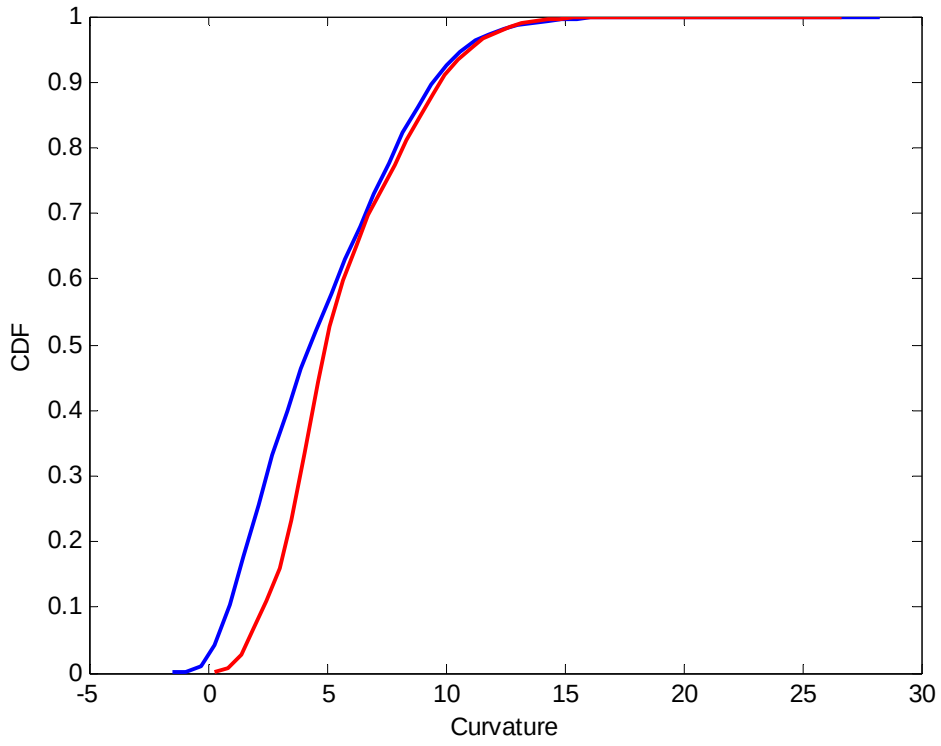
CDF
Curvature
0
0.1
0.2
0.3
0.4
0.5
0.6
0.7
0.8
0.9
1
-5
0
5
10
15
20
25
30

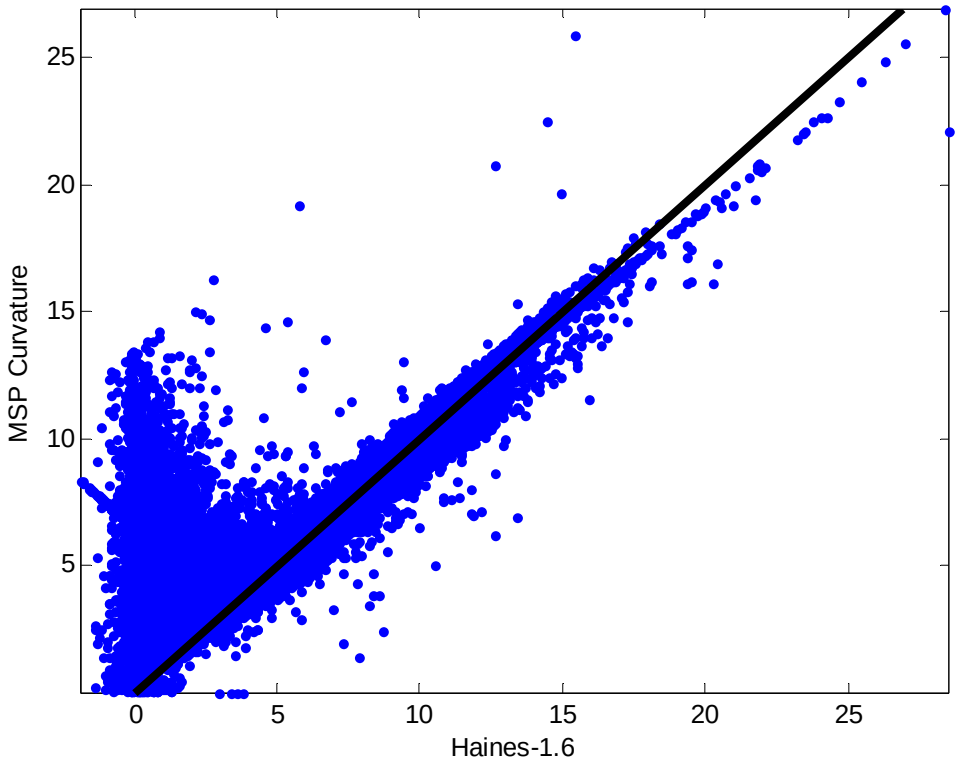
MSP Curvature
Haines-1.6
5
10
15
20
25
0
5
10
15
20
25

Example of generalized MSP calculation: Pack 53

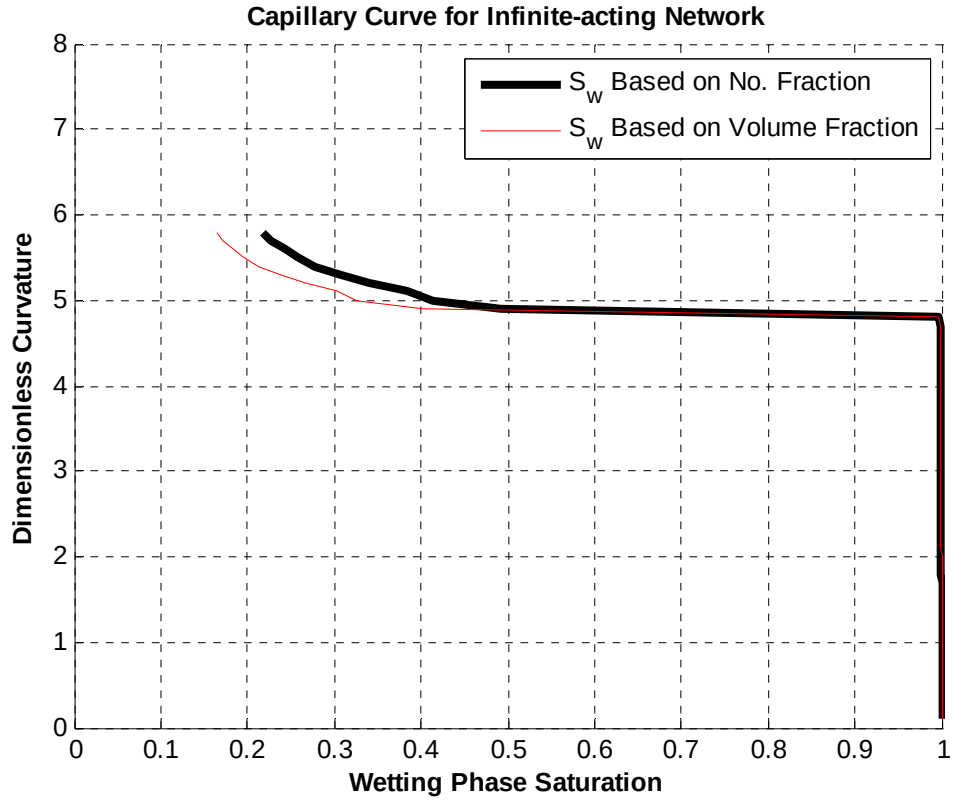

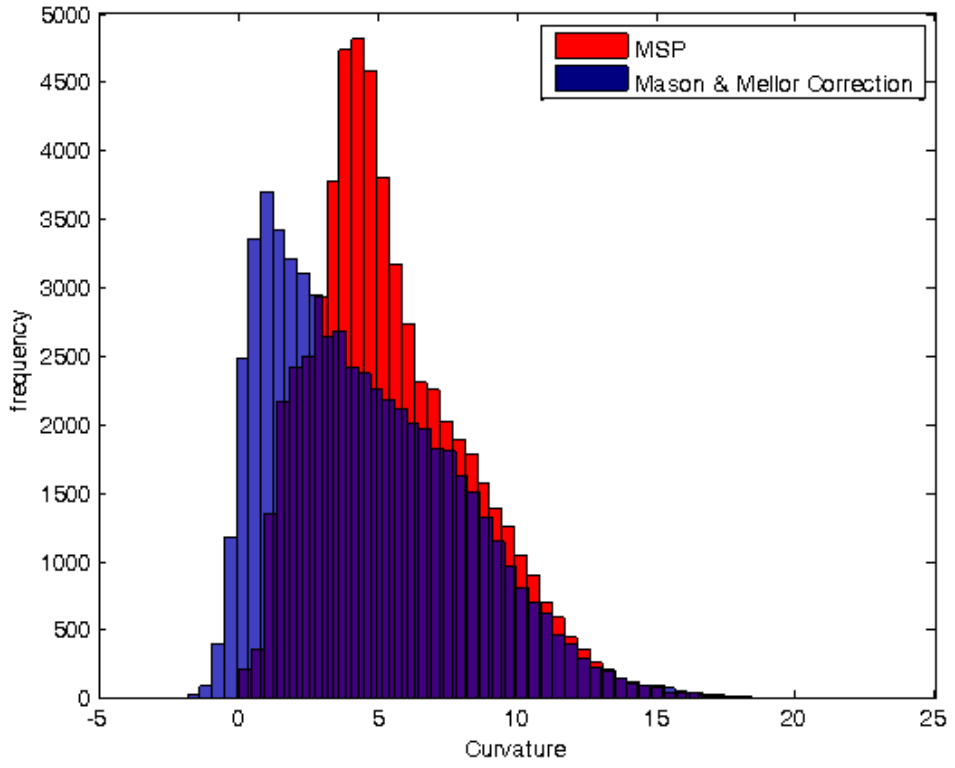

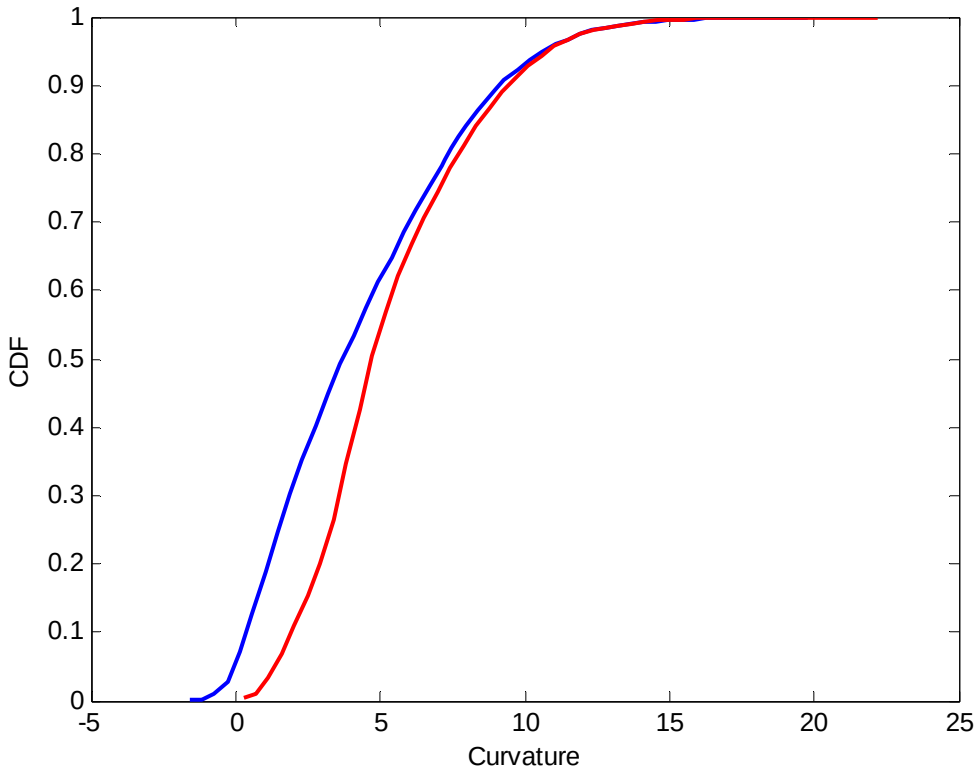
CDF
Curvature
1
0.9
0.8
0.7
0.6
0.5
0.4
0.3
0.2
0.1
0
-5
0
5
10
15
20
25

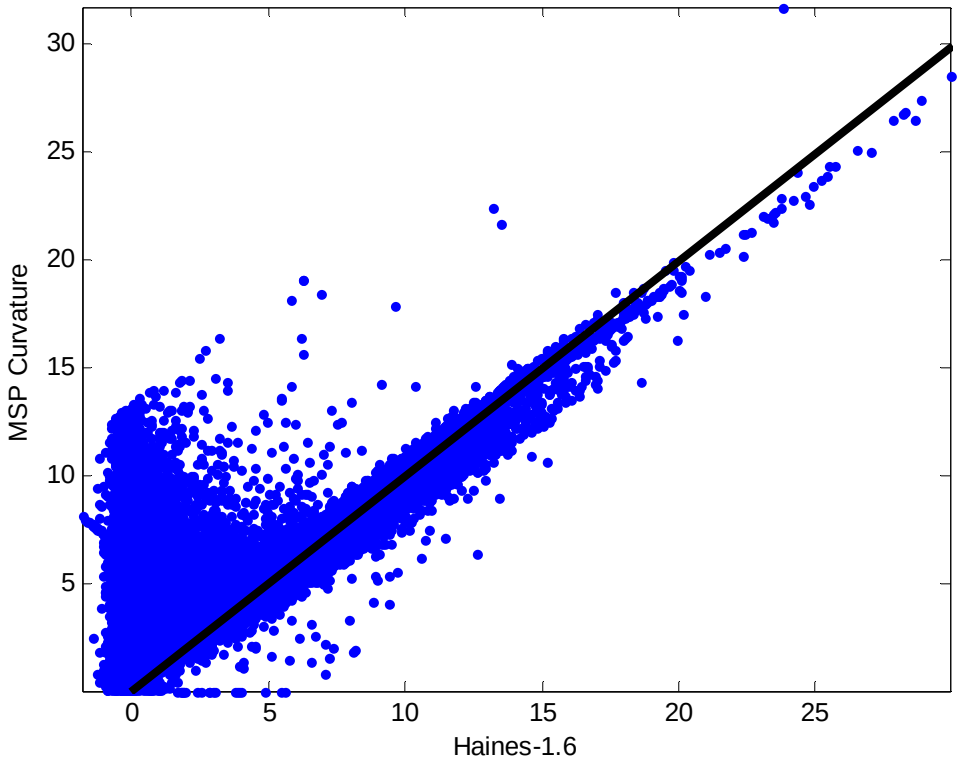
MSP Curvature
Haines-1.6
30
25
20
15
10
5
0
5
10
15
20
25

5.2.2 Imbibition Simulation from Drainage Endpoint in Model Sediments

The full set of simulations is reported in Appendix C. Here we review the approach taken.

We implemented a invasion percolation algorithm for imbibition. The simulation is analogous to the drainage simulation. Key differences are the initial condition (we start from the drainage endpoint, i.e. from irreducible water saturation as described in previous section) and the critical curvature for imbibition of a pore. An important similarity is the condition for trapping the displaced phase (gas in this case). A pore containing gas cannot be imbibed by water unless that pore is part of a cluster of connected, gas-filled pores which spans the network. Here "spans" means that the cluster is connected through at least one pair of periodic boundaries. If this condition is satisfied, the cluster is effectively infinite in extent, because it will be connected through any number of copies of the periodic unit cell placed adjacent to the original cell.

The simulations in very well sorted packings predict the same percolation threshold as observed in experiments, viz. at a dimensionless curvature of about 4. For most model sediments the residual saturations range from 30% to 40%, which are larger than observed in experiments. This is because the infinite-acting networks impose a more stringent condition for displacement of the gas phase, viz. percolation of the cluster of pores containing the gas. The predicted residual saturations are however consistent with typical observations in single well tracer tests applied to injection wells. The latter tests are conducted by injecting a solution containing a conservative tracer and a partitioning tracer into the reservoir around an injector, where all oil saturation is likely to be at or near residual. The injected fluid is then produced back from the same well. The difference in return times of the two tracers is a measure of residual oil saturation. Values are typically 40% or so.

Appendix A: Summary of Properties of Model Sediments

For convenience we reproduce from earlier reports that summary of the properties of the model sediments used in this research. All are dense, disordered, computer-generated packings of spheres. We use the nouns "sphere" and "grain" interchangeably. Packings with similar grain size distribution and similar sorting index values are grouped together:

Table 1. Summary of Properties of Model Sediments

	Grain sizes (arbitrary units)				Porosity (fraction)	Sorting Index			Notes*
Packing No.	Minimum Radius	Maximum radius	Mean radius	Standard deviation		Number fraction basis	Volume or weight fraction basis	Grain Surface Area/Bulk Volume	
1	0.32	2.58	2.18	0.11	0.37	1.04	1.04	0.873398	LN
2	1.84	2.64	2.18	0.11	0.36	1.03	1.03	0.873713	LN
3	1.8	2.6	2.18	0.11	0.37	1.03	1.03	0.871821	LN
4	0.32	2.59	2.18	0.11	0.35	1.03	1.03	0.874216	LN
5	1.82	2.52	2.15	0.11	0.41	1.03	1.03	0.845784	LN
Average	1.22	2.59	2.17	0.11	0.37	1.03	1.03		
6	1.5	3.22	2.17	0.22	0.36	1.07	1.07	0.870069	LN
7	1.5	3.08	2.16	0.22	0.36	1.07	1.07	0.862364	LN
8	1.48	2.99	2.17	0.22	0.36	1.07	1.07	0.867997	LN
9	1.47	3.06	2.16	0.22	0.37	1.07	1.07	0.862127	LN
Average	1.49	3.09	2.16	0.22	0.36	1.07	1.07		
10	0.96	4.12	2.12	0.42	0.35	1.14	1.14	0.853125	LN
11	0.93	4.64	2.12	0.43	0.34	1.14	1.14	0.855595	LN
12	1.07	4.49	2.11	0.42	0.35	1.14	1.14	0.852085	LN
13	0.99	4.27	2.11	0.43	0.35	1.14	1.14	0.846668	LN
Average	0.99	4.38	2.11	0.43	0.35	1.14	1.14		
14	4.24E-03	7.05	1.9	0.8	0.32	1.31	1.32	0.853125	LN
15	3.44E-03	6.44	1.9	0.79	0.35	1.31	1.31	0.855595	LN
16	3.91E-01	6.38	1.91	0.78	0.33	1.31	1.29	0.852085	LN
17	7.81E-03	7.01	1.9	0.79	0.32	1.31	1.3	0.846668	LN
18	1.59E-03	7.62	1.91	0.79	0.32	1.31	1.29	0.779363	LN
Average	8.17E-02	6.9	1.9	0.79	0.33	1.31	1.3		
19	1.86E-03	11.3	1.31	1.16	0.29	1.72	1.48	0.774083	LN; Trn
20	2.39E-03	10.16	1.31	1.17	0.25	1.72	1.54	0.782817	LN; Trn
21	7.85E-03	11.26	1.31	1.15	0.3	1.72	1.53	0.77599	LN; Trn
22	1.17E-03	11.17	1.3	1.16	0.3	1.69	1.53	0.780766	LN; Trn
Average	3.32E-03	10.97	1.31	1.16	0.29	1.71	1.52		
23	3.45E-05	11.31	0.69	1.25	0.31	3.11	1.32	0.561808	LN; Trn
24	1.63E-05	11.19	0.71	1.26	0.3	3.12	1.38	0.566764	LN; Trn
25	3.80E-05	11.28	0.7	1.25	0.37	3.16	1.3	0.556885	LN; Trn

26	1.44E-05	12.16	0.72	1.23	0.32	3.07	1.46	0.556307	LN; Trn
Average	2.58E-05	11.49	0.71	1.25	0.33	3.11	1.37		
27	8.10E-06	18.29	0.3	1.07	0.31	3.63	1.38	0.375571	LN; Trn
28	2.04E-06	21.32	0.3	1.04	0.29	3.77	1.37	0.385136	LN; Trn
29	6.94E-06	22.46	0.31	1.04	0.32	3.95	1.41	0.377781	LN; Trn
Average	5.69E-06	20.69	0.31	1.05	0.31	3.79	1.39		
30	1.24E-03	11.93	1.01	1.2	0.29	2	1.5	0.373962	LN; Trn
31	6.31E-04	11.99	1.04	1.22	0.32	2	1.56	0.227332	LN; Trn
32	5.70E-04	12.34	1.02	1.21	0.3	2.03	1.48	0.215402	LN; Trn
33	4.21E-05	12.57	1.07	1.22	0.31	1.94	1.51		LN; Trn
34	5.47E-04	11.63	1.03	1.19	0.34	2.01	1.49		LN; Trn
Average	6.06E-04	12.09	1.03	1.21	0.31	2	1.51		
35	4.62E-04	9.67	1.63	1.03	0.3	1.51	1.4	0.213955	LN
36	1.89E-03	9.7	1.61	1.04	0.3	1.5	1.43	0.451858	LN
37	1.35E-03	9.3	1.59	1.04	0.27	1.49	1.46	0.466817	LN
38	3.98E-03	9.41	1.6	1.05	0.27	1.51	1.44	0.457397	LN
Average	1.92E-03	9.52	1.6	1.04	0.29	1.5	1.43		
39	2	2.4	2.19	0.07	0.34	1.02	1.02	0.679516	N
40	2	2.41	2.19	0.07	0.35	1.02	1.02	0.671683	N
41	2	2.39	2.17	0.07	0.38	1.02	1.02	0.662955	N
42	2	2.4	2.19	0.07	0.37	1.02	1.02	0.666658	N
Averages	2	2.4	2.18	0.07	0.36	1.02	1.02		
43	1	3.2	2.14	0.35	0.36	1.12	1.1	0.878862	N
44	1	3.2	2.14	0.35	0.36	1.12	1.1	0.879162	N
45	1	3.2	2.14	0.36	0.35	1.12	1.11	0.86555	N
46	1	3.2	2.14	0.35	0.37	1.12	1.11	0.877698	N
Averages	1	3.2	2.14	0.35	0.36	1.12	1.1		
47	#	4.01	2.01	0.68	0.34	1.27	1.17	0.862418	
48	#	4.01	2.01	0.66	0.33	1.25	1.17	0.861402	
49	#	4.03	2.01	0.67	0.34	1.25	1.18	0.864378	
50	#	4.04	2.02	0.66	0.33	1.25	1.17	0.86135	
Averages	#	4.02	2.01	0.67	0.34	1.26	1.17		
51	#	4.59	1.85	0.9	0.32	1.42	1.21		
52	#	4.51	1.85	0.91	0.34	1.42	1.21		
53	#	4.44	1.86	0.89	0.35	1.4	1.21		
54	#	4.59	1.86	0.9	0.32	1.42	1.2		
Averages	#	4.53	1.86	0.9	0.33	1.42	1.21		
55	#	5	1.73	1.04	0.32	1.6	1.23		
56	#	5.06	1.71	1.05	0.31	1.64	1.22		
57	#	5.07	1.71	1.05	0.35	1.62	1.22		
58	#	5.08	1.71	1.05	0.34	1.65	1.23		
59	#	5.01	1.7	1.05	0.33	1.63	1.22		

Averages	#	5.04	1.71	1.05	0.33	1.63	1.22		
60	#	4.56	1.84	0.91	0.32	1.43	1.21		
61	#	4.82	1.77	1	0.31	1.53	1.22	0.752922	
62	#	4.85	1.76	1	0.35	1.53	1.23	0.749431	
63	#	4.81	1.76	1	0.33	1.53	1.22	0.752072	
64	#	4.82	1.77	0.99	0.33	1.51	1.22	0.75331	
65	#	4.88	1.76	1	0.34	1.54	1.23	0.752684	
Averages	#	4.79	1.78	0.98	0.33	1.51	1.22		
66	#	5.36	1.6	1.15	0.33	1.89	1.24	0.711901	
67	#	5.38	1.61	1.14	0.32	1.85	1.24	0.712101	
68	#	5.44	1.6	1.15	0.33	1.94	1.23	0.708131	
69	#	5.43	1.6	1.14	0.33	1.91	1.24	0.704996	
70	#	5.32	1.59	1.14	0.33	1.9	1.25	0.704055	
Averages	#	5.39	1.6	1.14	0.33	1.9	1.24		
71	#	5.46	1.54	1.19	0.33	2.12	1.23	0.693023	
72	#	5.47	1.53	1.2	0.33	2.2	1.23	0.692432	
73	#	5.49	1.52	1.2	0.32	2.27	1.24		
74	#	5.64	1.53	1.2	0.33	2.18	1.24	0.690997	
75	#	5.65	1.53	1.19	0.33	2.13	1.26	0.688666	
76	#	5.52	1.53	1.2	0.32	2.23	1.24	0.692512	
Averages	#	5.54	1.53	1.2	0.32	2.19	1.24		

# indicates packings in which small grains were removed. Here "small" means less than one tenth the average grain size. In the following graphs packings with "_reduced" in their names show that we have eliminated these grains.

Appendix B: Drainage in All Model Sediments

Drainage curves based on MSP critical curvatures along with the graphs of water/gas interfacial area for several packings are shown in the following graphs. The curves are labeled as "resultXX" where XX indicates the number of the model sediment in the table in Appendix A. Packings with "_reduced" in their names show that we have eliminated grains of size less than one tenth of the average grain size. This removes artifacts (very large nominal throat sizes) without affecting the essential physics so that the overall drainage behavior is consistent.

B.1 Drainage capillary pressure curves

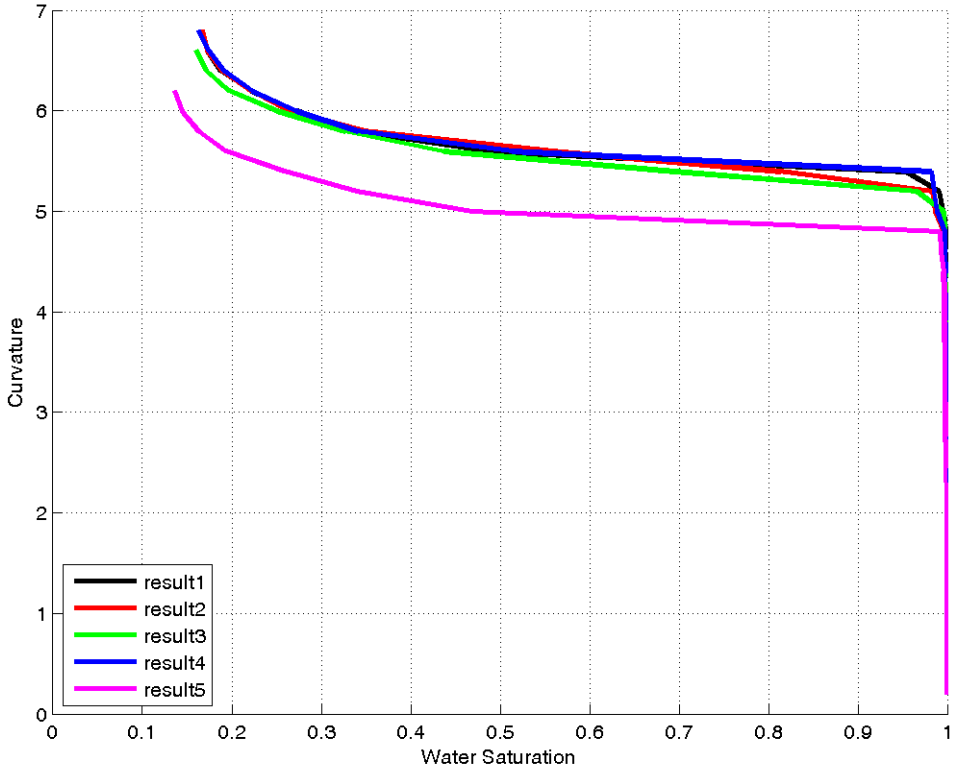
Curvature
Water Saturation
result1
result2
result3
result4
result5
0
1
2
3
4
5
6
7
0
0.1
0.2
0.3
0.4
0.5
0.6
0.7
0.8
0.9
1

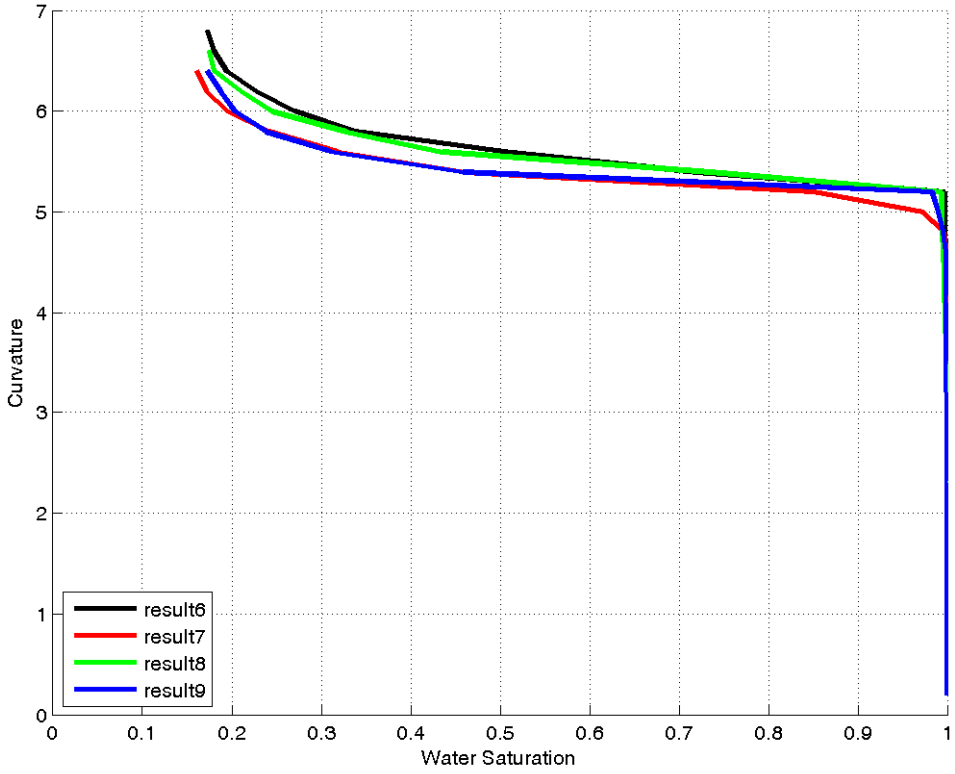
Curvature
Water Saturation
result6
result7
result8
result9
0
1
2
3
4
5
6
7
0
0.1
0.2
0.3
0.4
0.5
0.6
0.7
0.8
0.9
1

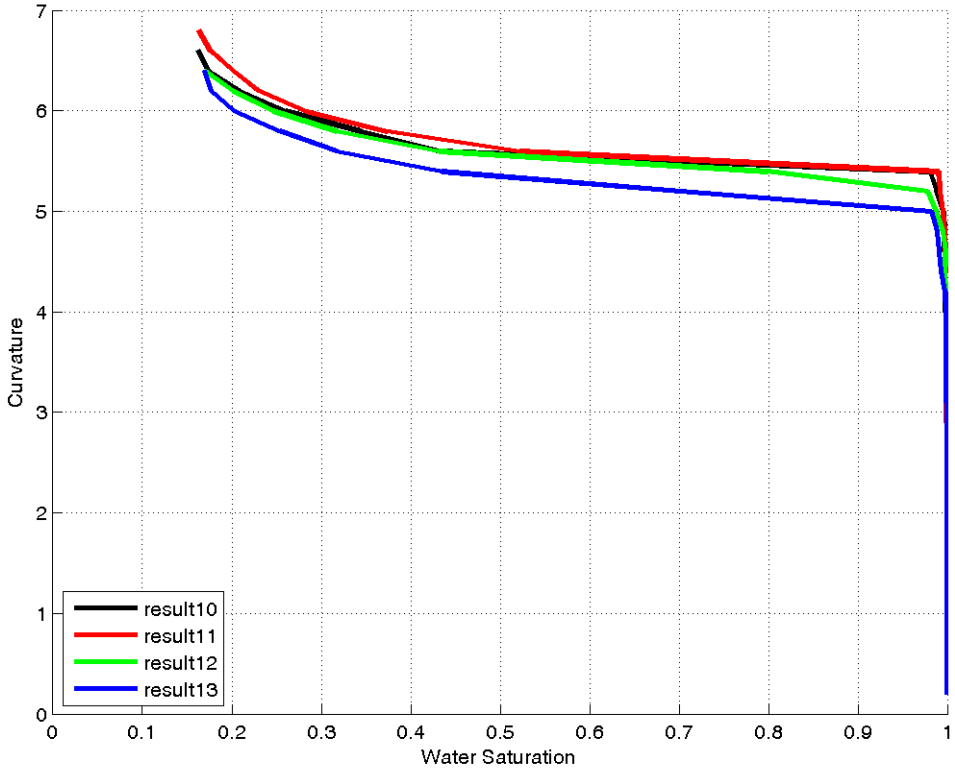
Curvature
Water Saturation
result10
result11
result12
result13
0
1
2
3
4
5
6
7
0
0.1
0.2
0.3
0.4
0.5
0.6
0.7
0.8
0.9
1

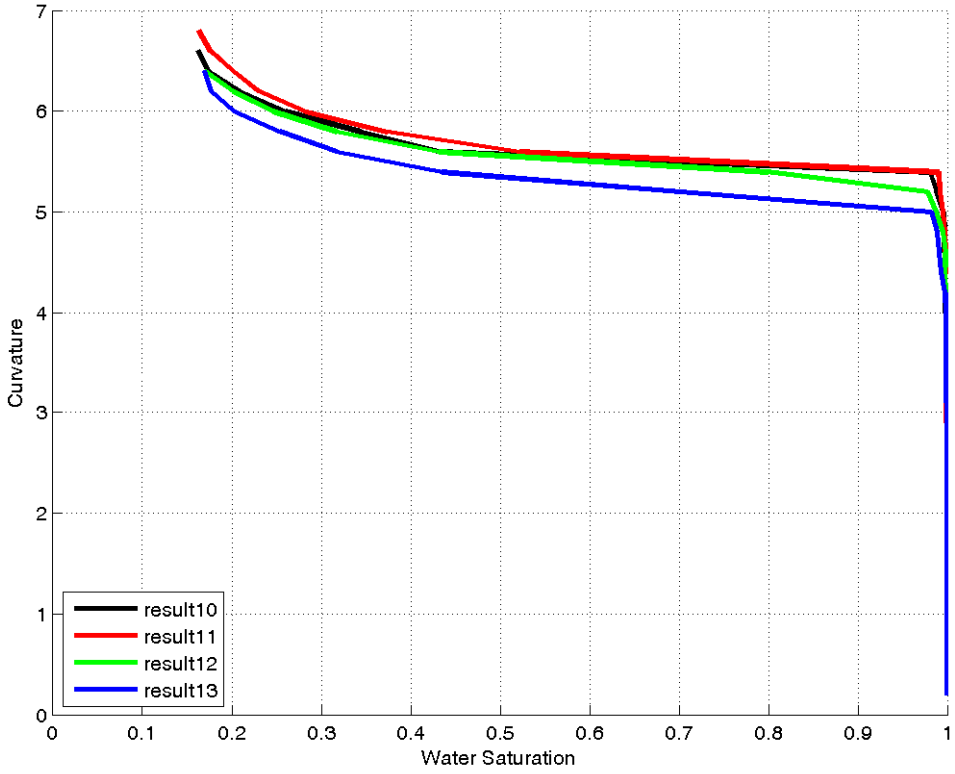
Curvature
Water Saturation
result10
result11
result12
result13
0
1
2
3
4
5
6
7
0
0.1
0.2
0.3
0.4
0.5
0.6
0.7
0.8
0.9
1

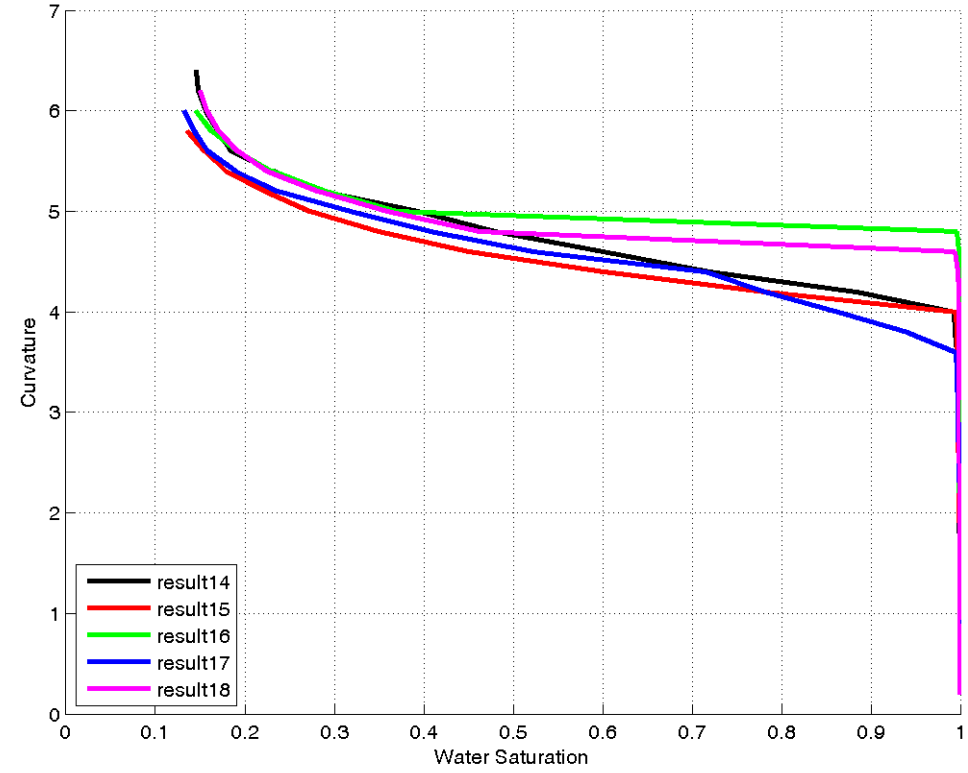
Curvature
Water Saturation
result14
result15
result16
result17
result18

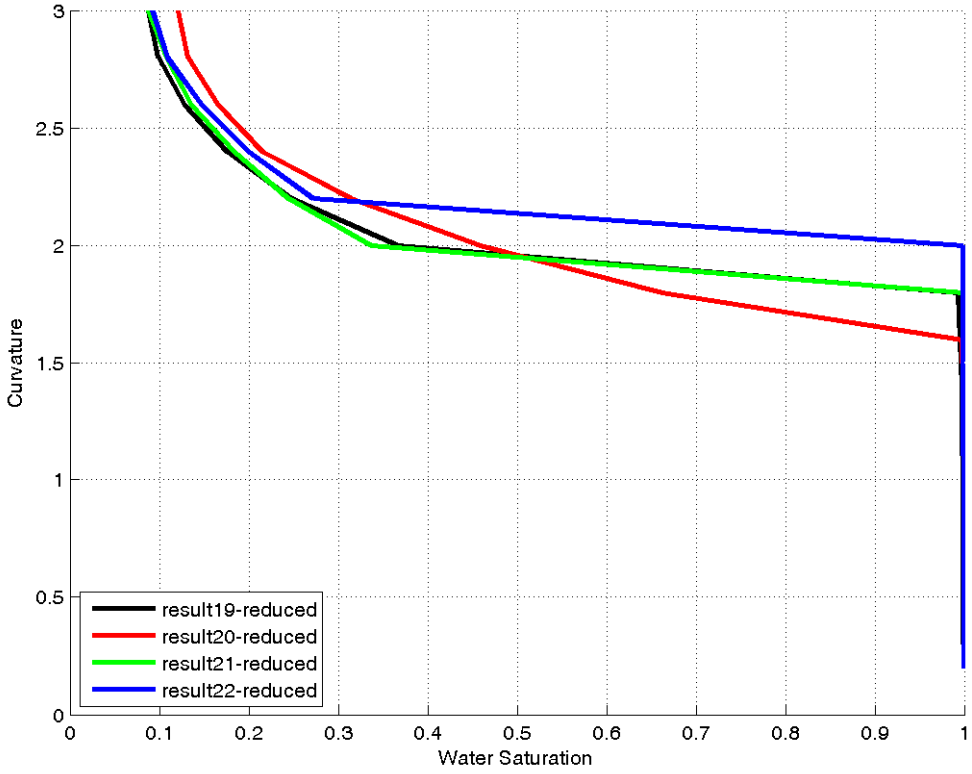
Curvature
Water Saturation
result19-reduced
result20-reduced
result21-reduced
result22-reduced

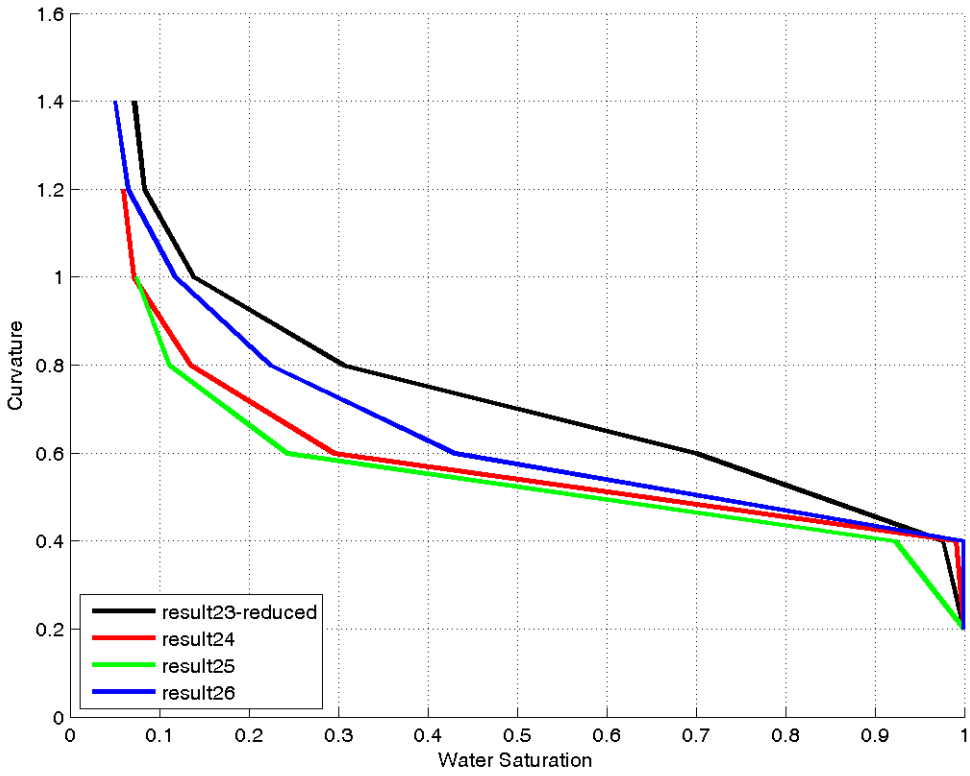
Curvature
Water Saturation
result23-reduced
result24
result25
result26

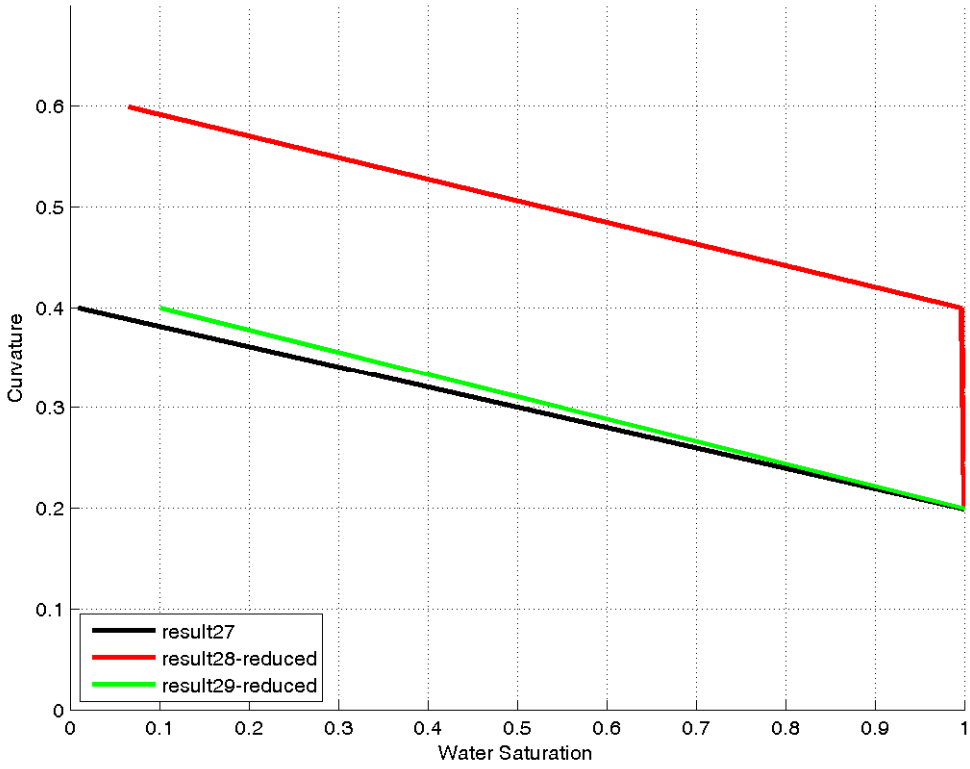
Curvature
Water Saturation
result27
result28-reduced
result29-reduced

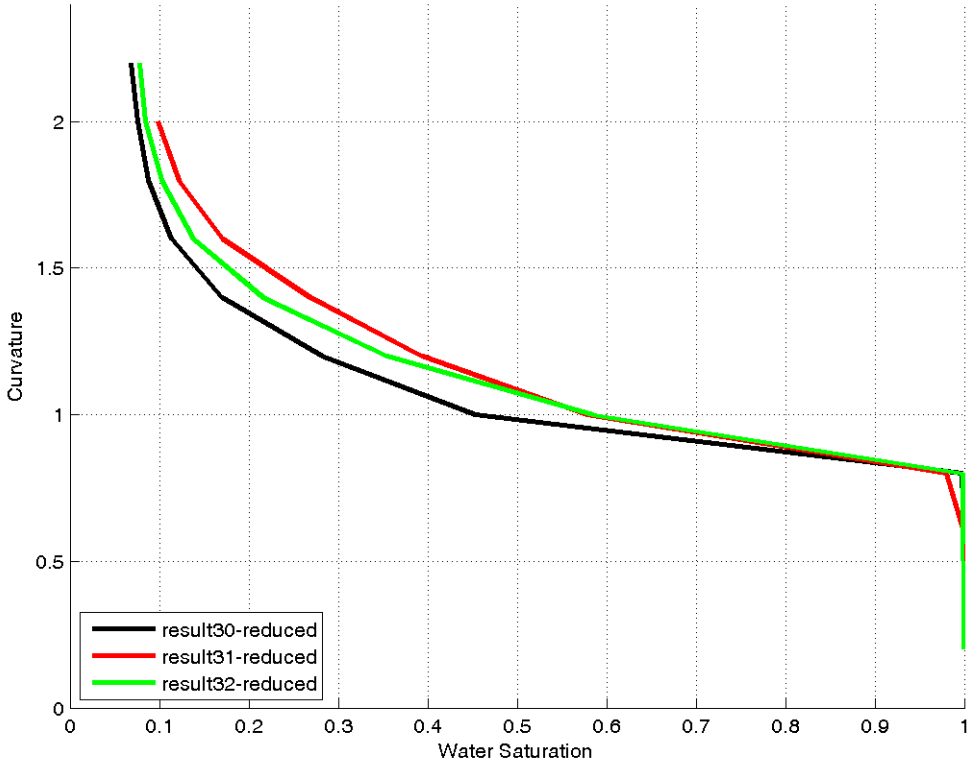
Curvature
Water Saturation
result30-reduced
result31-reduced
result32-reduced
0
0.5
1
1.5
2
0.1
0.2
0.3
0.4
0.5
0.6
0.7
0.8
0.9

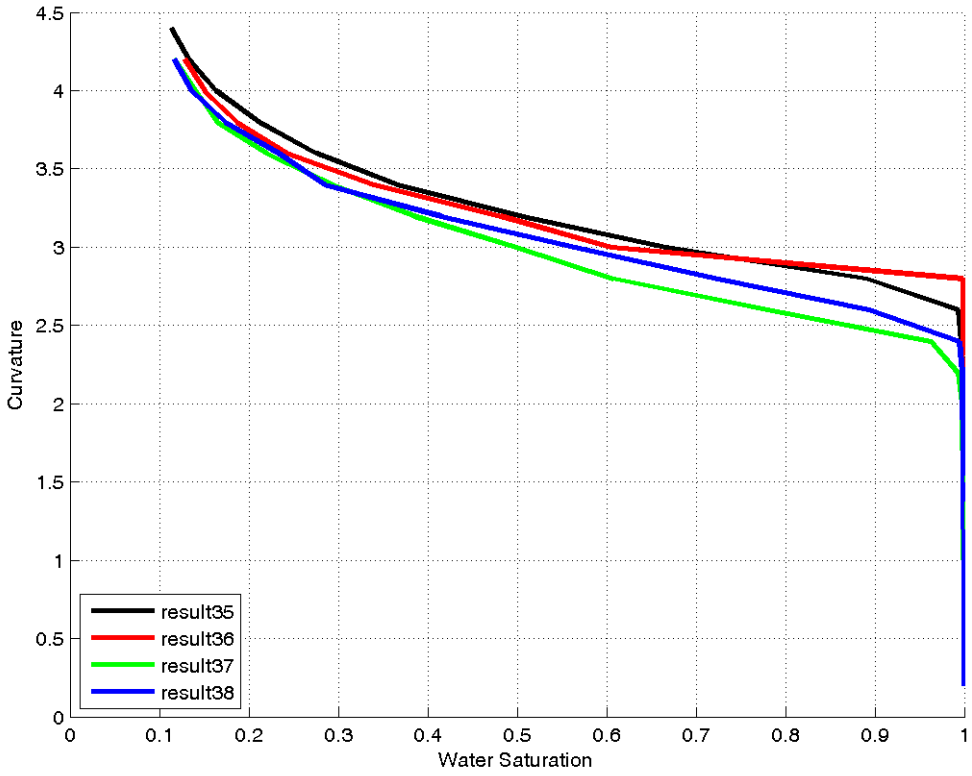
Curvature
Water Saturation
result35
result36
result37
result38
0
0.5
1
1.5
2
2.5
3
3.5
4
4.5
0.1
0.2
0.3
0.4
0.5
0.6
0.7
0.8
0.9

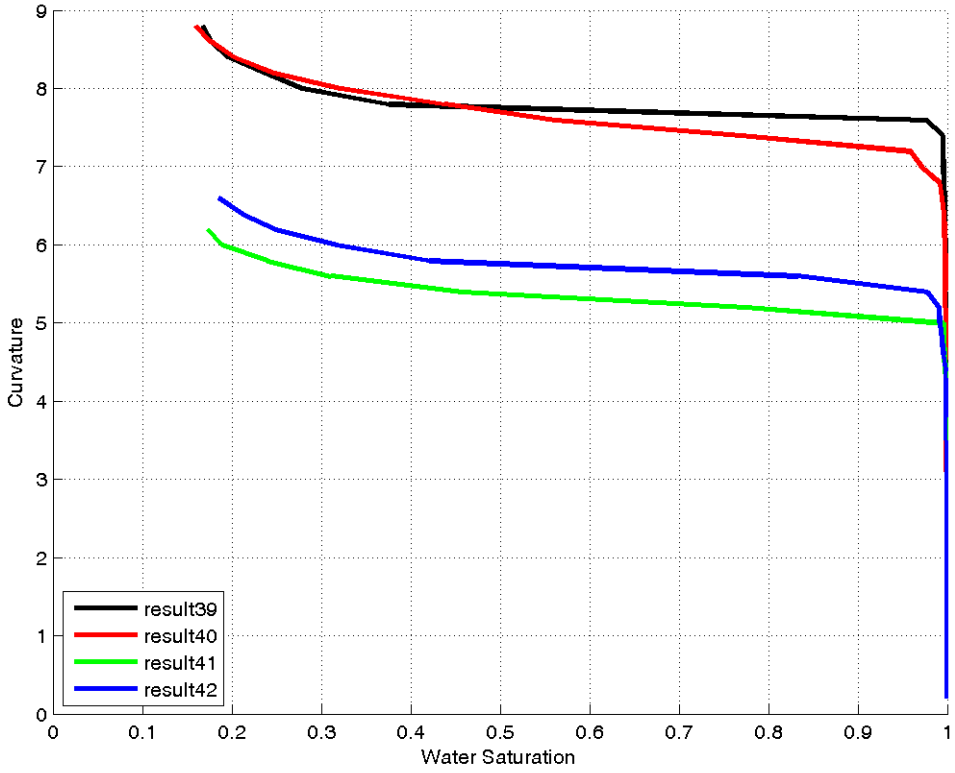
Curvature
Water Saturation
result39
result40
result41
result42

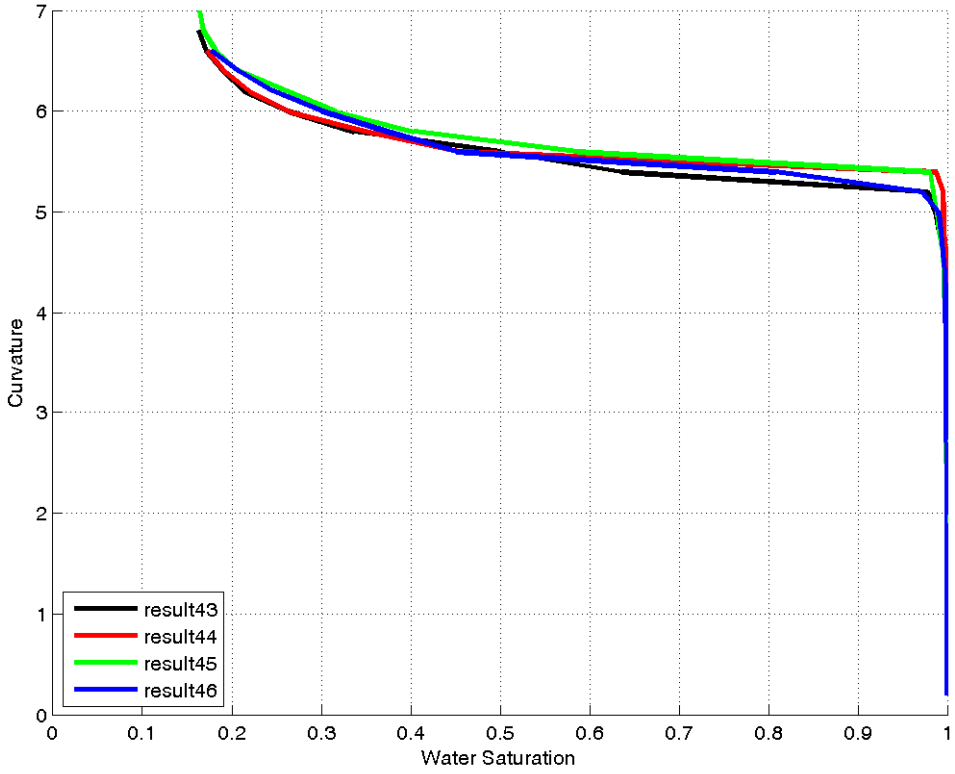
Curvature
Water Saturation
result43
result44
result45
result46

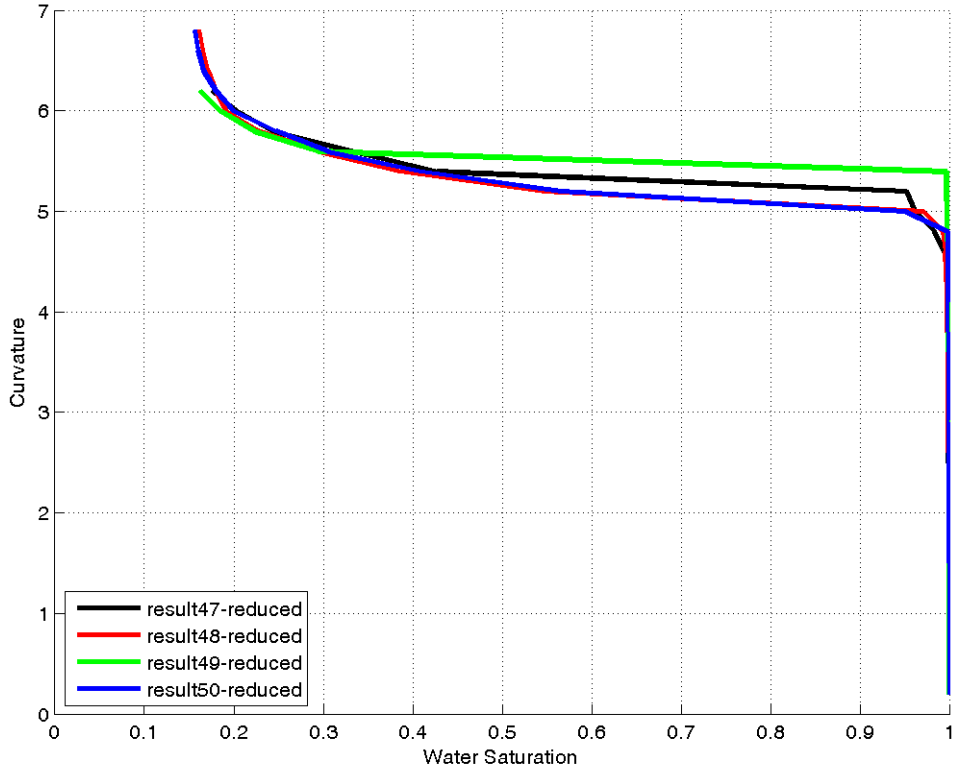
Curvature
Water Saturation
result47-reduced
result48-reduced
result49-reduced
result50-reduced

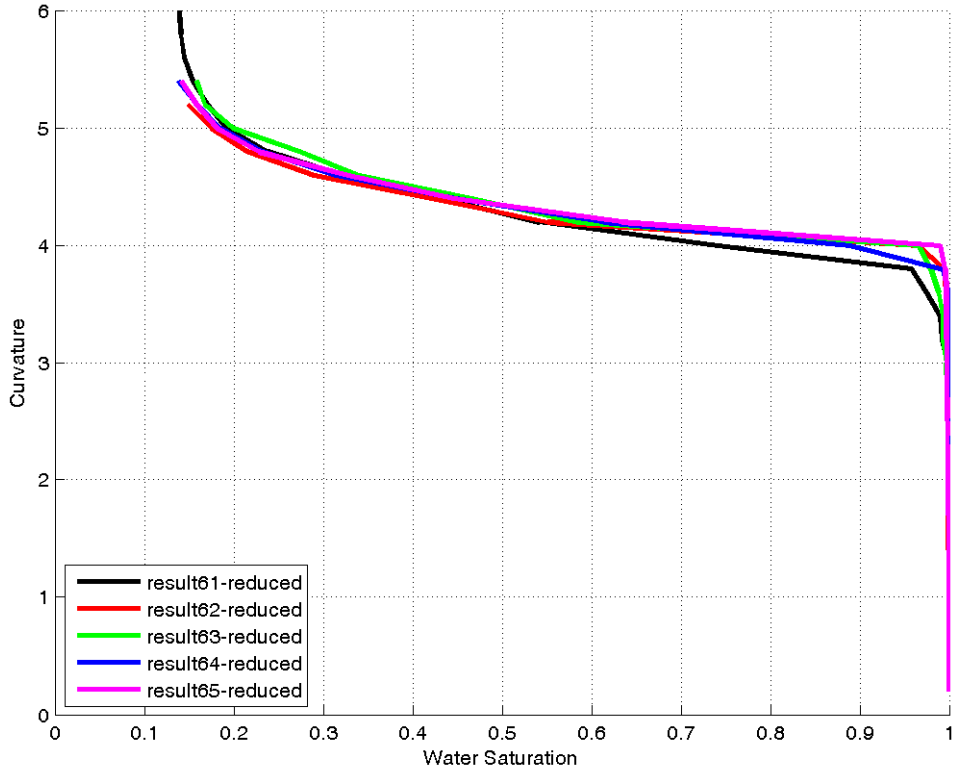
Curvature
Water Saturation
result61-reduced
result62-reduced
result63-reduced
result64-reduced
result65-reduced

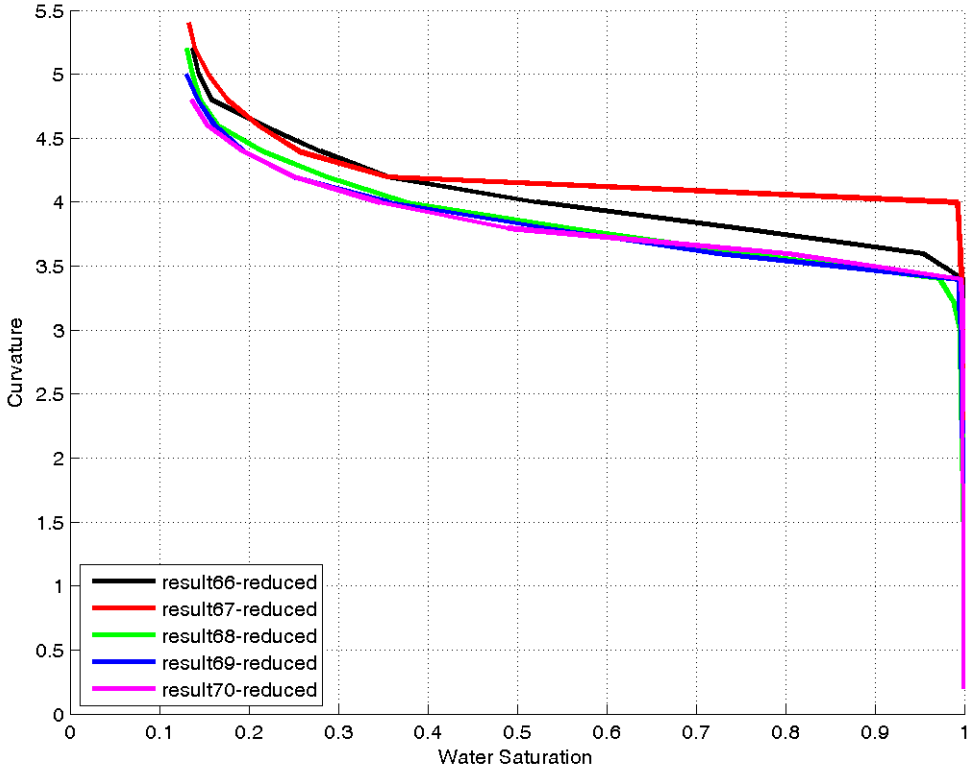
Curvature
Water Saturation
result66-reduced
result67-reduced
result68-reduced
result69-reduced
result70-reduced

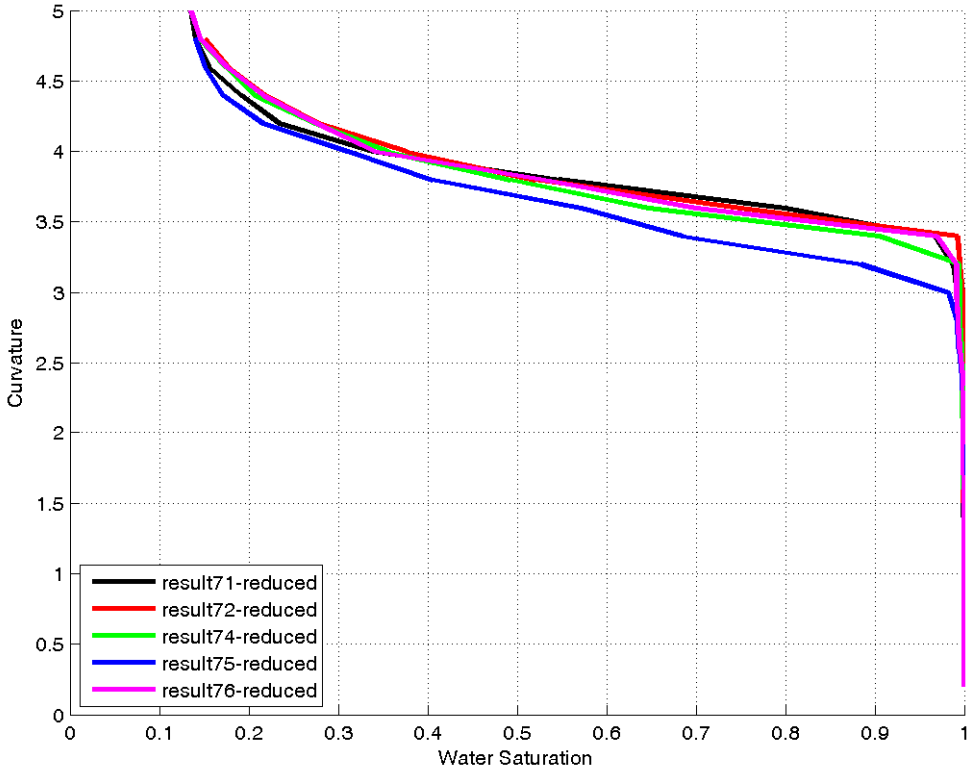
Curvature
Water Saturation
result71-reduced
result72-reduced
result74-reduced
result75-reduced
result76-reduced

B.2 Normalized gas/water interfacial area during drainage.

The interfacial area between gas and water was determined during drainage. The values have been normalized to the total grain surface area in the packing. The naming convention in the figure legends is same as in previous section.

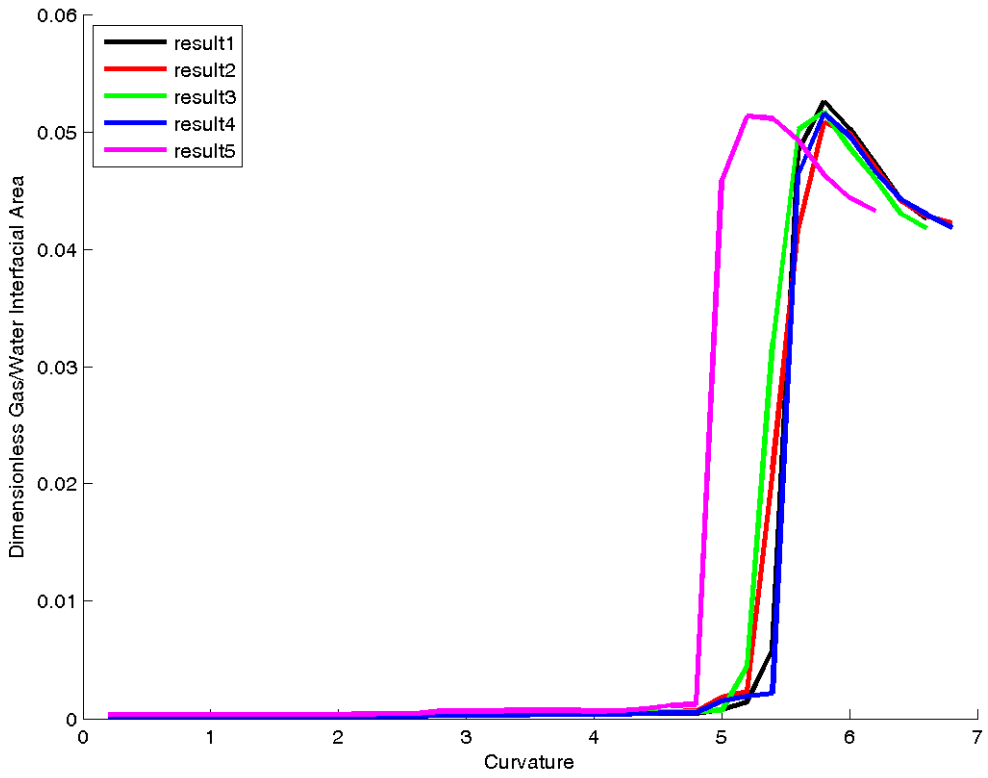

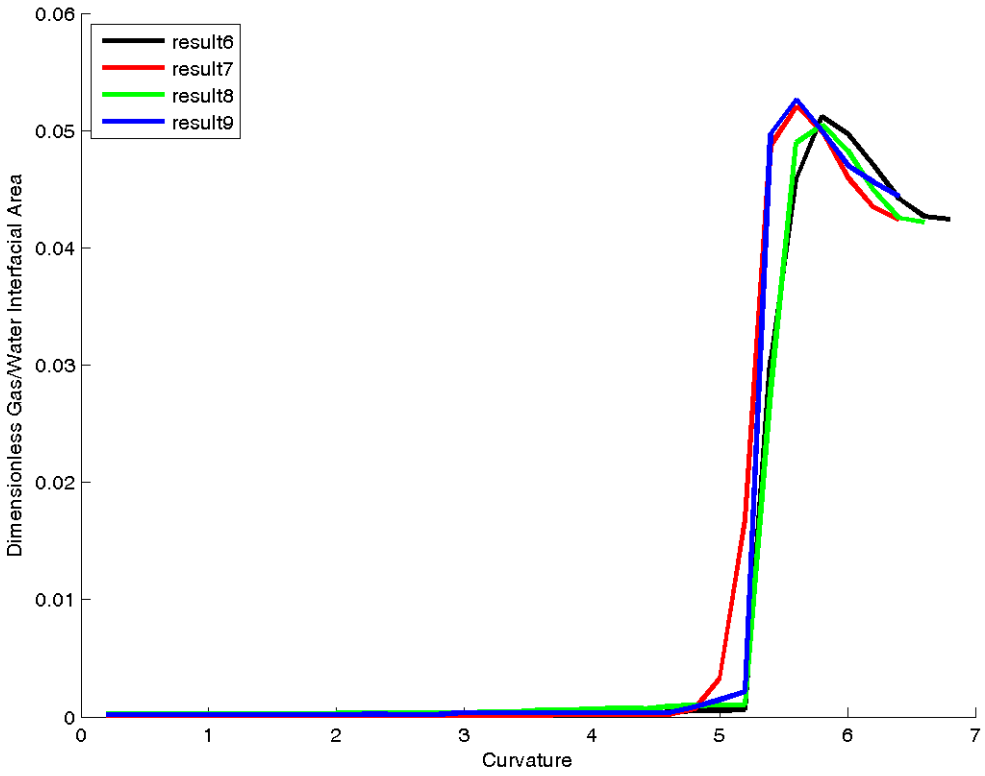
result6
result7
result8
result9
Dimensionless Gas/Water Interfacial Area
Curvature
0.06
0.05
0.04
0.03
0.02
0.01
0
0
1
2
3
4
5
6
7

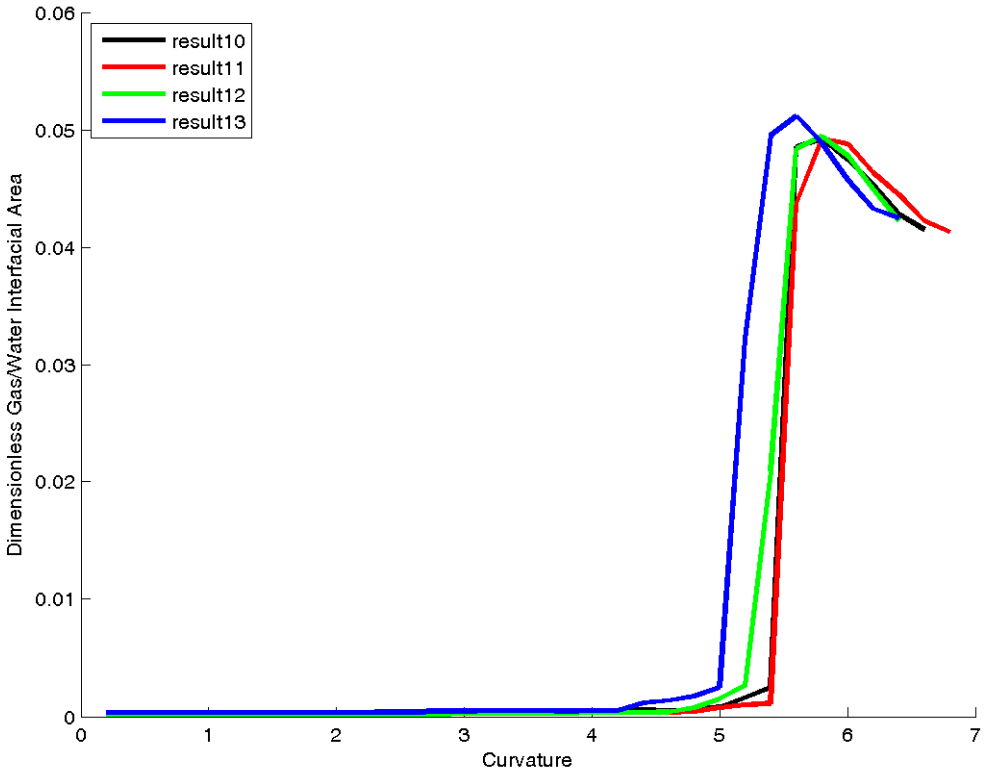
result10
result11
result12
result13
Dimensionless Gas/Water Interfacial Area
Curvature
0.06
0.05
0.04
0.03
0.02
0.01
0
0
1
2
3
4
5
6
7

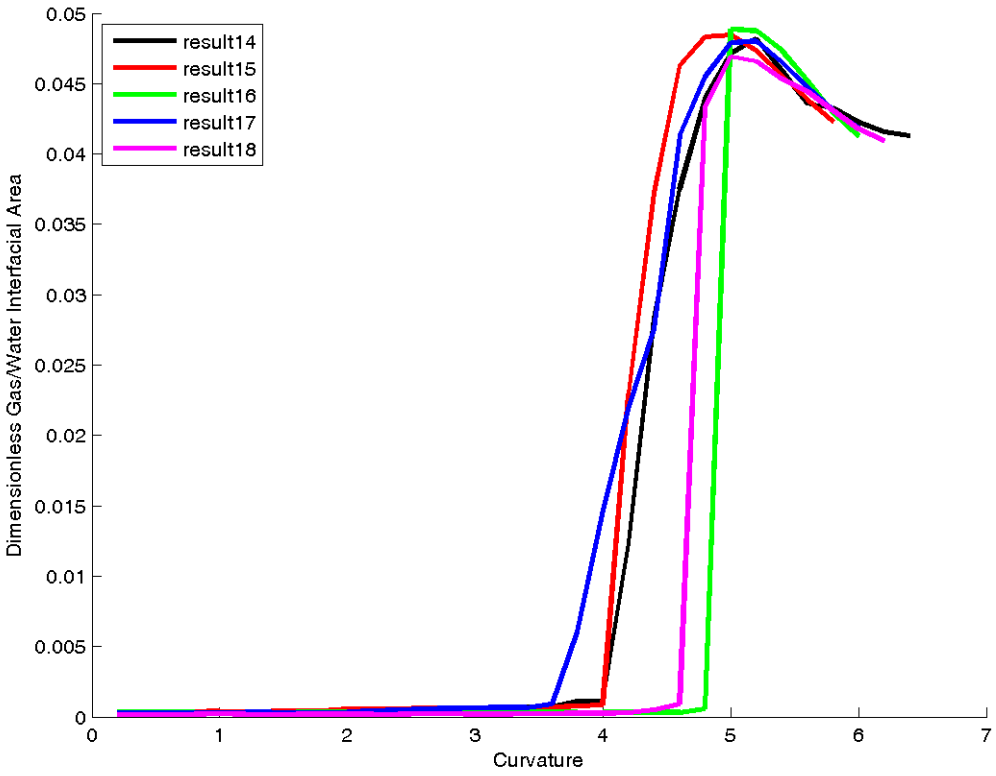
result14
result15
result16
result17
result18
Dimensionless Gas/Water Interfacial Area
Curvature
0.05
0.045
0.04
0.035
0.03
0.025
0.02
0.015
0.01
0.005
0
0
1
2
3
4
5
6
7

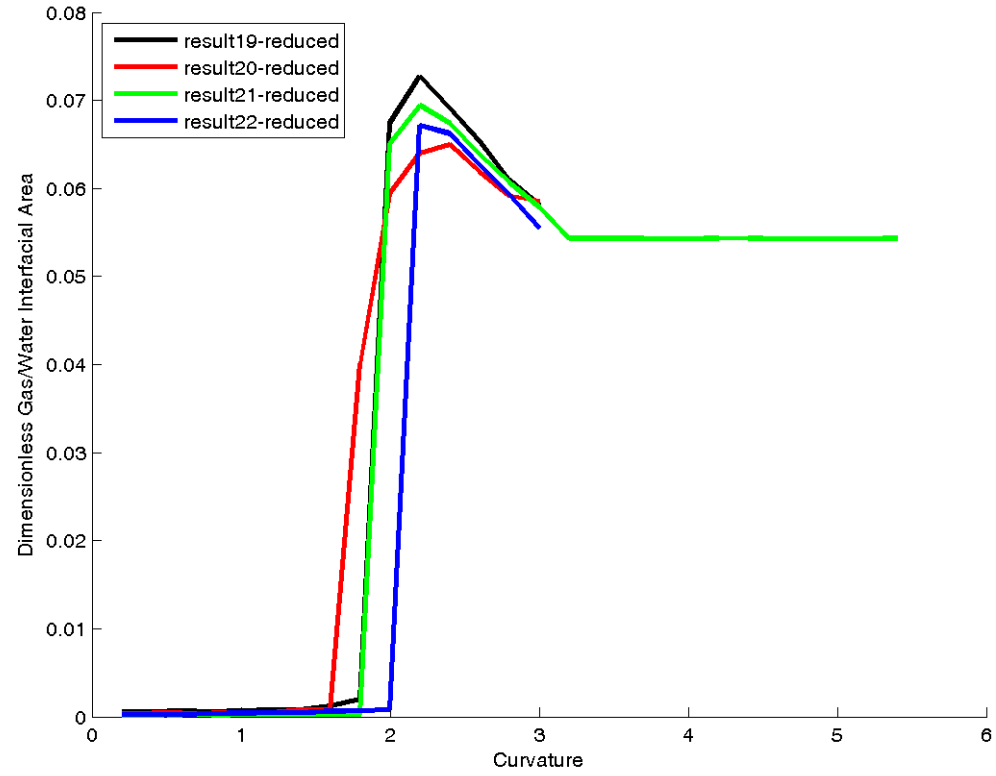
result19-reduced
result20-reduced
result21-reduced
result22-reduced
Dimensionless Gas/Water Interfacial Area
Curvature
0.08
0.07
0.06
0.05
0.04
0.03
0.02
0.01
0
0
1
2
3
4
5
6

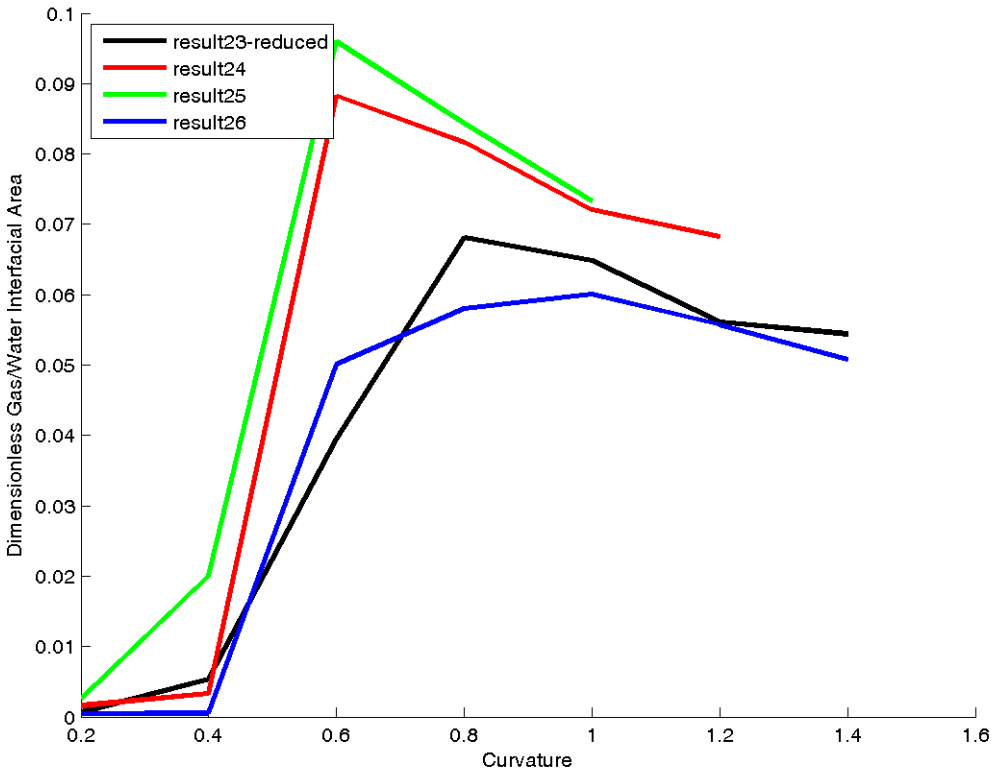
result23-reduced
result24
result25
result26
Dimensionless Gas/Water Interfacial Area
Curvature
0.1
0.09
0.08
0.07
0.06
0.05
0.04
0.03
0.02
0.01
0
0.2
0.4
0.6
0.8
1
1.2
1.4
1.6

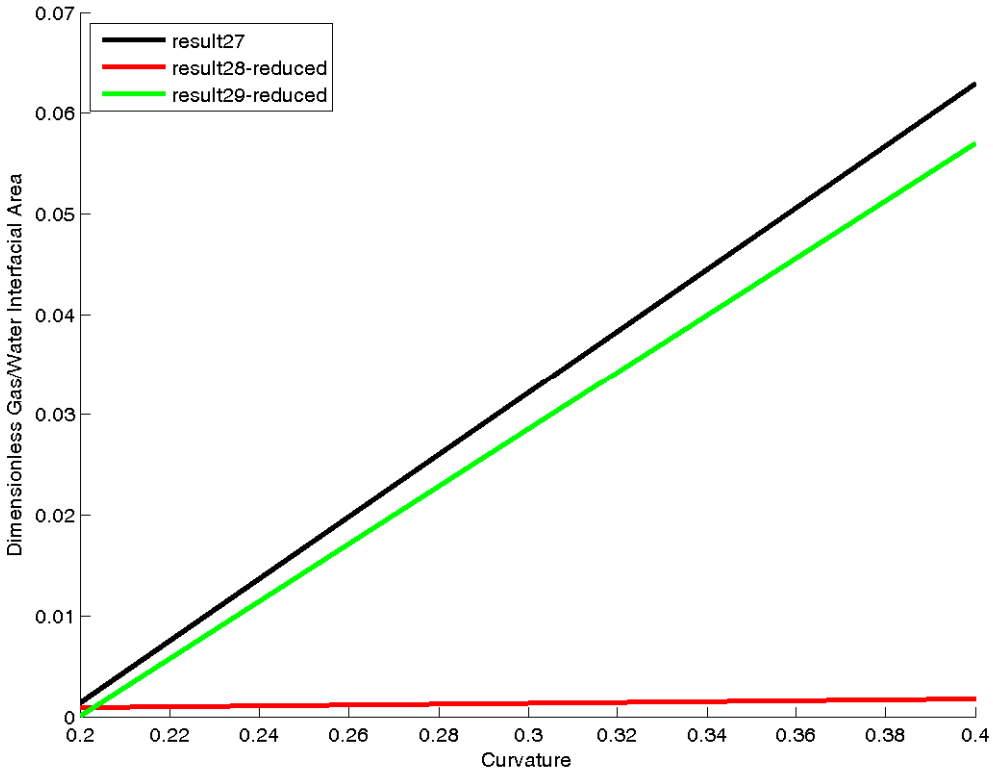
result27
result28-reduced
result29-reduced
Dimensionless Gas/Water Interfacial Area
Curvature
0.07
0.06
0.05
0.04
0.03
0.02
0.01
0
0.2
0.22
0.24
0.26
0.28
0.3
0.32
0.34
0.36
0.38
0.4

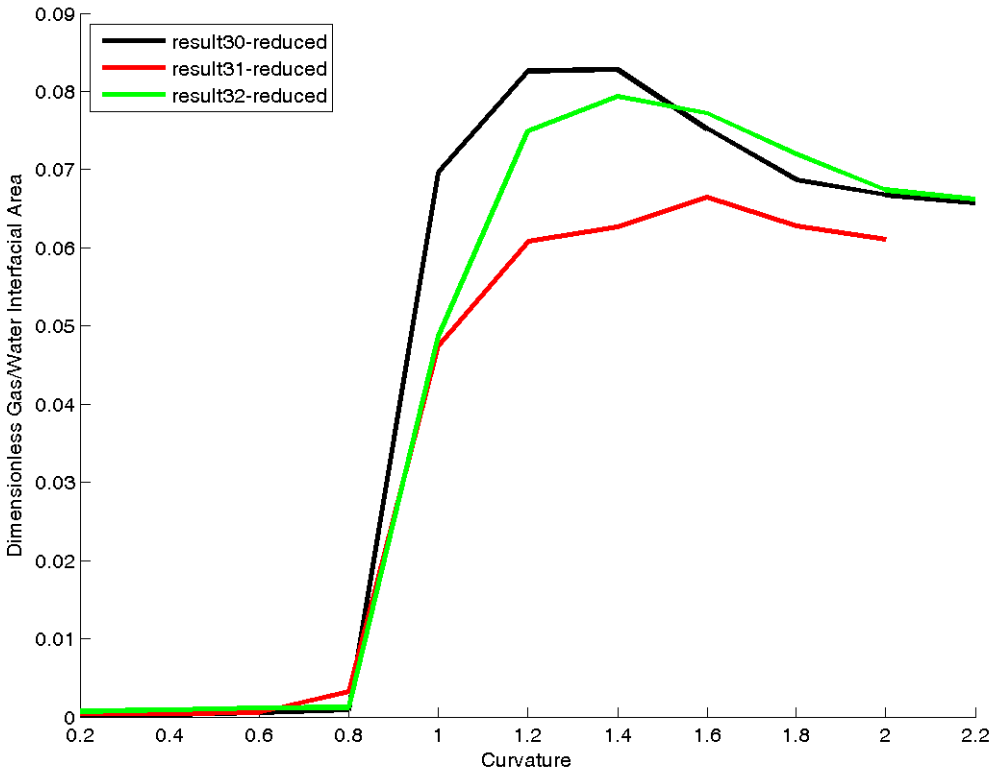
result30-reduced
result31-reduced
result32-reduced
Dimensionless Gas/Water Interfacial Area
Curvature
0.09
0.08
0.07
0.06
0.05
0.04
0.03
0.02
0.01
0
0.2
0.4
0.6
0.8
1
1.2
1.4
1.6
1.8
2
2.2

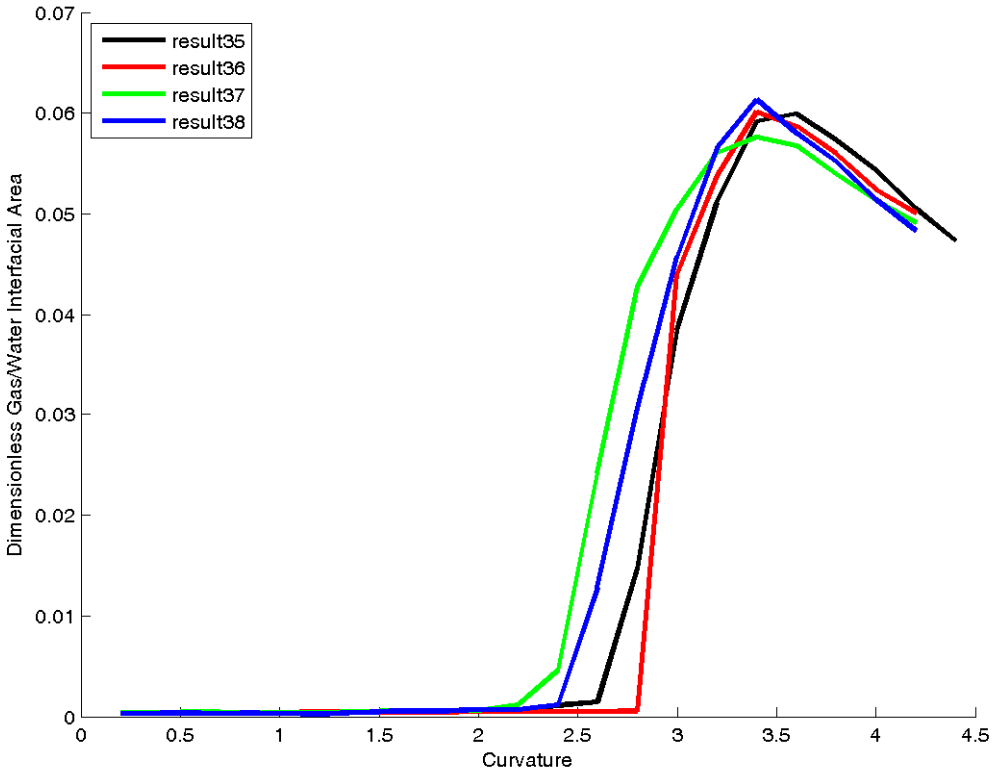
result35
result36
result37
result38
Dimensionless Gas/Water Interfacial Area
Curvature
0.07
0.06
0.05
0.04
0.03
0.02
0.01
0
0
0.5
1
1.5
2
2.5
3
3.5
4
4.5

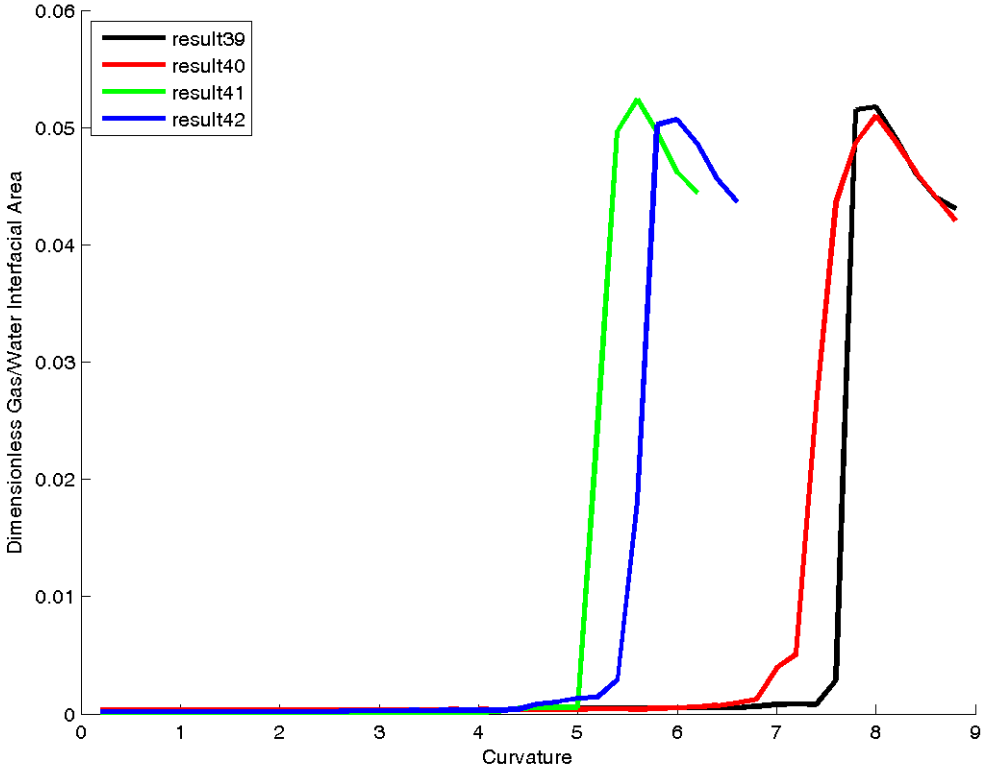
result39
result40
result41
result42
Dimensionless Gas/Water Interfacial Area
Curvature
0.06
0.05
0.04
0.03
0.02
0.01
0
0
1
2
3
4
5
6
7
8
9

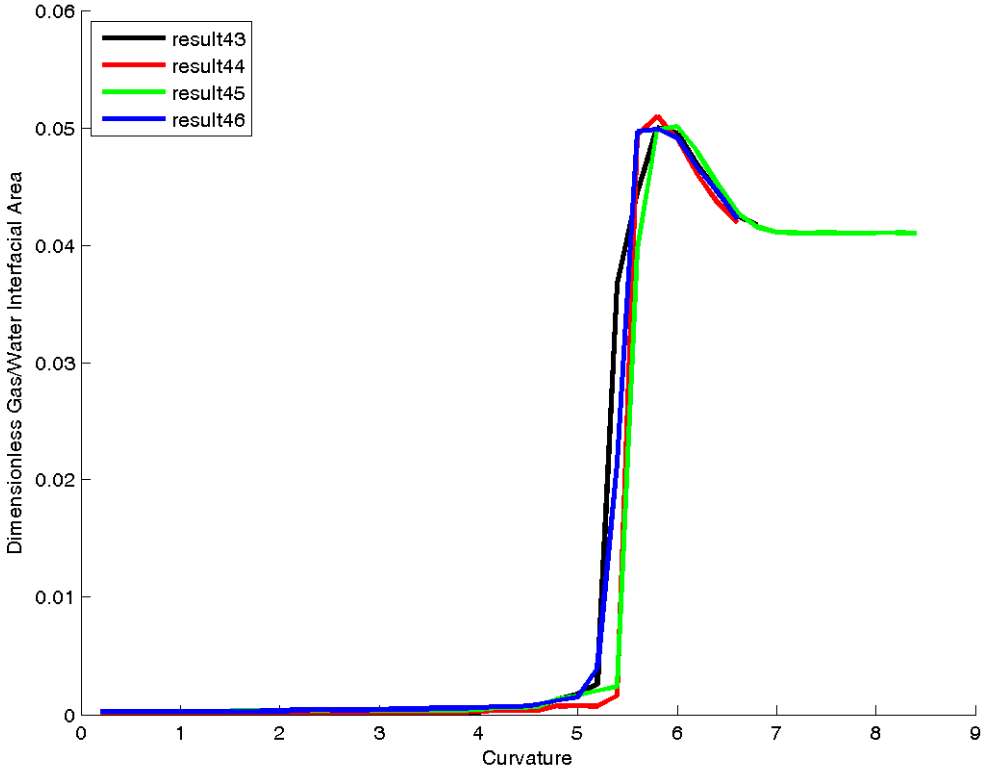
result43
result44
result45
result46
Dimensionless Gas/Water Interfacial Area
Curvature
0.06
0.05
0.04
0.03
0.02
0.01
0
0
1
2
3
4
5
6
7
8
9

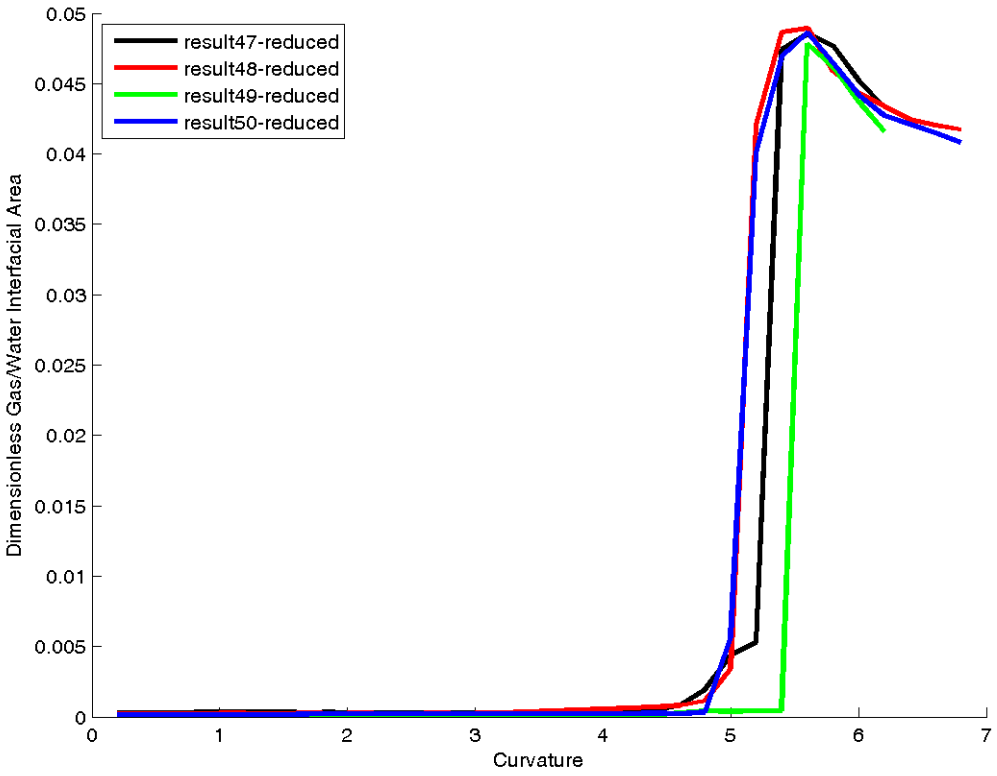
result47-reduced
result48-reduced
result49-reduced
result50-reduced
Dimensionless Gas/Water Interfacial Area
Curvature
0.05
0.045
0.04
0.035
0.03
0.025
0.02
0.015
0.01
0.005
0
0
1
2
3
4
5
6
7

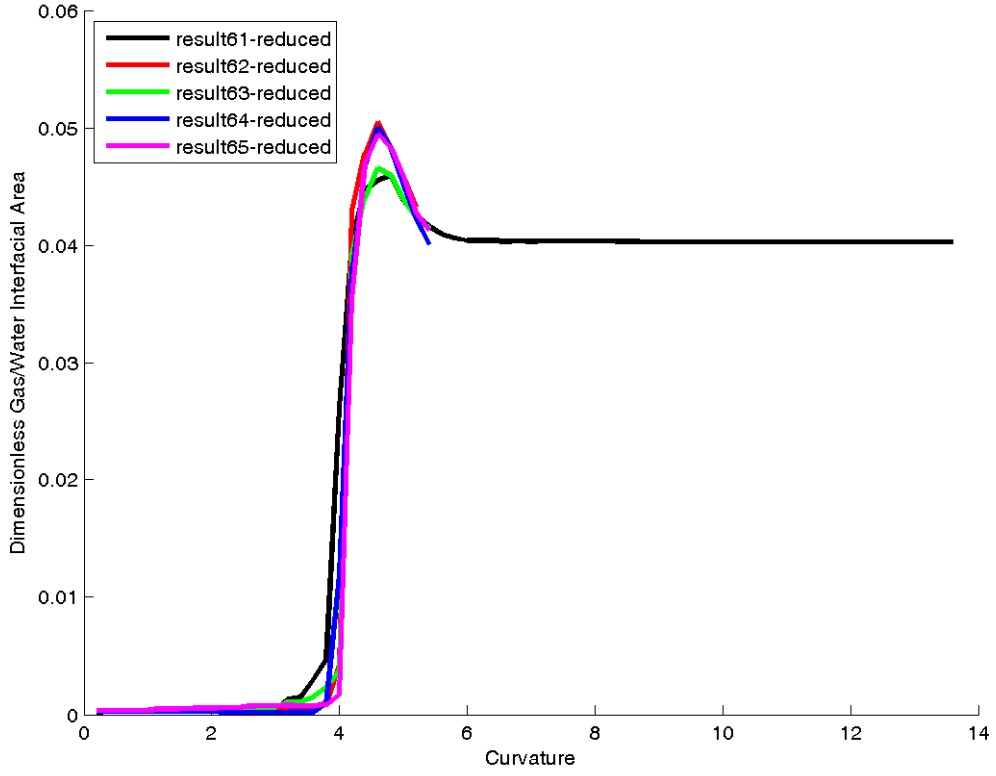
result61-reduced
result62-reduced
result63-reduced
result64-reduced
result65-reduced
Dimensionless Gas/Water Interfacial Area
Curvature
0.06
0.05
0.04
0.03
0.02
0.01
0
0
2
4
6
8
10
12
14

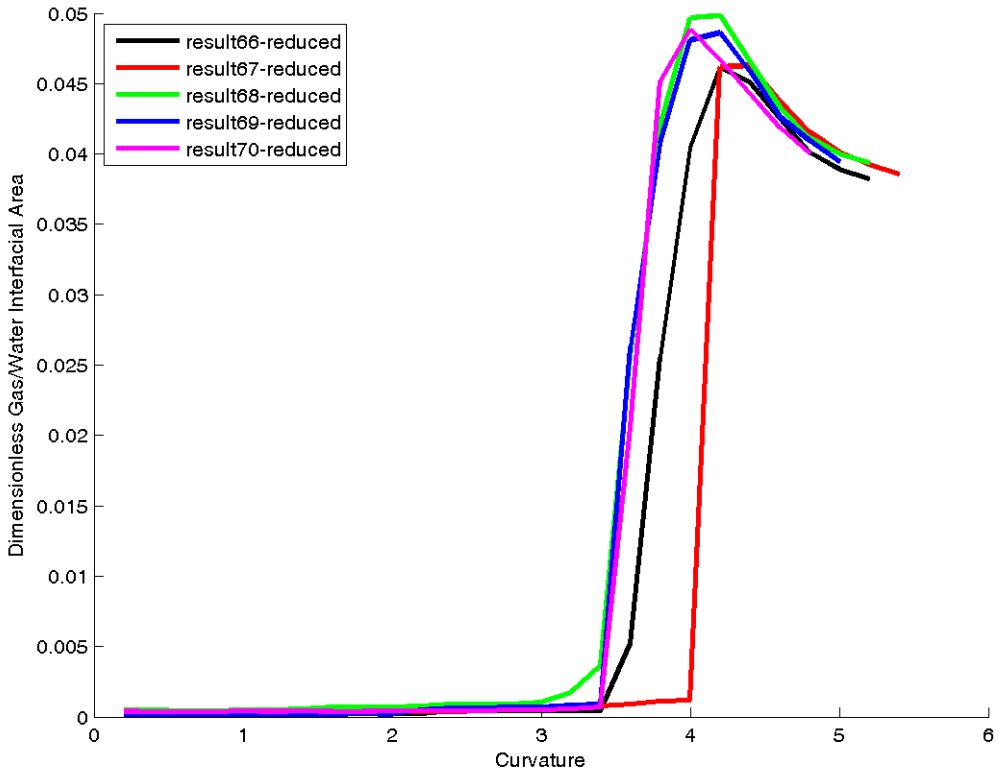
result66-reduced
result67-reduced
result68-reduced
result69-reduced
result70-reduced
Dimensionless Gas/Water Interfacial Area
Curvature
0
0.005
0.01
0.015
0.02
0.025
0.03
0.035
0.04
0.045
0.05
0
1
2
3
4
5
6

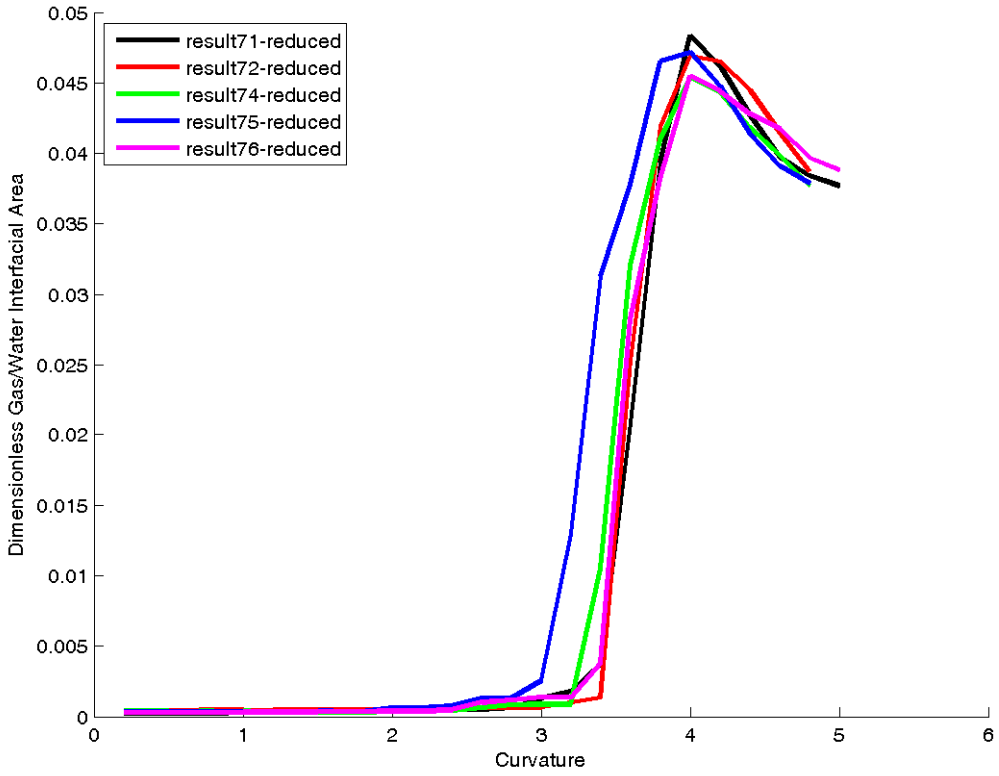
result71-reduced
result72-reduced
result74-reduced
result75-reduced
result76-reduced
Dimensionless Gas/Water Interfacial Area
Curvature
0
0.005
0.01
0.015
0.02
0.025
0.03
0.035
0.04
0.045
0.05
0
1
2
3
4
5
6

Appendix C: Imbibition in All Model Sediments

Imbibition curves based on the criterion for critical curvature in a pore reported previously are shown in the following graphs. The curves are labeled as "resultXX" where XX indicates the number of the model sediment in the table in Appendix A.

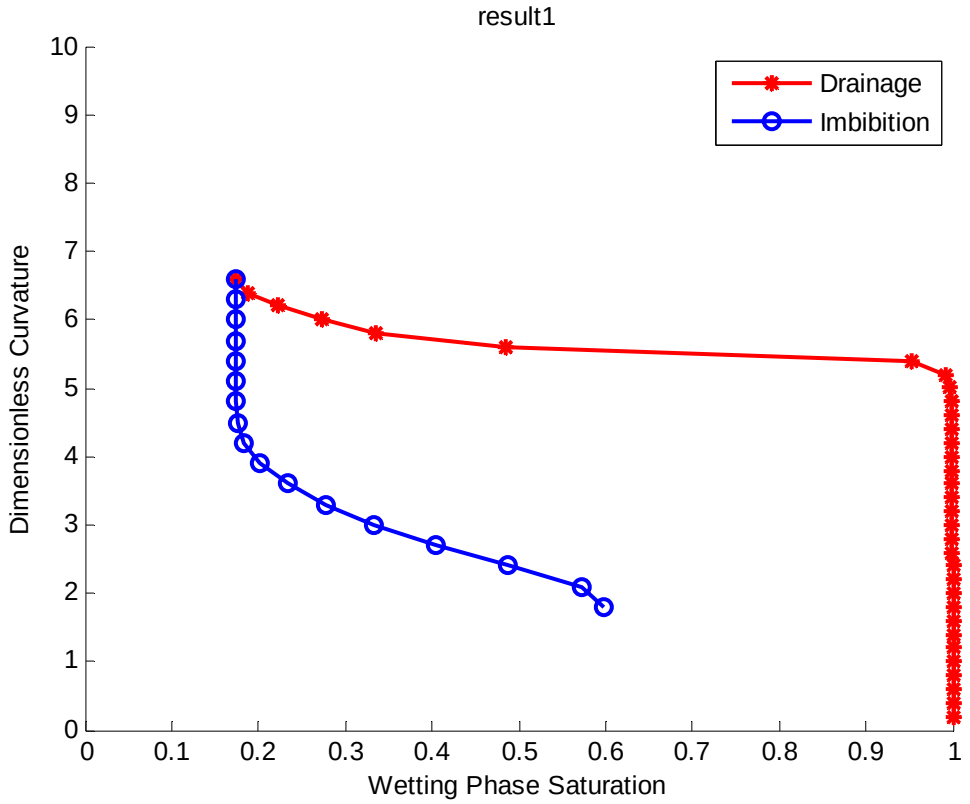

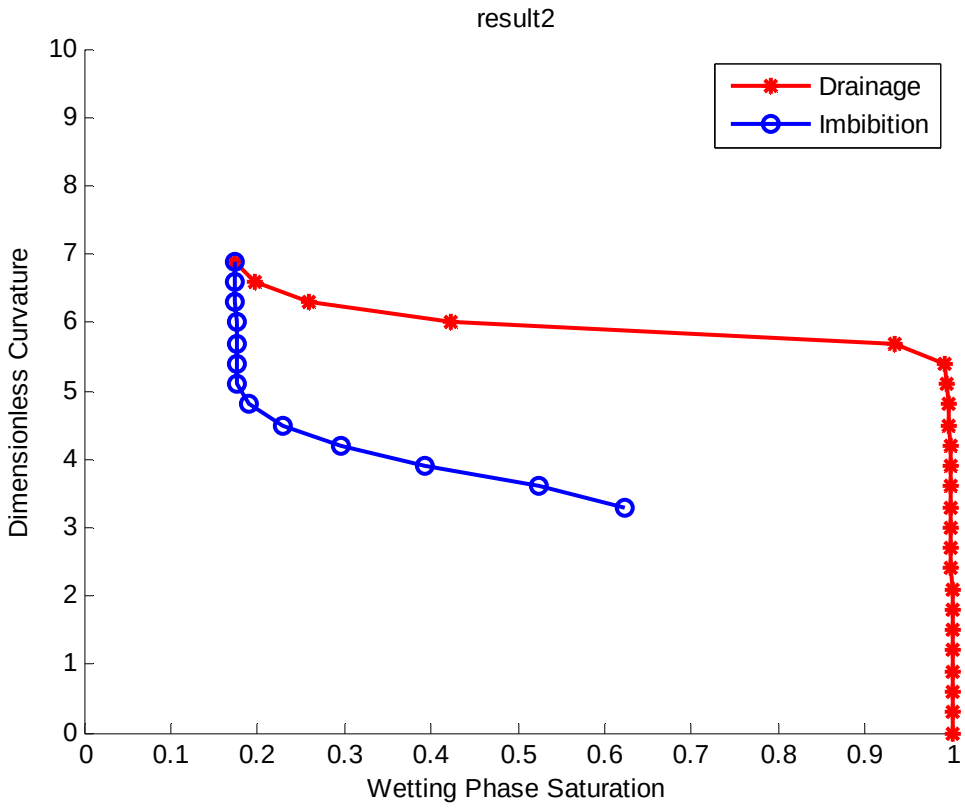
result2
Drainage
Imbibition
Dimensionless Curvature
Wetting Phase Saturation
0
1
2
3
4
5
6
7
8
9
10
0
0.1
0.2
0.3
0.4
0.5
0.6
0.7
0.8
0.9
1

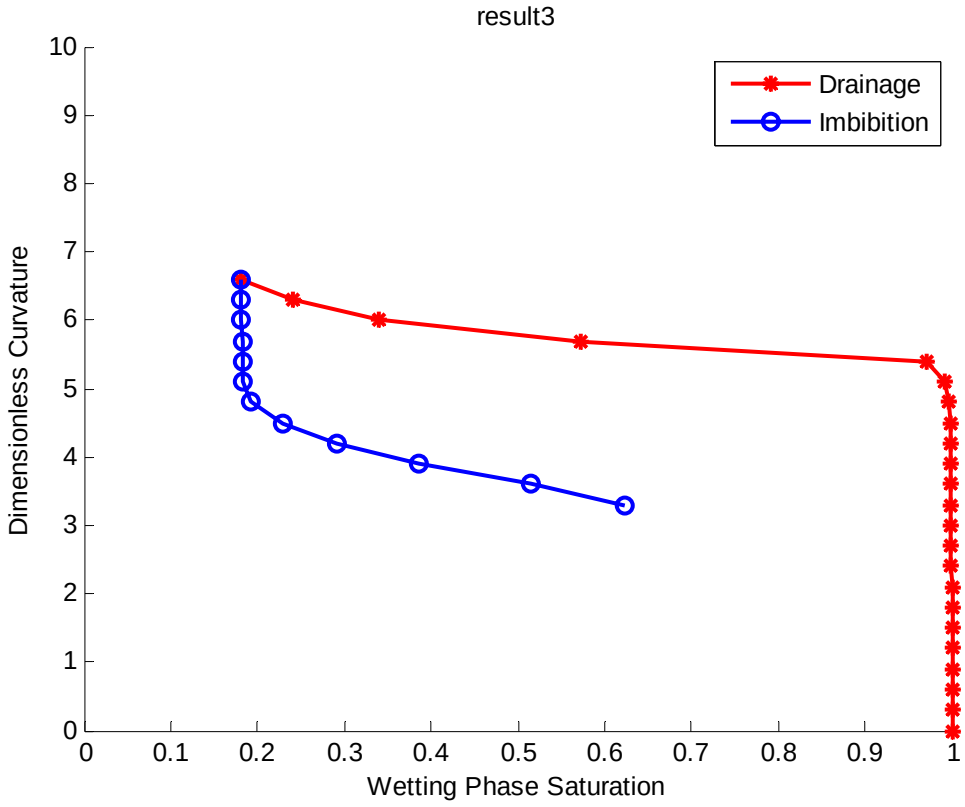
result3
Drainage
Imbibition
Dimensionless Curvature
Wetting Phase Saturation
0
1
2
3
4
5
6
7
8
9
10
0
0.1
0.2
0.3
0.4
0.5
0.6
0.7
0.8
0.9
1

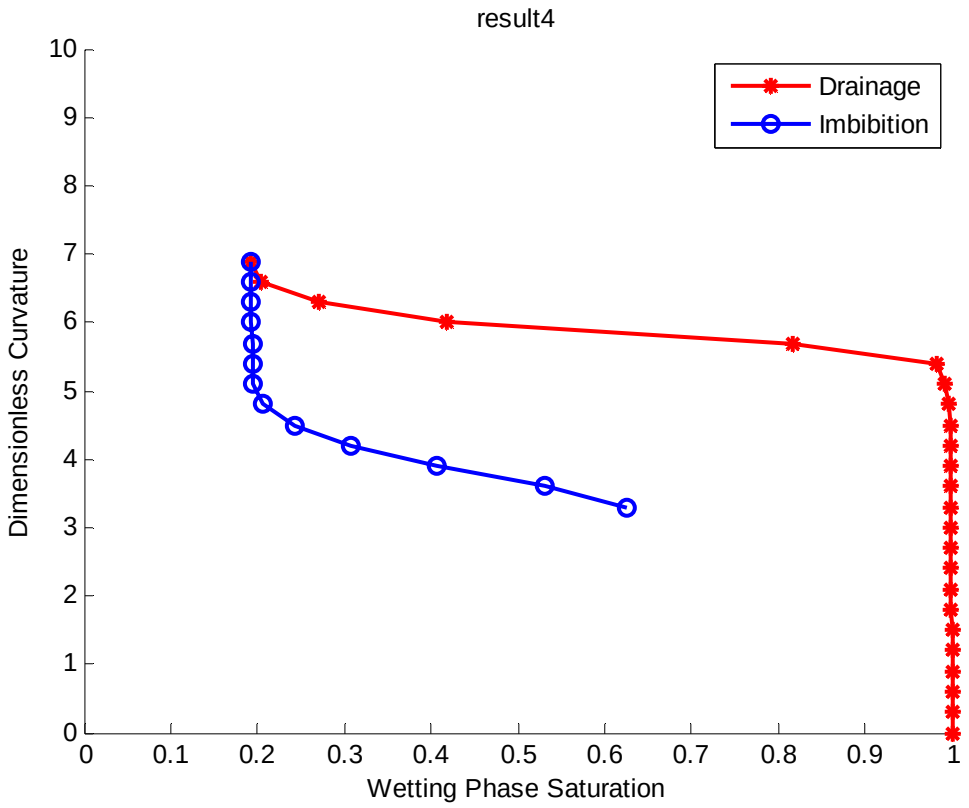
result4
Drainage
Imbibition
Dimensionless Curvature
Wetting Phase Saturation
0
1
2
3
4
5
6
7
8
9
10
0
0.1
0.2
0.3
0.4
0.5
0.6
0.7
0.8
0.9
1

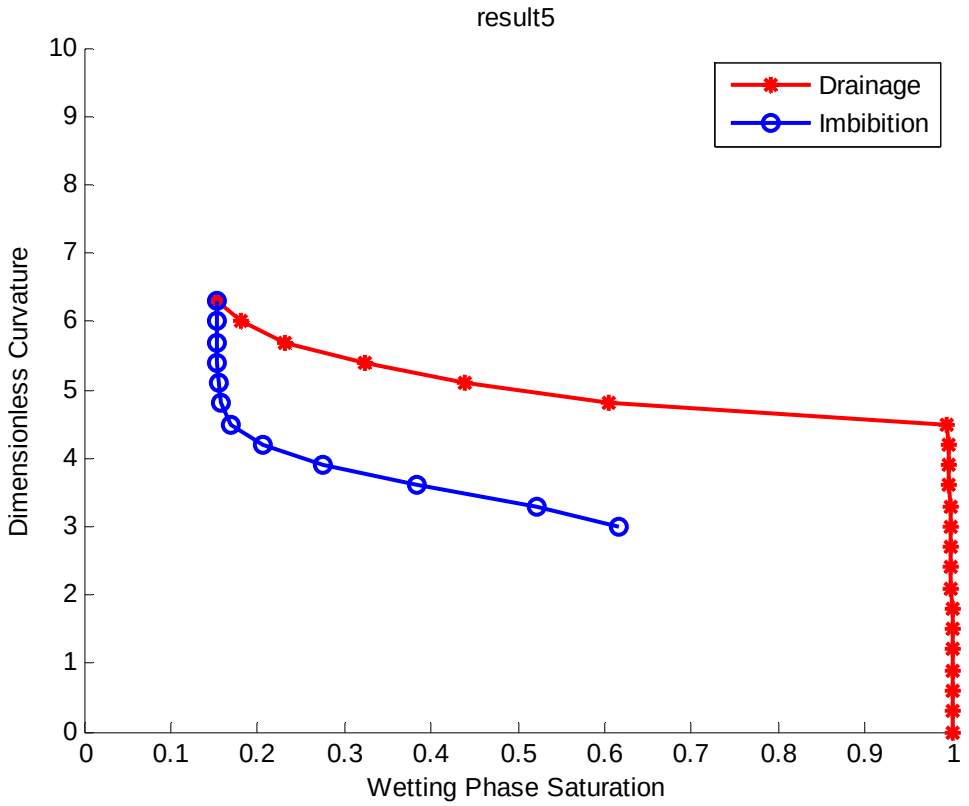
result5
Drainage
Imbibition
Dimensionless Curvature
Wetting Phase Saturation
0
1
2
3
4
5
6
7
8
9
10
0
0.1
0.2
0.3
0.4
0.5
0.6
0.7
0.8
0.9
1

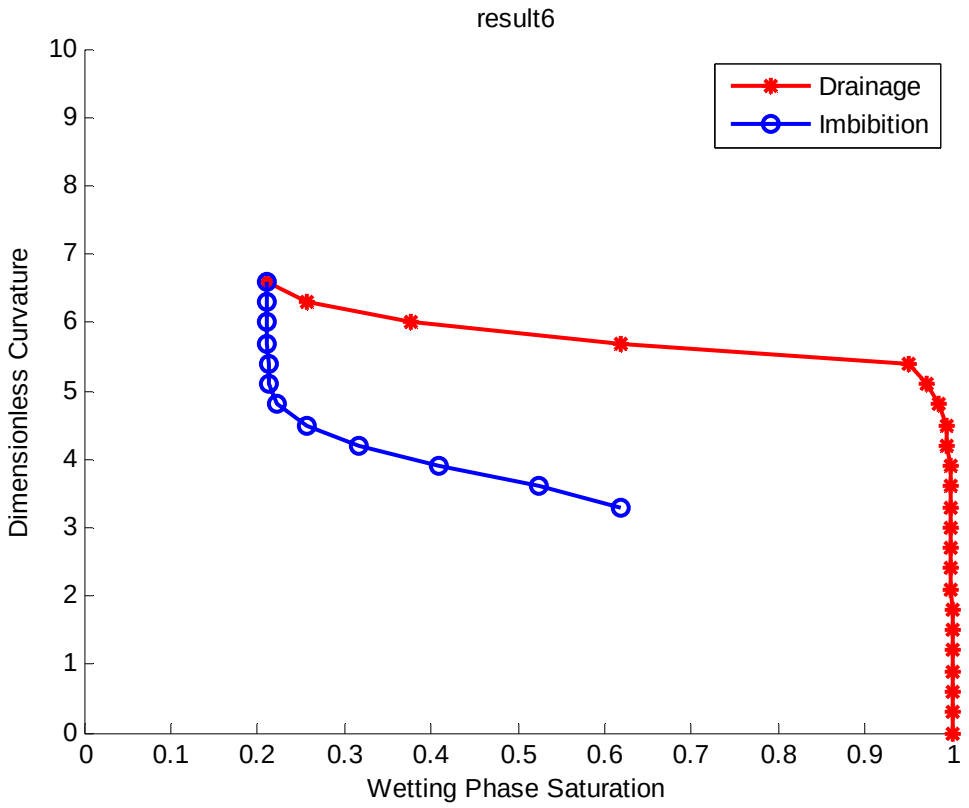
result6
Drainage
Imbibition
Dimensionless Curvature
Wetting Phase Saturation
0
1
2
3
4
5
6
7
8
9
10
0
0.1
0.2
0.3
0.4
0.5
0.6
0.7
0.8
0.9
1

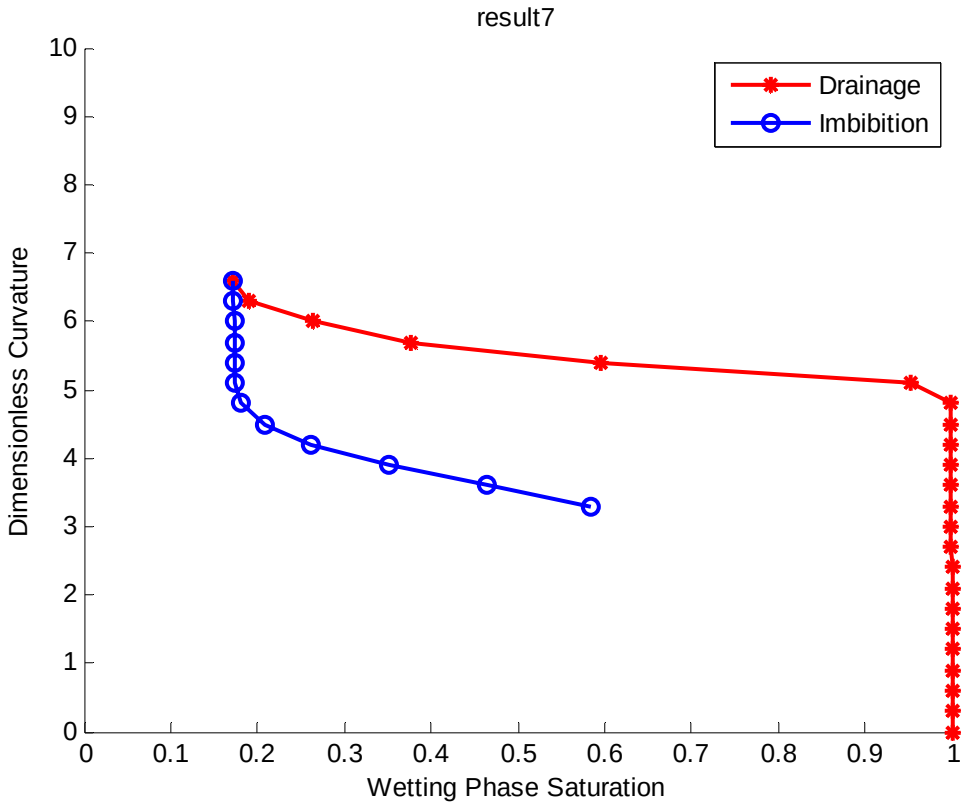
result7
Drainage
Imbibition
Dimensionless Curvature
Wetting Phase Saturation
0
1
2
3
4
5
6
7
8
9
10
0
0.1
0.2
0.3
0.4
0.5
0.6
0.7
0.8
0.9
1

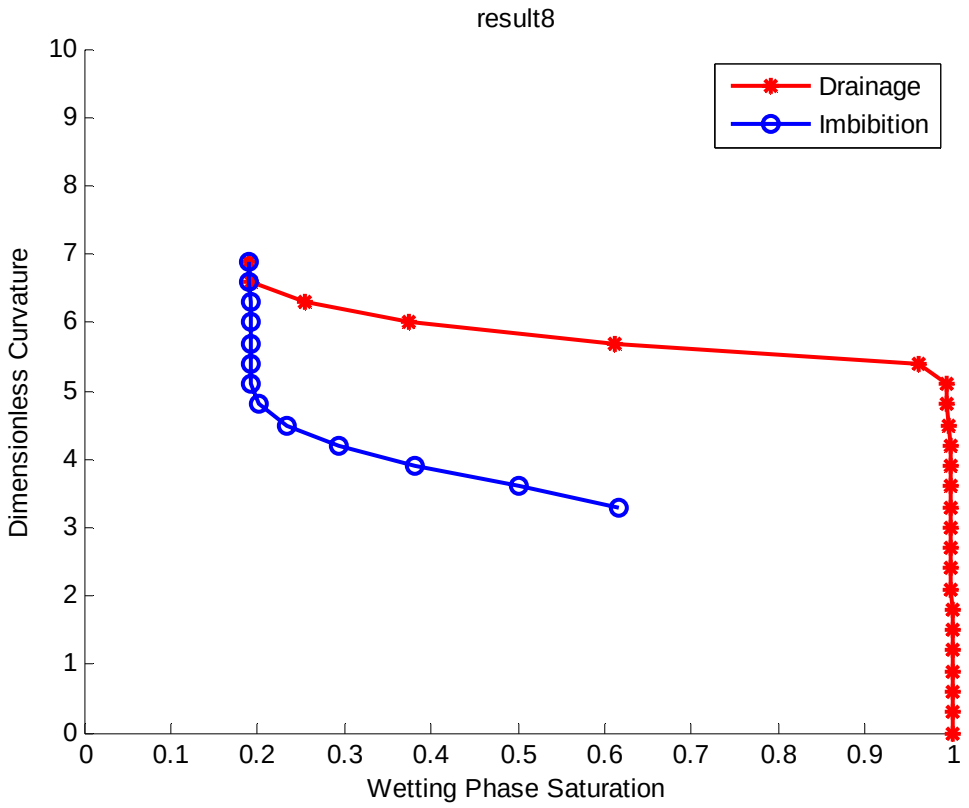
result8
Drainage
Imbibition
Dimensionless Curvature
Wetting Phase Saturation
0
1
2
3
4
5
6
7
8
9
10
0
0.1
0.2
0.3
0.4
0.5
0.6
0.7
0.8
0.9
1

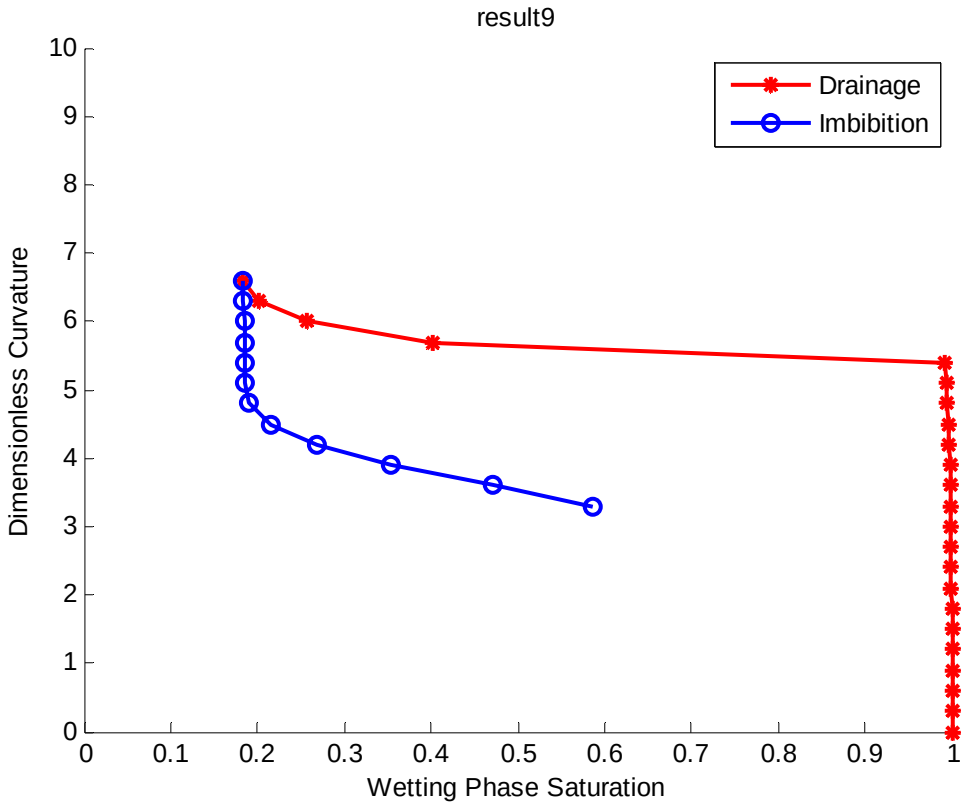
result9
Drainage
Imbibition
Dimensionless Curvature
Wetting Phase Saturation
0
1
2
3
4
5
6
7
8
9
10
0
0.1
0.2
0.3
0.4
0.5
0.6
0.7
0.8
0.9
1

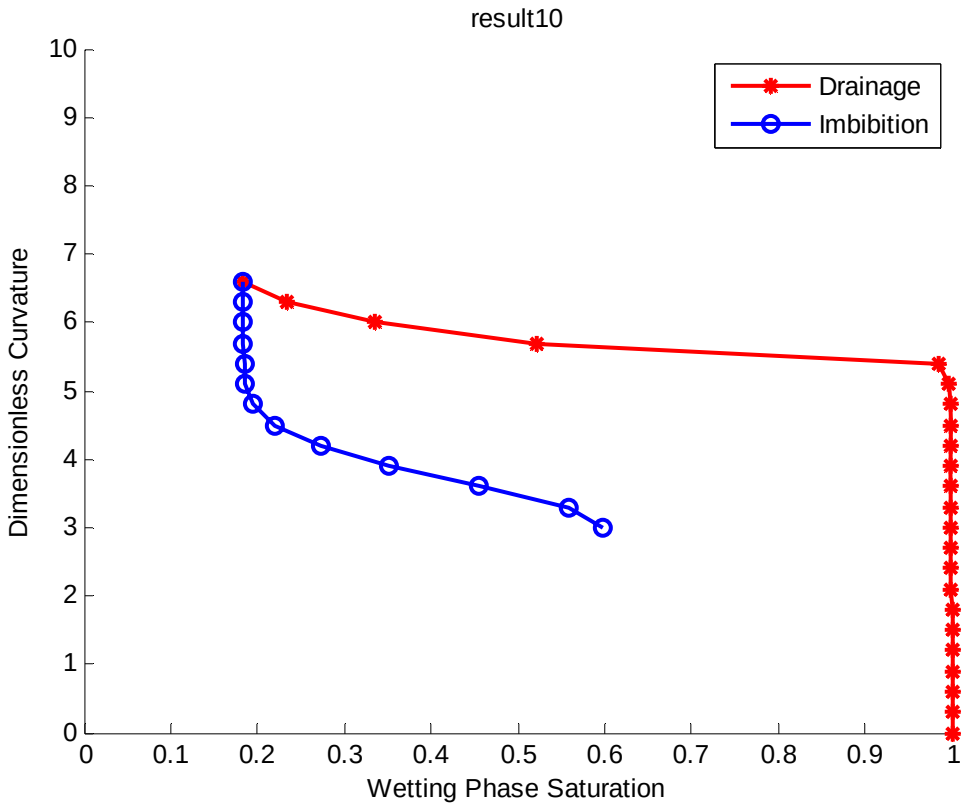
result10
Drainage
Imbibition
Dimensionless Curvature
Wetting Phase Saturation
0
1
2
3
4
5
6
7
8
9
10
0
0.1
0.2
0.3
0.4
0.5
0.6
0.7
0.8
0.9
1

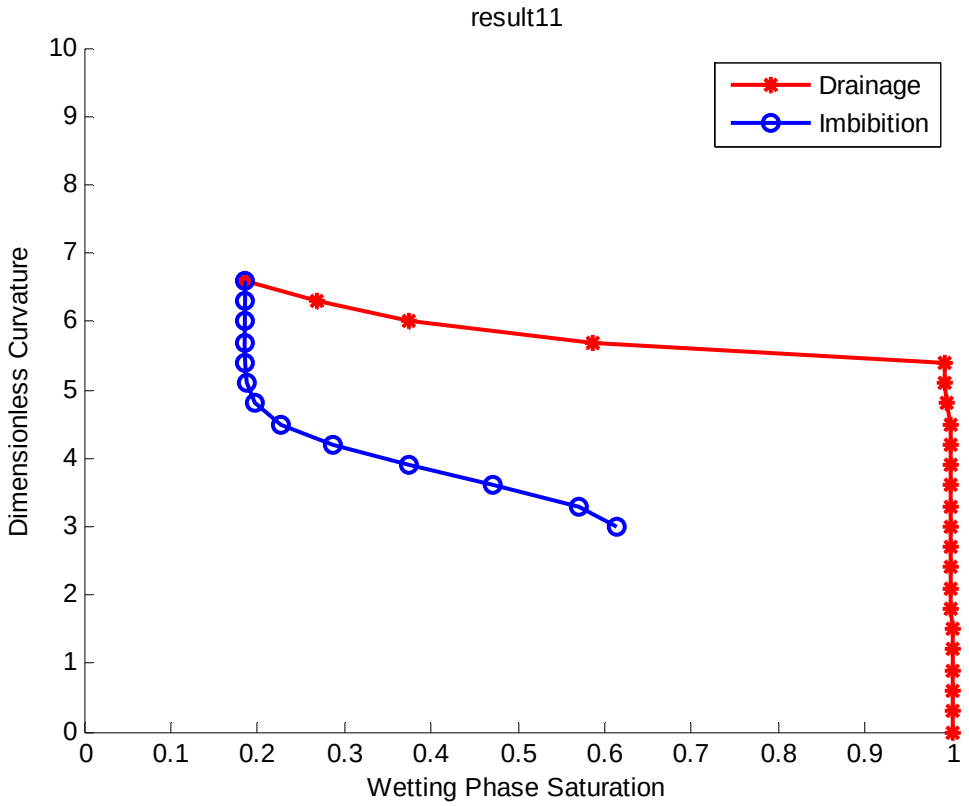
result11
Drainage
Imbibition
Dimensionless Curvature
Wetting Phase Saturation
0
1
2
3
4
5
6
7
8
9
10
0
0.1
0.2
0.3
0.4
0.5
0.6
0.7
0.8
0.9
1

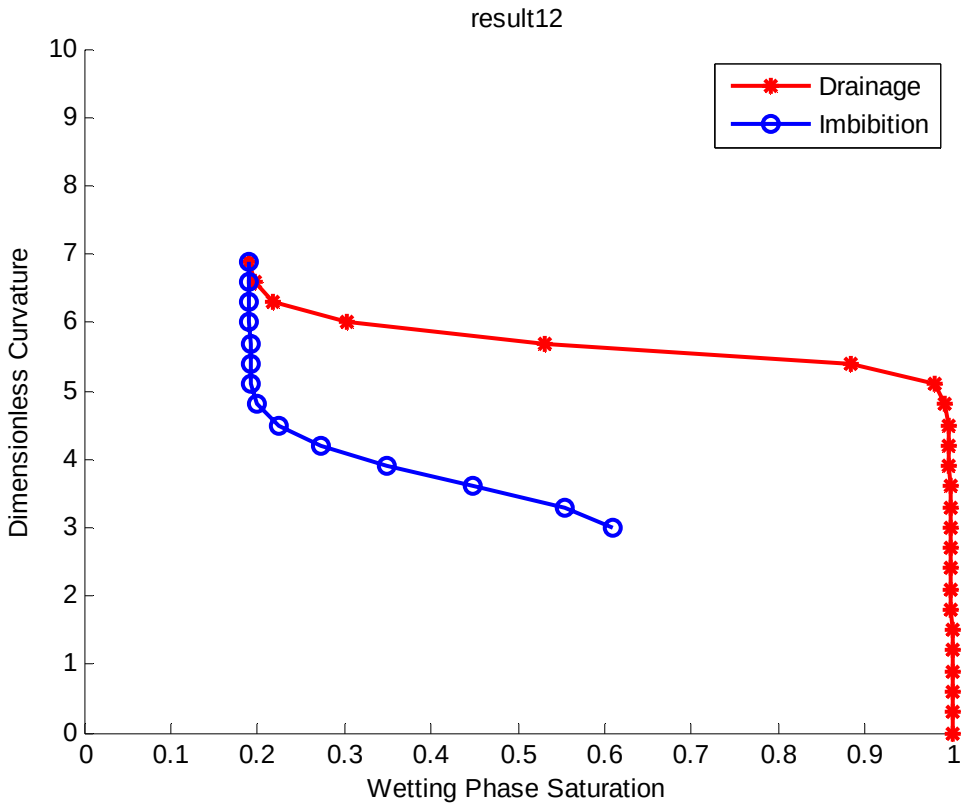
result12
Drainage
Imbibition
Dimensionless Curvature
Wetting Phase Saturation
0
1
2
3
4
5
6
7
8
9
10
0
0.1
0.2
0.3
0.4
0.5
0.6
0.7
0.8
0.9
1

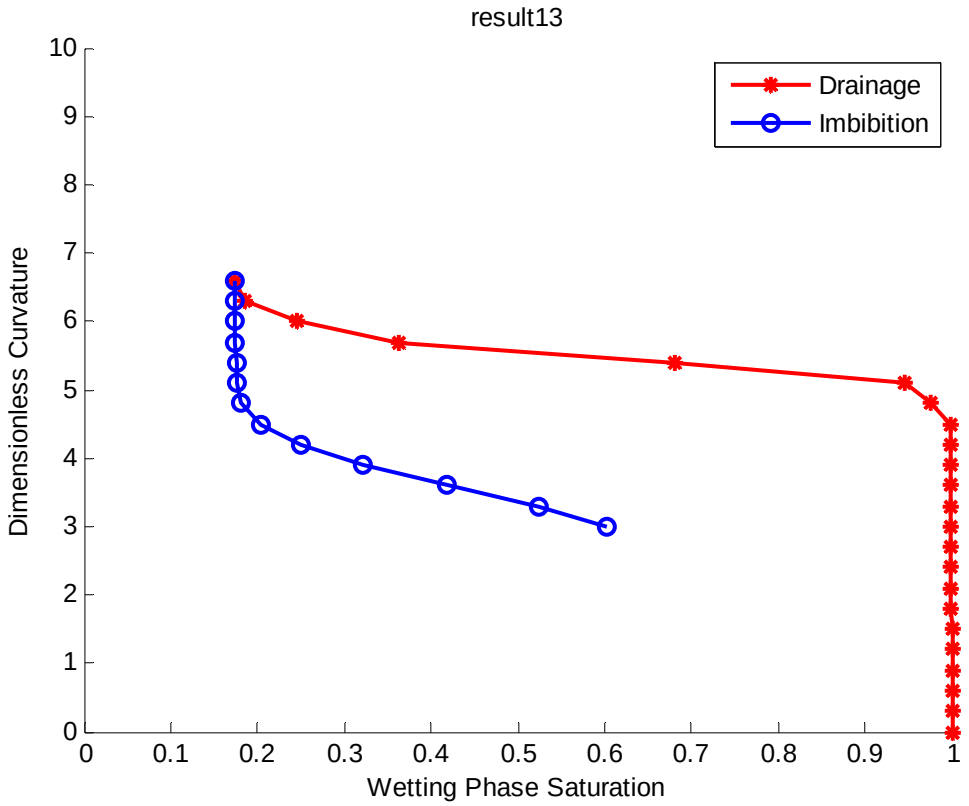
result13
Drainage
Imbibition
Dimensionless Curvature
Wetting Phase Saturation
0
1
2
3
4
5
6
7
8
9
10
0
0.1
0.2
0.3
0.4
0.5
0.6
0.7
0.8
0.9
1

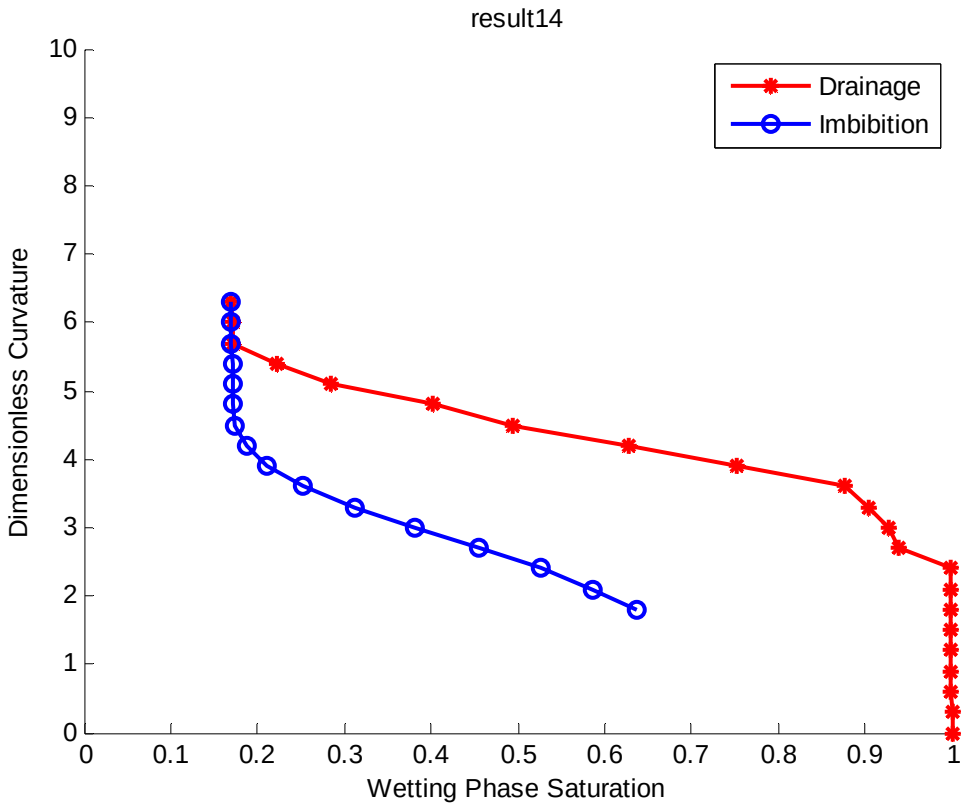
result14
Drainage
Imbibition
Dimensionless Curvature
Wetting Phase Saturation
0
1
2
3
4
5
6
7
8
9
10
0
0.1
0.2
0.3
0.4
0.5
0.6
0.7
0.8
0.9
1

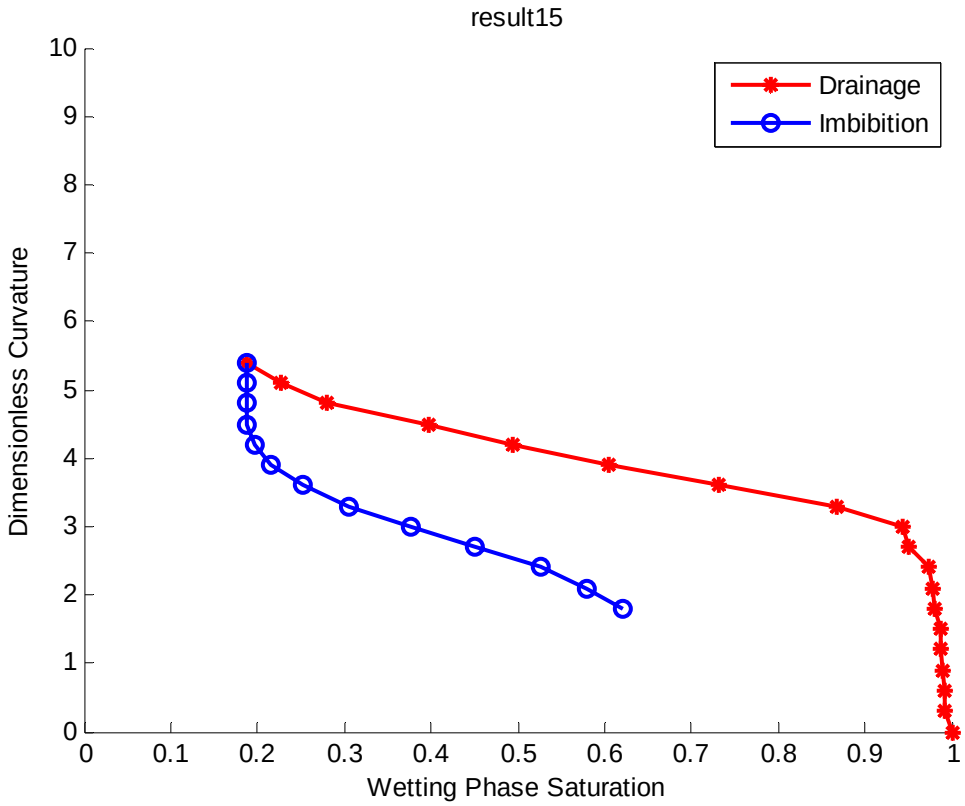
result15
Drainage
Imbibition
Dimensionless Curvature
Wetting Phase Saturation
0
1
2
3
4
5
6
7
8
9
10
0
0.1
0.2
0.3
0.4
0.5
0.6
0.7
0.8
0.9
1

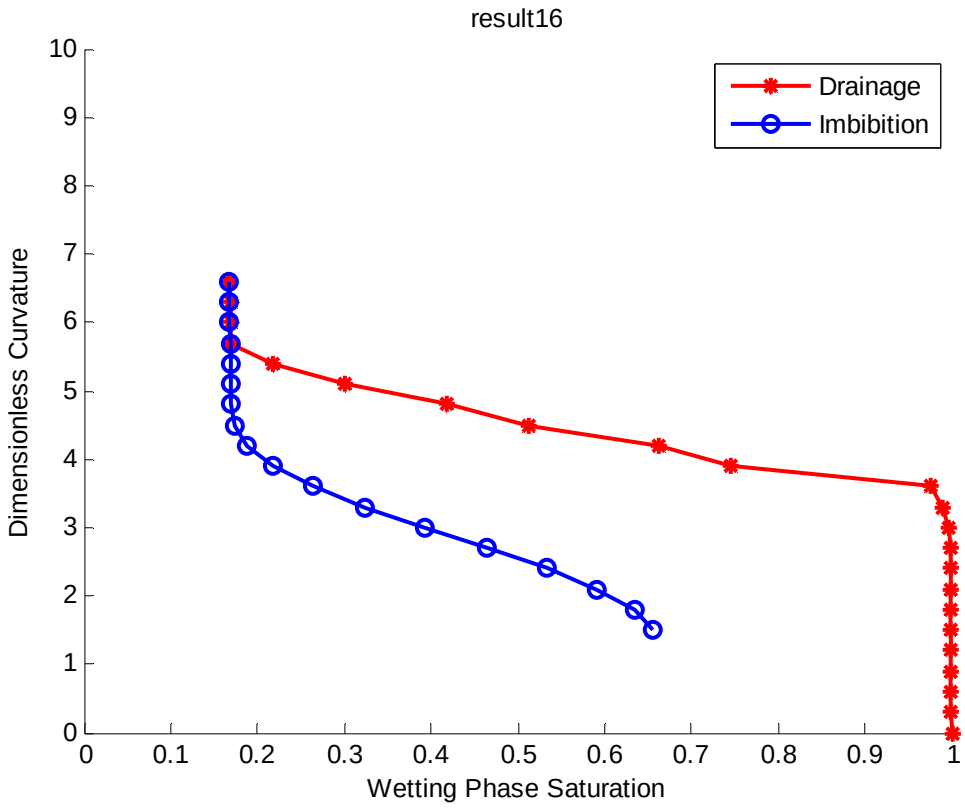
result16
Drainage
Imbibition
Dimensionless Curvature
Wetting Phase Saturation
0
1
2
3
4
5
6
7
8
9
10
0
0.1
0.2
0.3
0.4
0.5
0.6
0.7
0.8
0.9
1

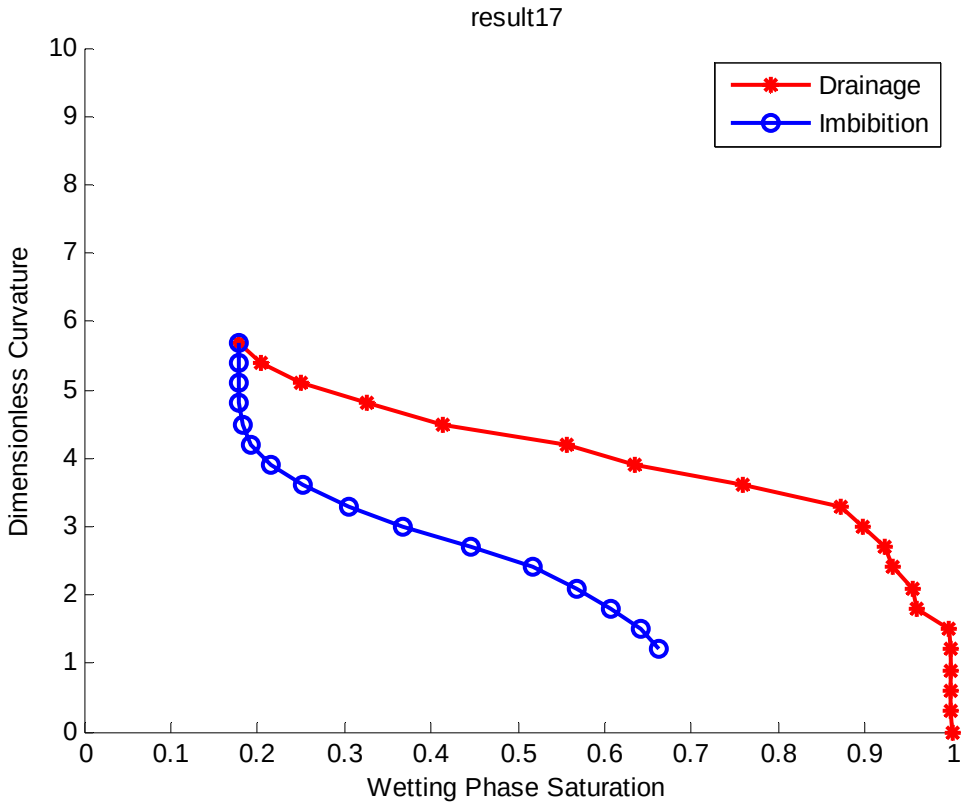
result17
Drainage
Imbibition
Dimensionless Curvature
Wetting Phase Saturation
0
1
2
3
4
5
6
7
8
9
10
0
0.1
0.2
0.3
0.4
0.5
0.6
0.7
0.8
0.9
1

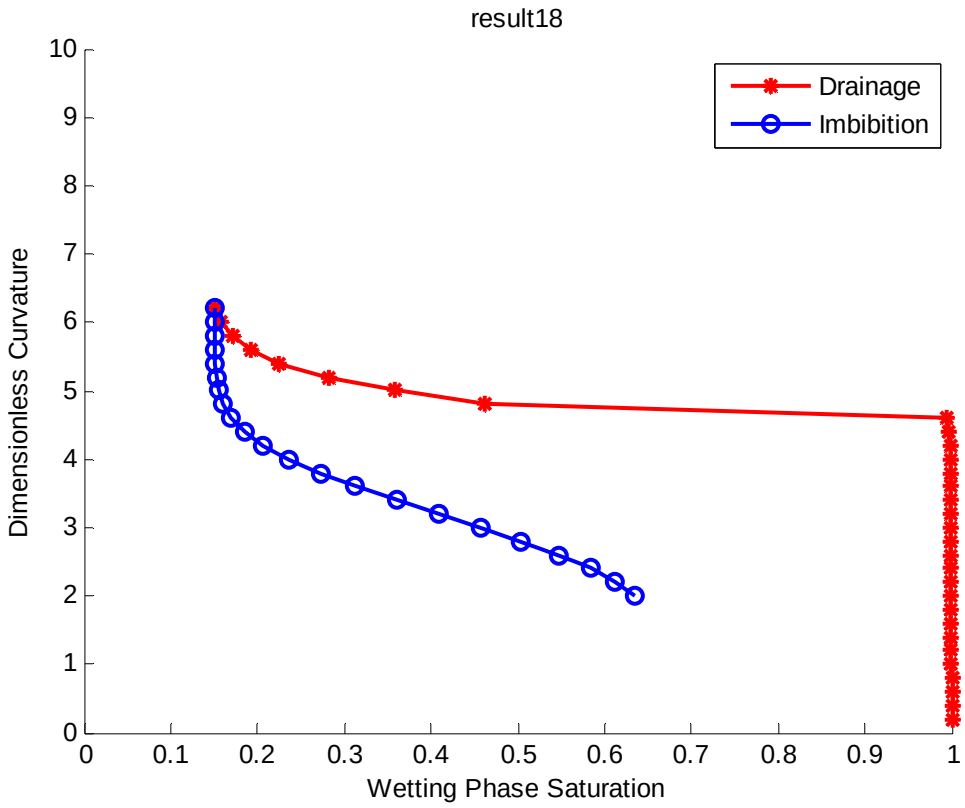
result18
Drainage
Imbibition
Dimensionless Curvature
Wetting Phase Saturation
0
1
2
3
4
5
6
7
8
9
10
0
0.1
0.2
0.3
0.4
0.5
0.6
0.7
0.8
0.9
1

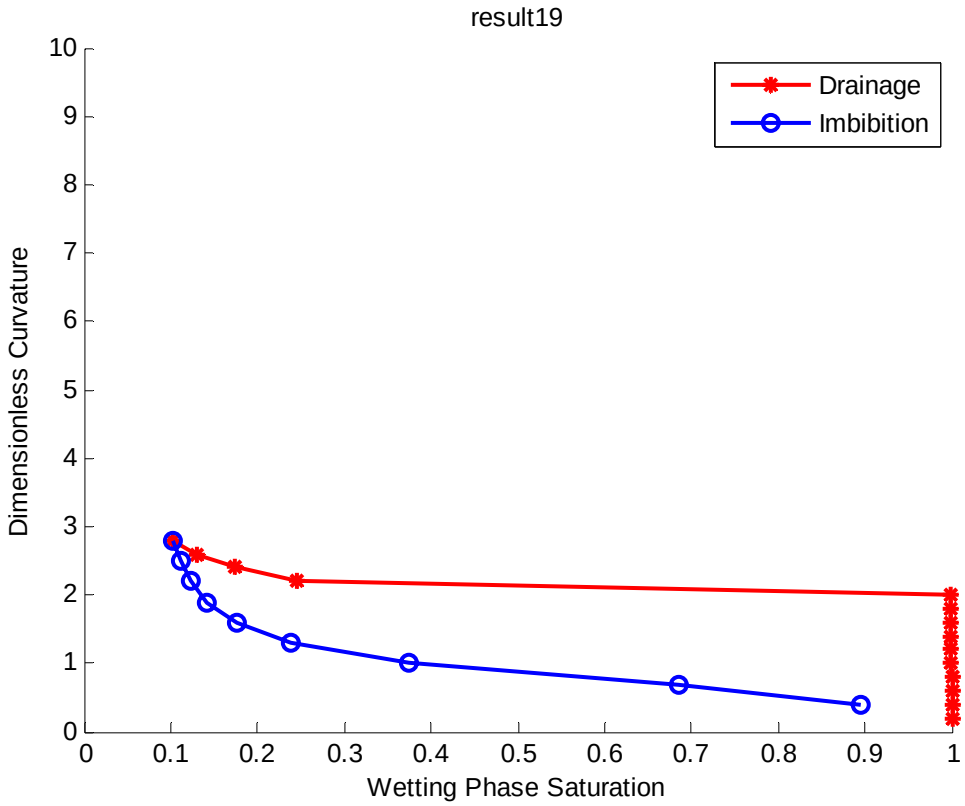
result19
Drainage
Imbibition
Dimensionless Curvature
Wetting Phase Saturation
0
1
2
3
4
5
6
7
8
9
10
0
0.1
0.2
0.3
0.4
0.5
0.6
0.7
0.8
0.9
1

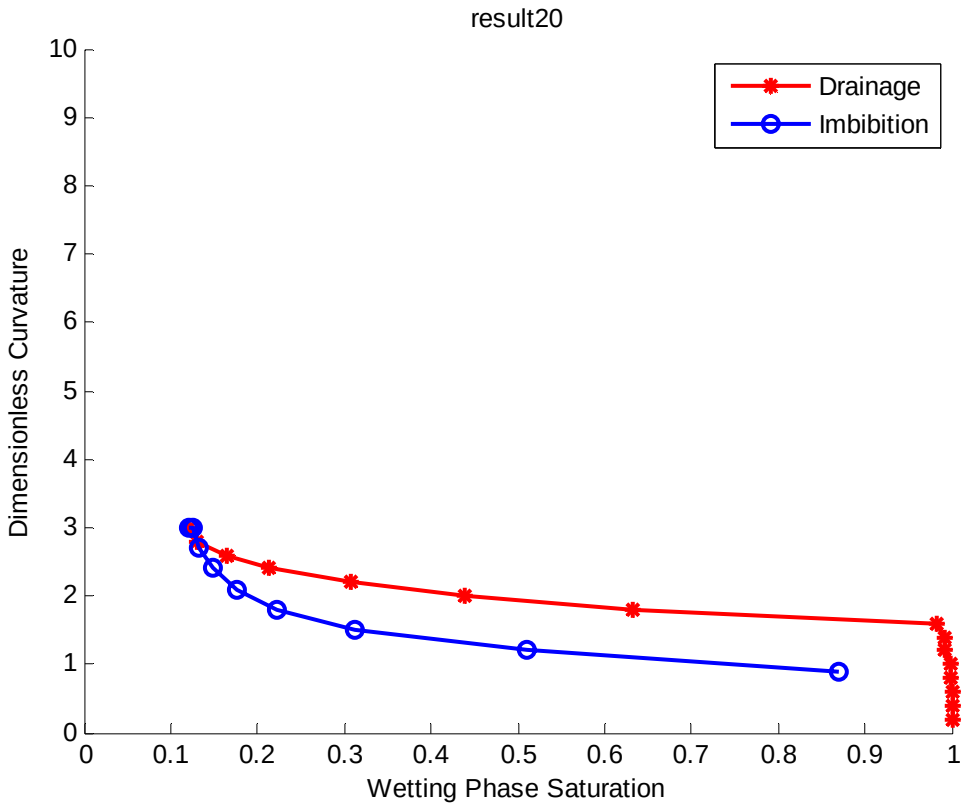
result20
Drainage
Imbibition
Dimensionless Curvature
Wetting Phase Saturation
0
1
2
3
4
5
6
7
8
9
10
0
0.1
0.2
0.3
0.4
0.5
0.6
0.7
0.8
0.9
1

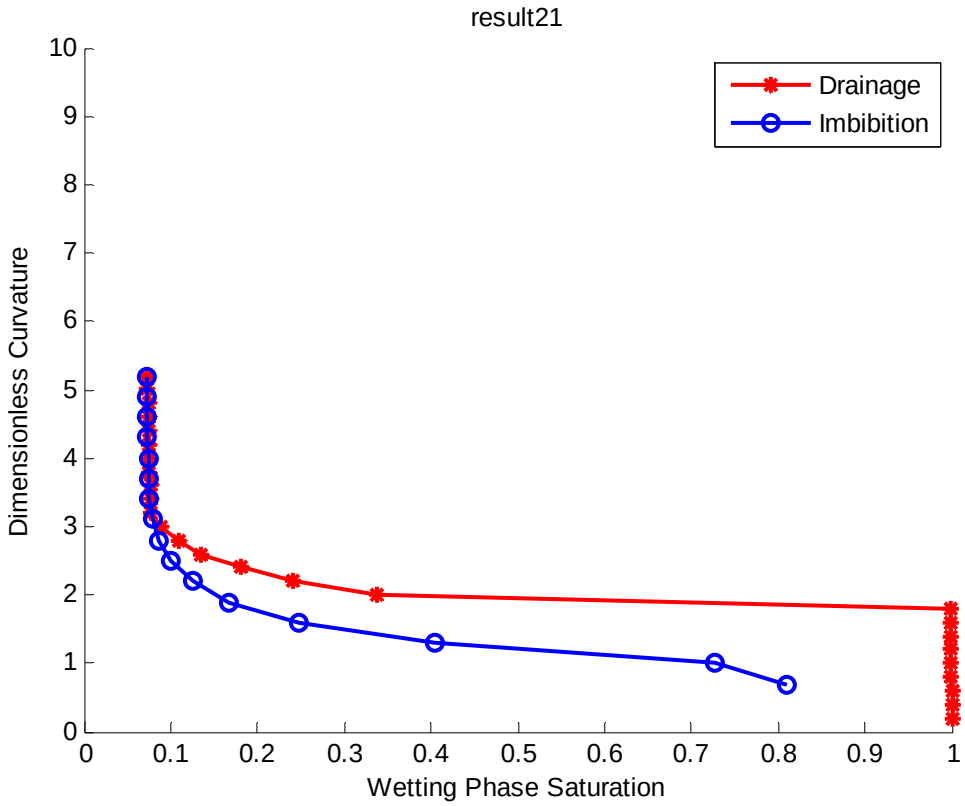
result21
Drainage
Imbibition
Dimensionless Curvature
Wetting Phase Saturation
0
1
2
3
4
5
6
7
8
9
10
0
0.1
0.2
0.3
0.4
0.5
0.6
0.7
0.8
0.9
1

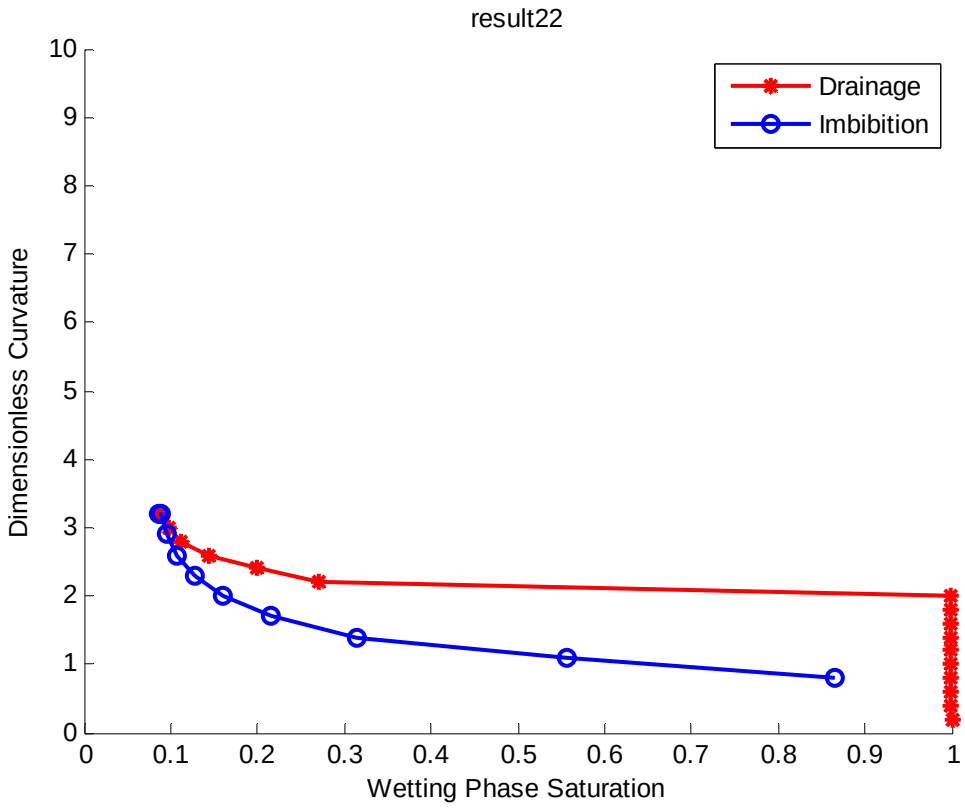
result22
Drainage
Imbibition
Dimensionless Curvature
Wetting Phase Saturation
0
1
2
3
4
5
6
7
8
9
10
0
0.1
0.2
0.3
0.4
0.5
0.6
0.7
0.8
0.9
1

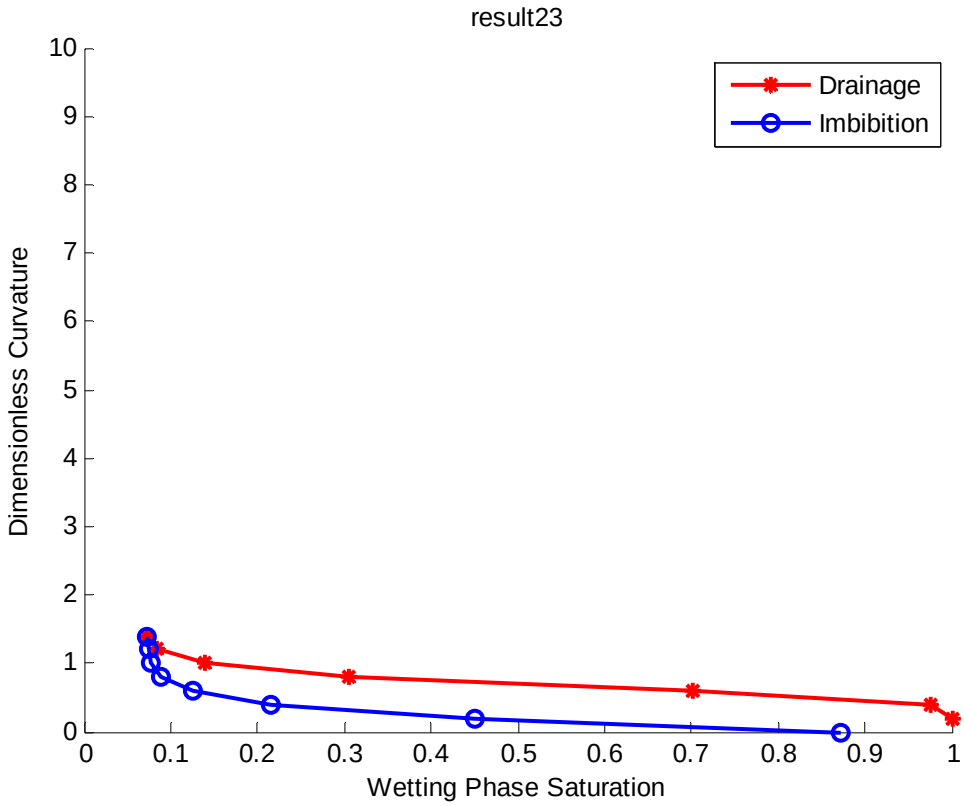
result23
Drainage
Imbibition
Dimensionless Curvature
Wetting Phase Saturation
0
1
2
3
4
5
6
7
8
9
10
0
0.1
0.2
0.3
0.4
0.5
0.6
0.7
0.8
0.9
1

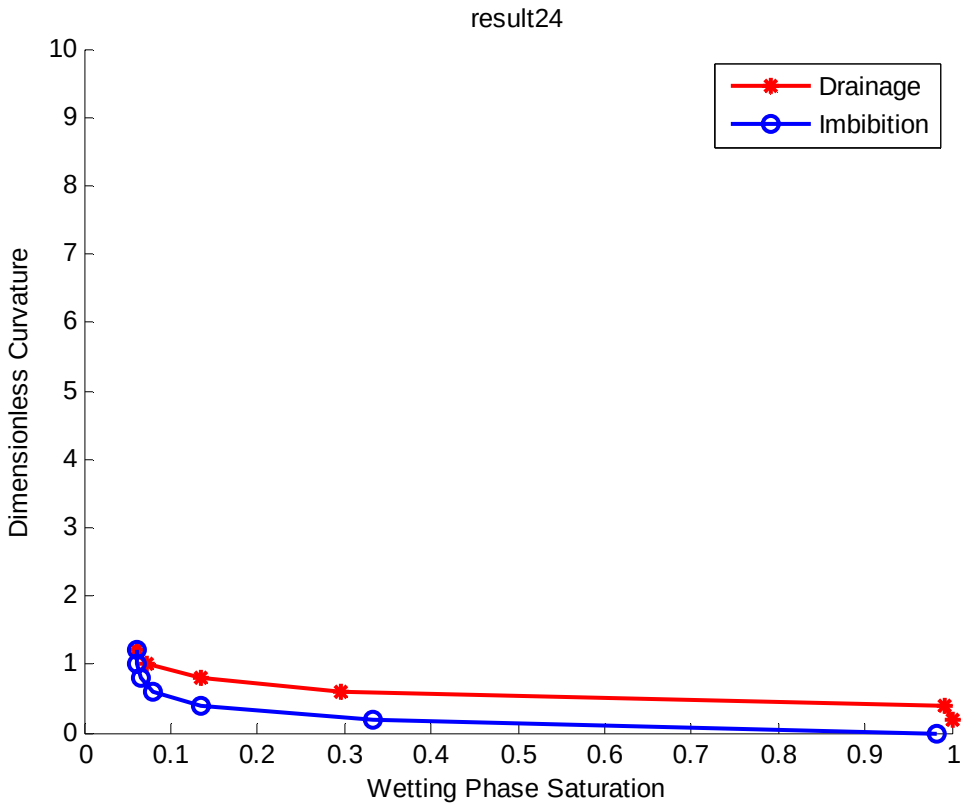
result24
Drainage
Imbibition
Dimensionless Curvature
Wetting Phase Saturation
0
1
2
3
4
5
6
7
8
9
10
0
0.1
0.2
0.3
0.4
0.5
0.6
0.7
0.8
0.9
1

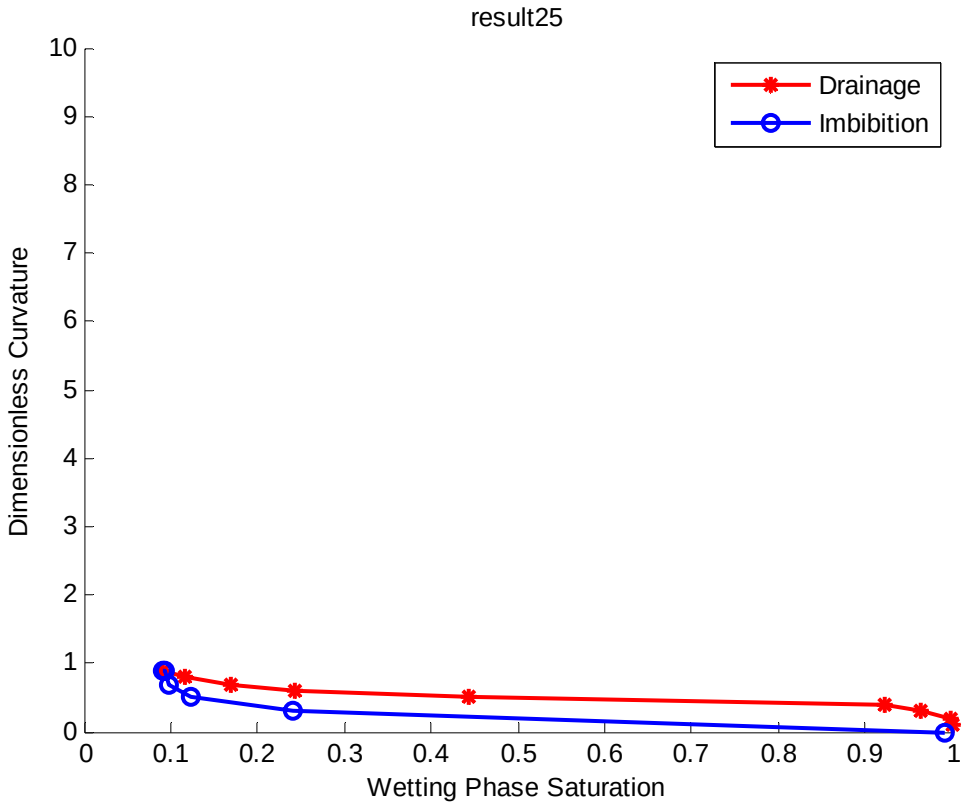
result25
Drainage
Imbibition
Dimensionless Curvature
Wetting Phase Saturation
0
1
2
3
4
5
6
7
8
9
10
0
0.1
0.2
0.3
0.4
0.5
0.6
0.7
0.8
0.9
1

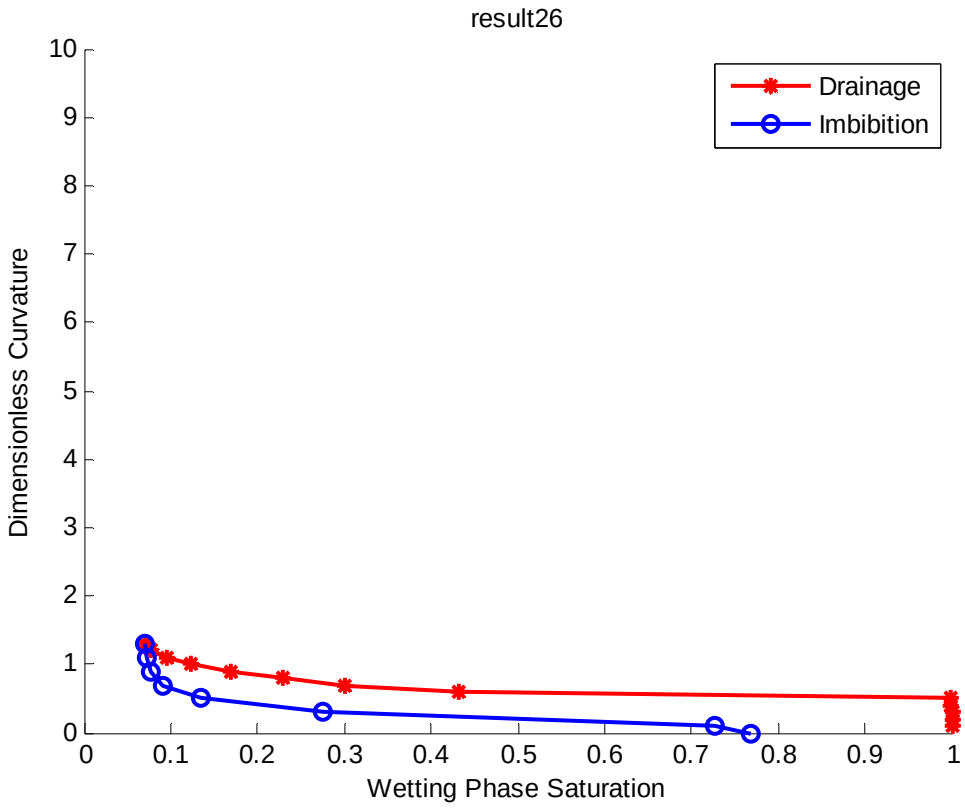
result26
Drainage
Imbibition
Dimensionless Curvature
Wetting Phase Saturation
0
1
2
3
4
5
6
7
8
9
10
0
0.1
0.2
0.3
0.4
0.5
0.6
0.7
0.8
0.9
1

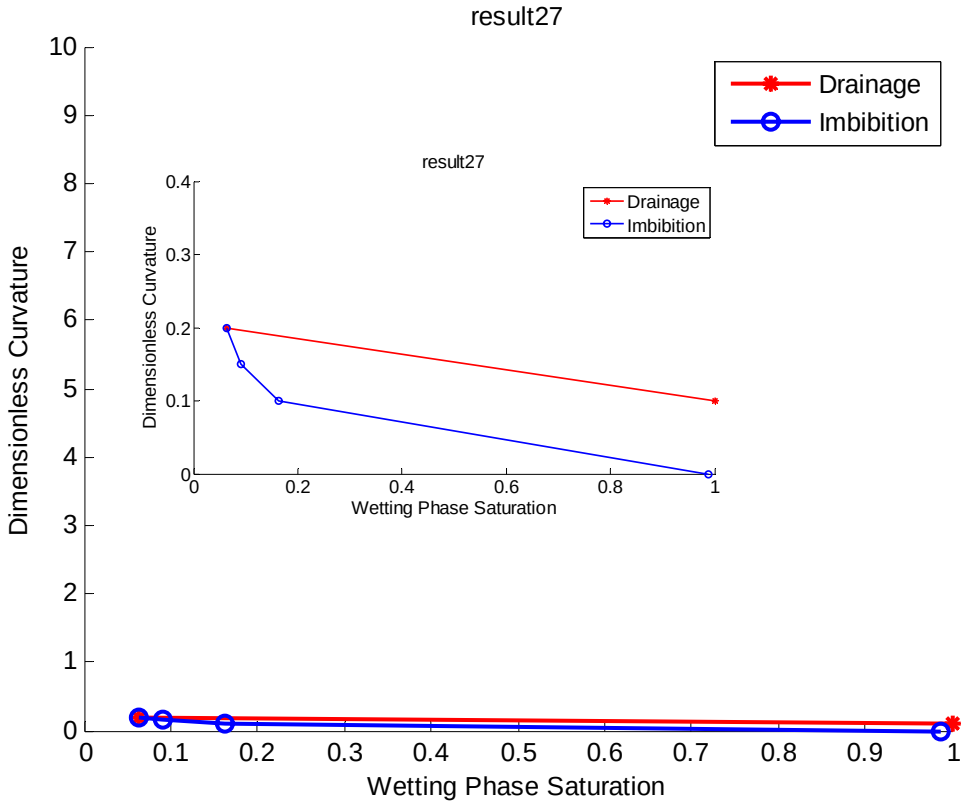
result27
Drainage
Imbibition
Dimensionless Curvature
Wetting Phase Saturation
result27
Drainage
Imbibition
Dimensionless Curvature
Wetting Phase Saturation
0
0.1
0.2
0.3
0.4
0
0.2
0.4
0.6
0.8
1

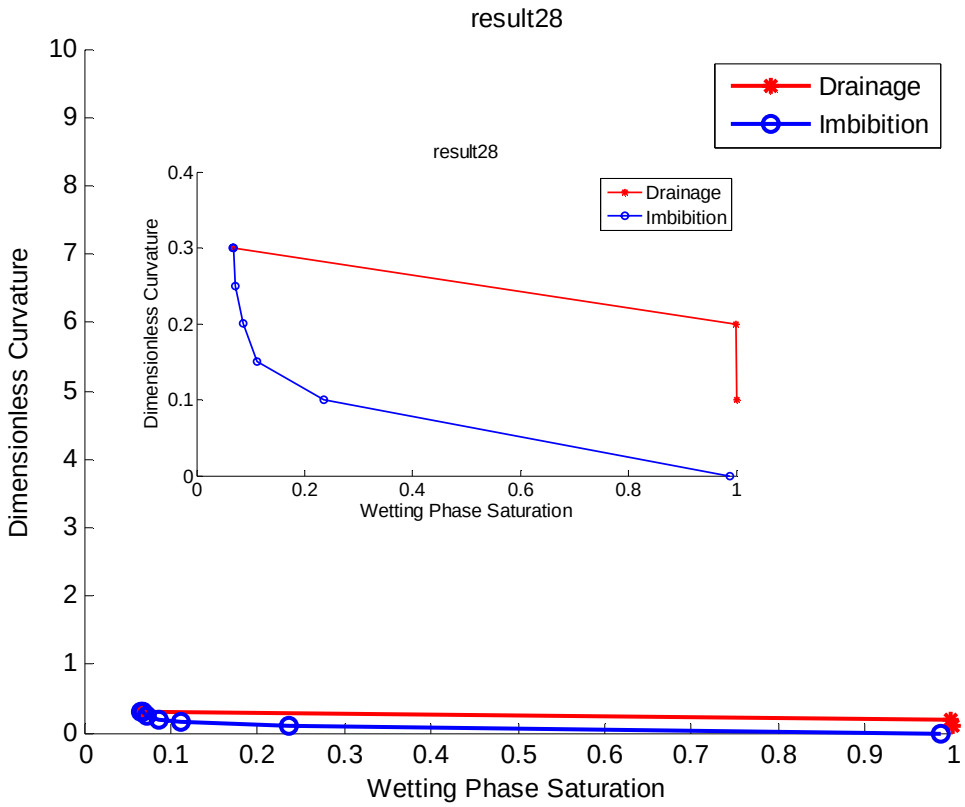
result28
Drainage
Imbibition
Dimensionless Curvature
Wetting Phase Saturation
result28
Drainage
Imbibition
Dimensionless Curvature
Wetting Phase Saturation

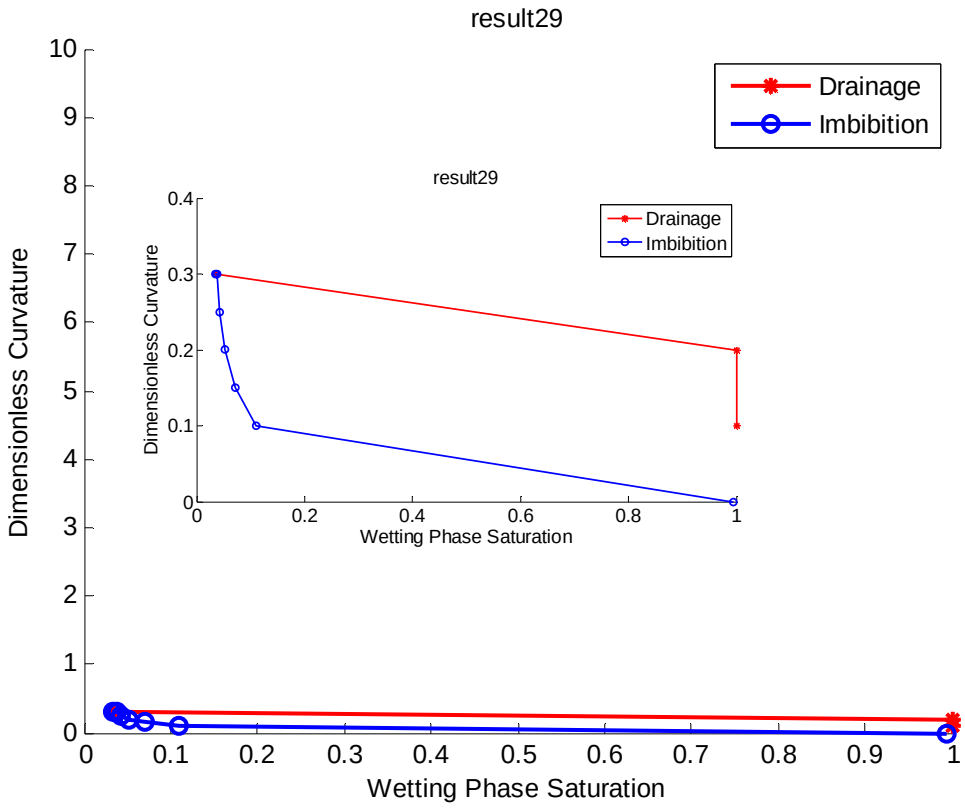
result29
Drainage
Imbibition
Dimensionless Curvature
Wetting Phase Saturation
result29
Drainage
Imbibition
Dimensionless Curvature
Wetting Phase Saturation

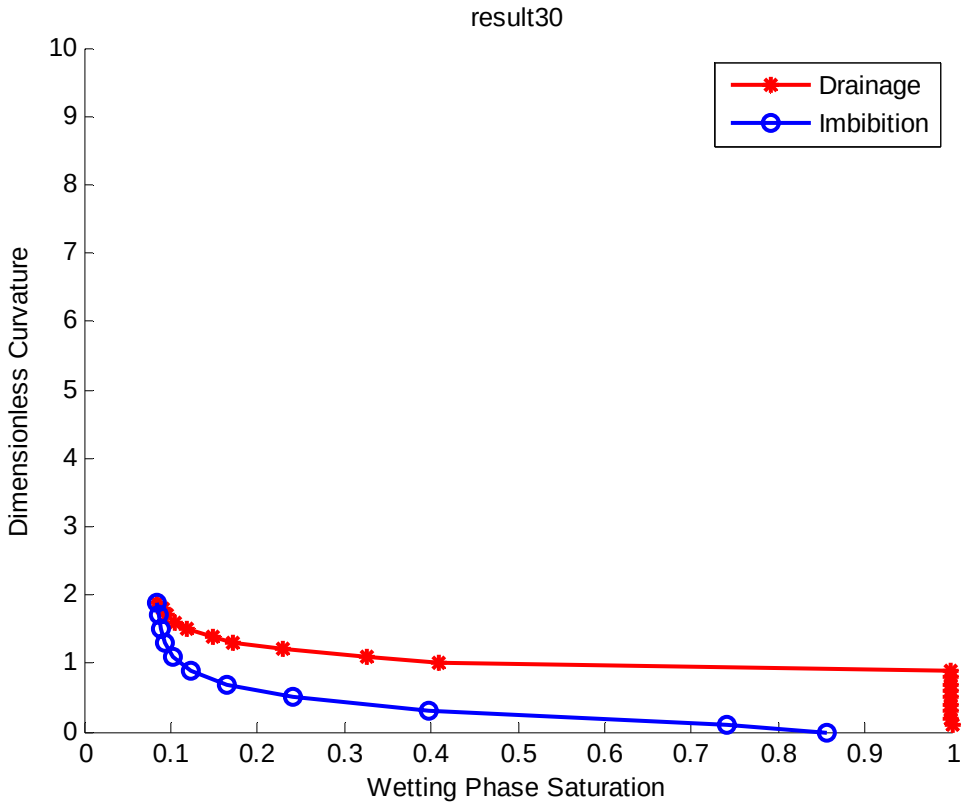
result30
Drainage
Imbibition
Dimensionless Curvature
Wetting Phase Saturation

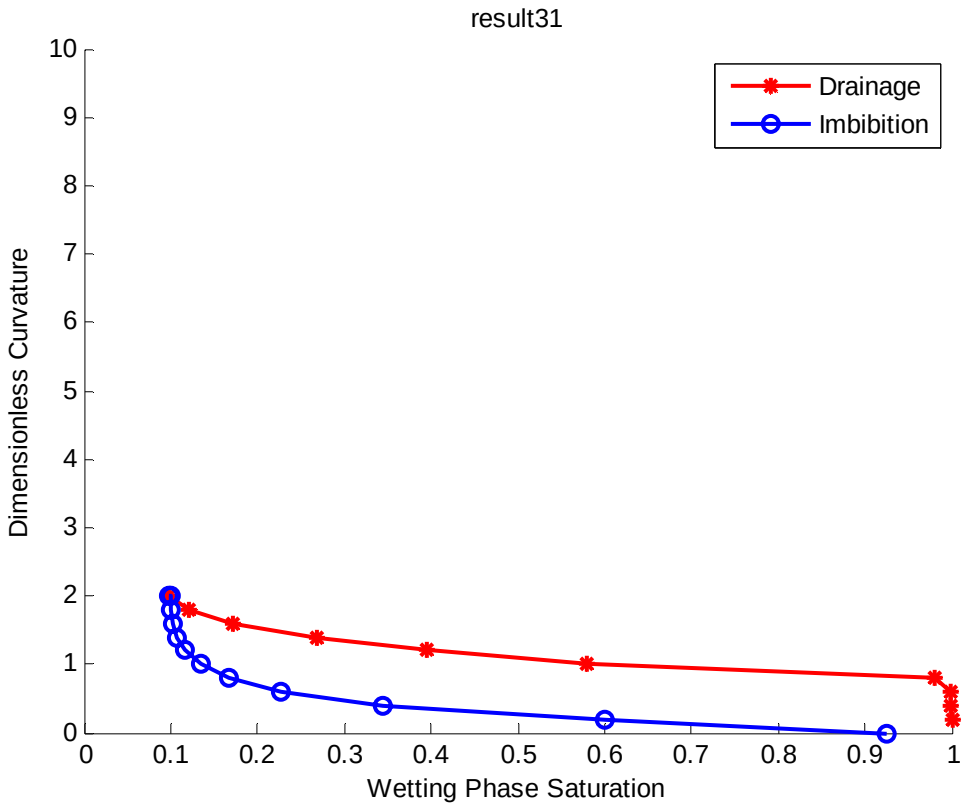
result31
Drainage
Imbibition
Dimensionless Curvature
Wetting Phase Saturation
0
1
2
3
4
5
6
7
8
9
10
0
0.1
0.2
0.3
0.4
0.5
0.6
0.7
0.8
0.9
1

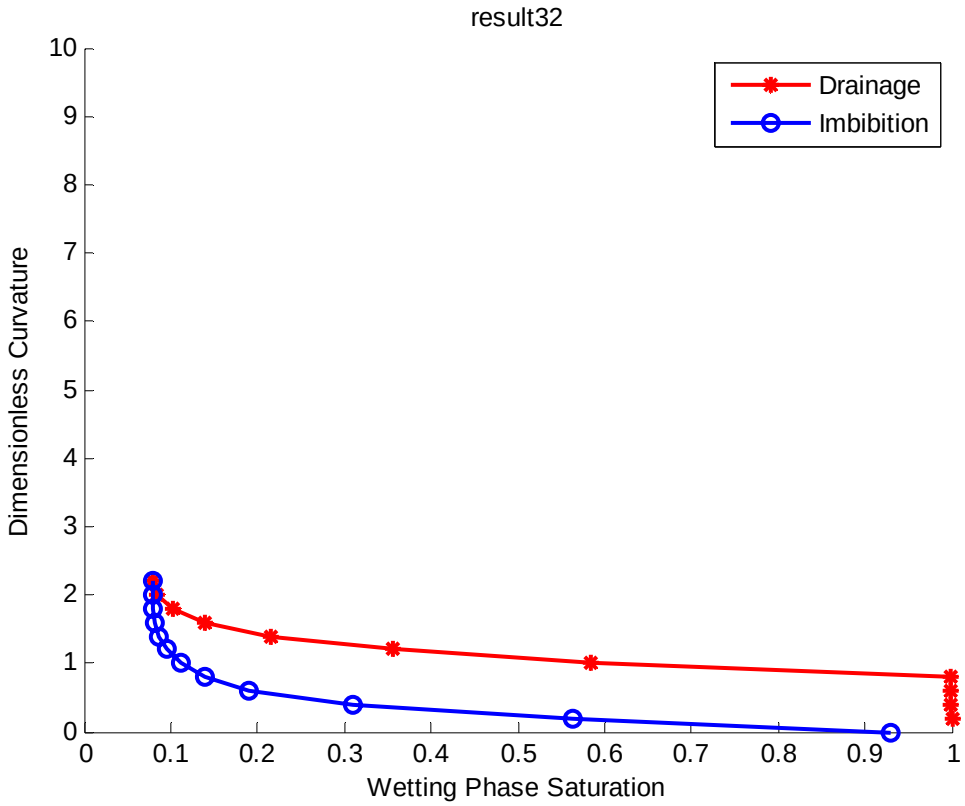
result32
Drainage
Imbibition
Dimensionless Curvature
Wetting Phase Saturation
0
1
2
3
4
5
6
7
8
9
10
0
0.1
0.2
0.3
0.4
0.5
0.6
0.7
0.8
0.9
1

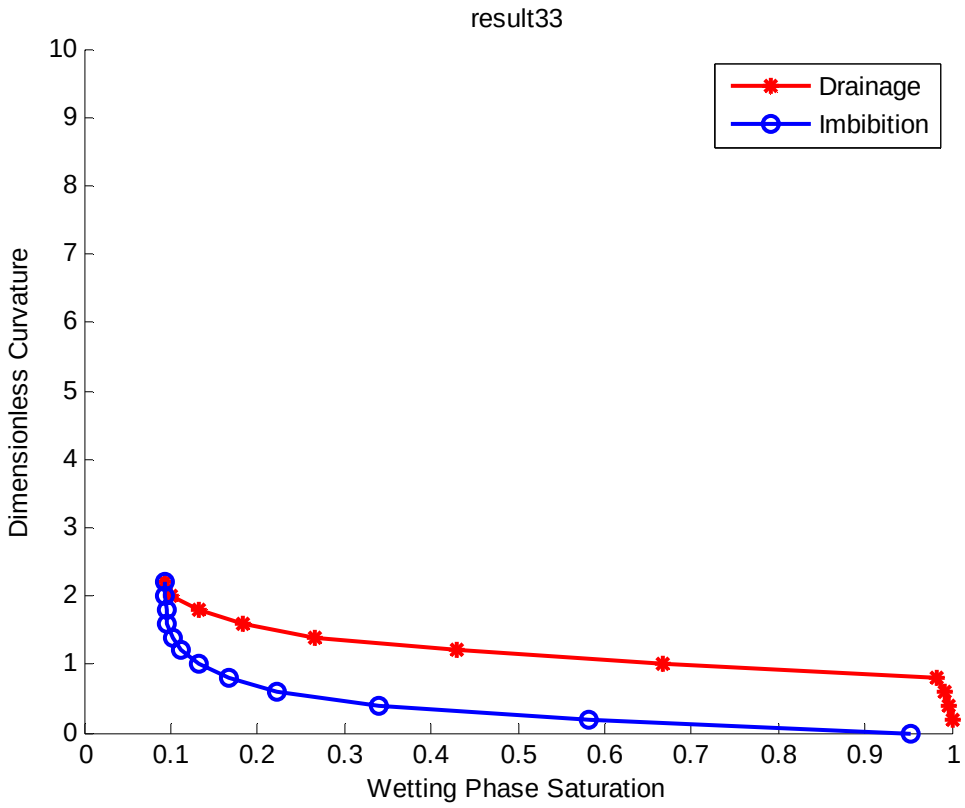
result33
Drainage
Imbibition
Dimensionless Curvature
Wetting Phase Saturation
0
1
2
3
4
5
6
7
8
9
10
0
0.1
0.2
0.3
0.4
0.5
0.6
0.7
0.8
0.9
1

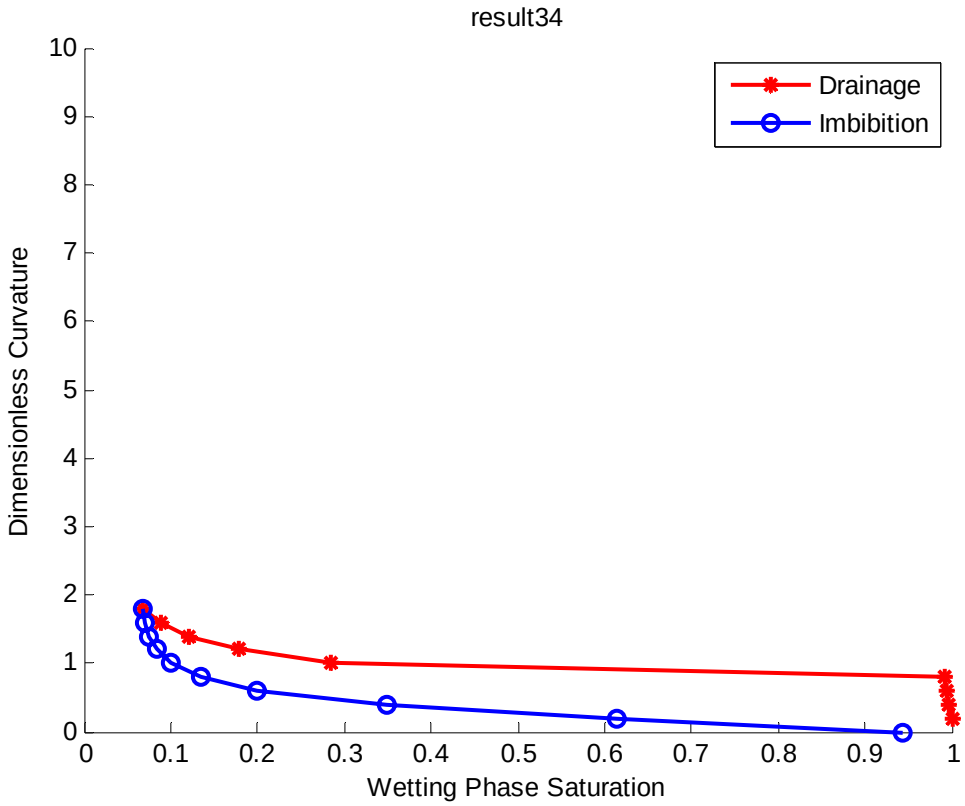
result34
Drainage
Imbibition
Dimensionless Curvature
Wetting Phase Saturation
0
1
2
3
4
5
6
7
8
9
10
0
0.1
0.2
0.3
0.4
0.5
0.6
0.7
0.8
0.9
1

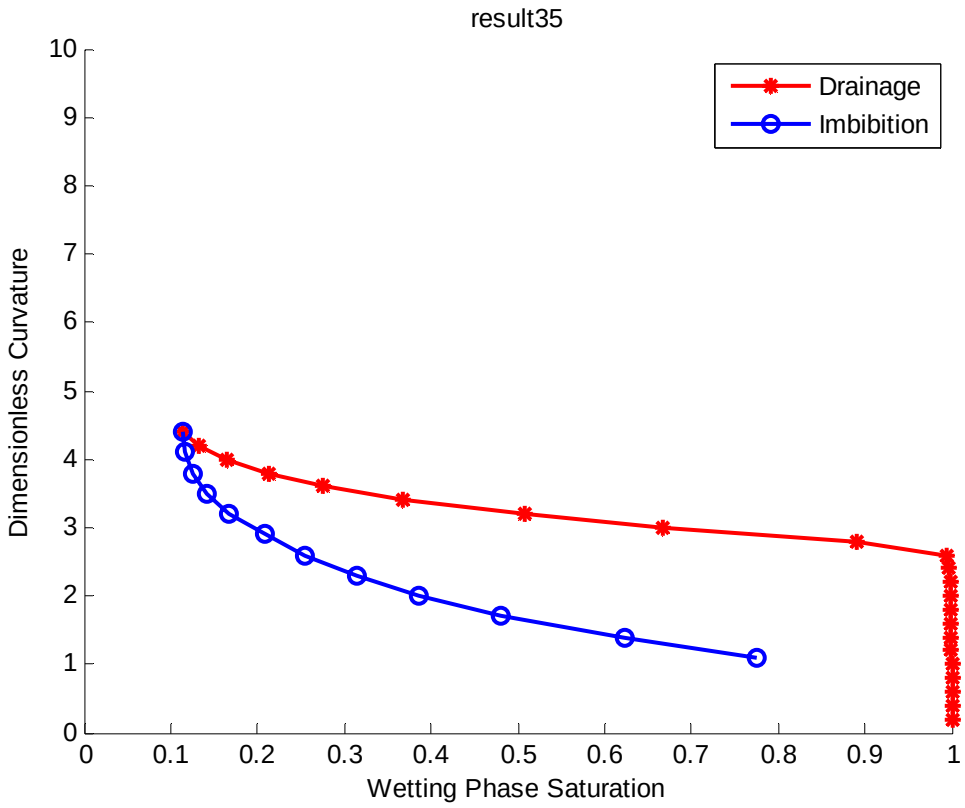
result35
Drainage
Imbibition
Dimensionless Curvature
Wetting Phase Saturation
0
1
2
3
4
5
6
7
8
9
10
0
0.1
0.2
0.3
0.4
0.5
0.6
0.7
0.8
0.9
1

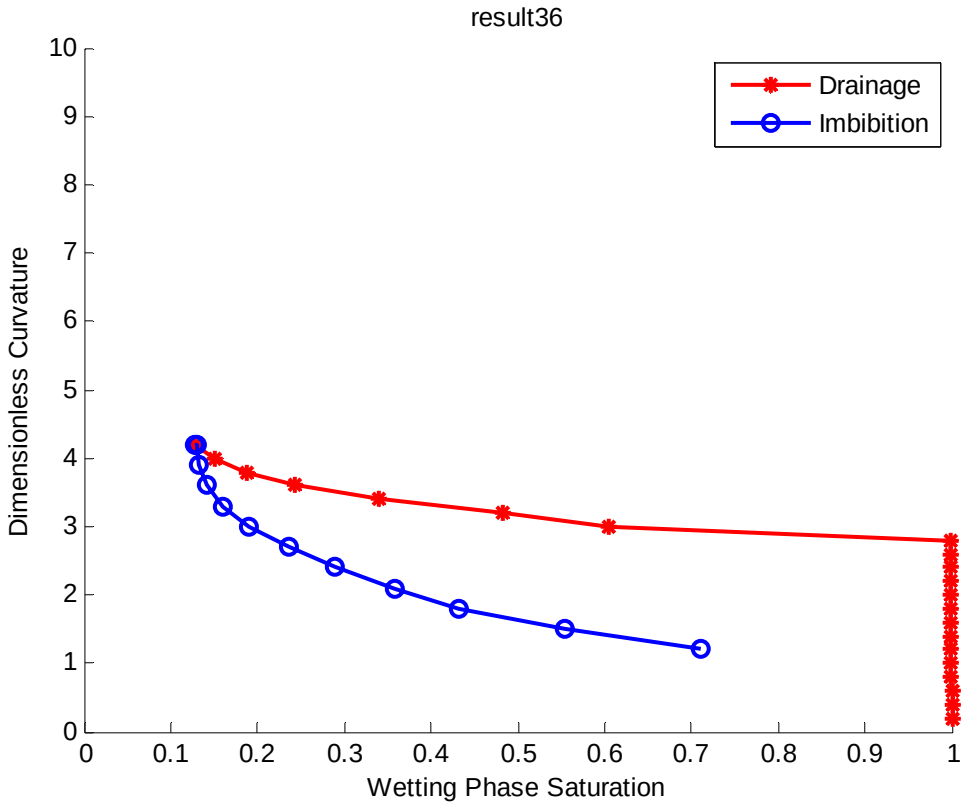
result36
Drainage
Imbibition
Dimensionless Curvature
Wetting Phase Saturation
0
1
2
3
4
5
6
7
8
9
10
0
0.1
0.2
0.3
0.4
0.5
0.6
0.7
0.8
0.9
1

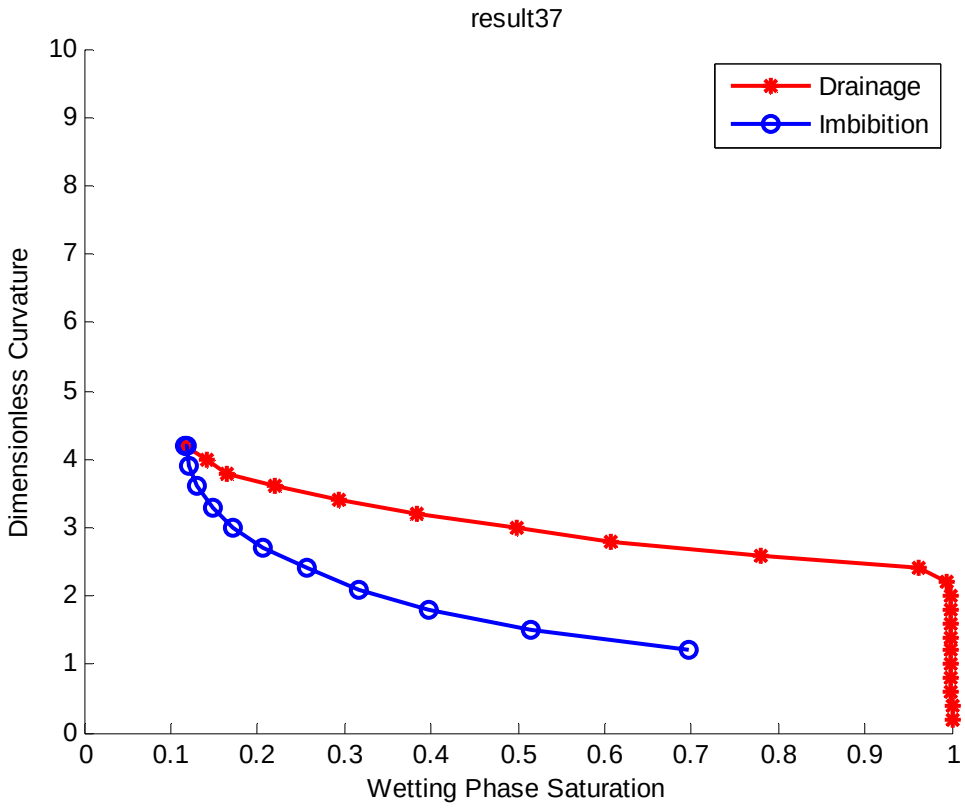
result37
Drainage
Imbibition
Dimensionless Curvature
Wetting Phase Saturation
0
1
2
3
4
5
6
7
8
9
10
0
0.1
0.2
0.3
0.4
0.5
0.6
0.7
0.8
0.9
1

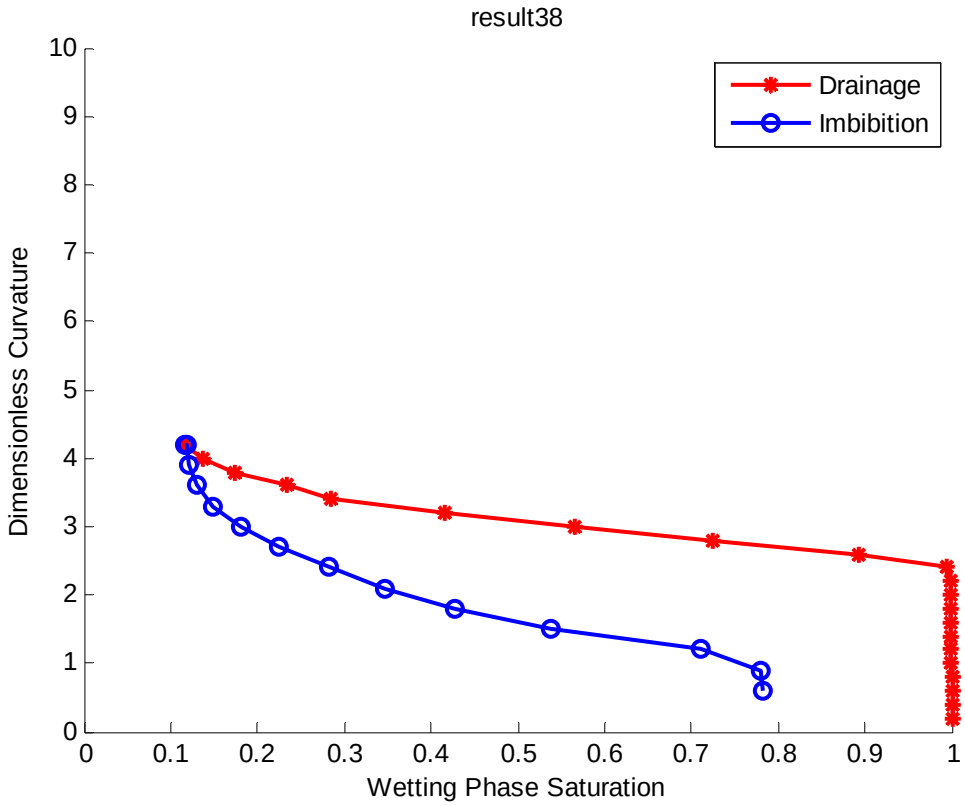
result38
Drainage
Imbibition
Dimensionless Curvature
Wetting Phase Saturation
0
1
2
3
4
5
6
7
8
9
10
0
0.1
0.2
0.3
0.4
0.5
0.6
0.7
0.8
0.9
1

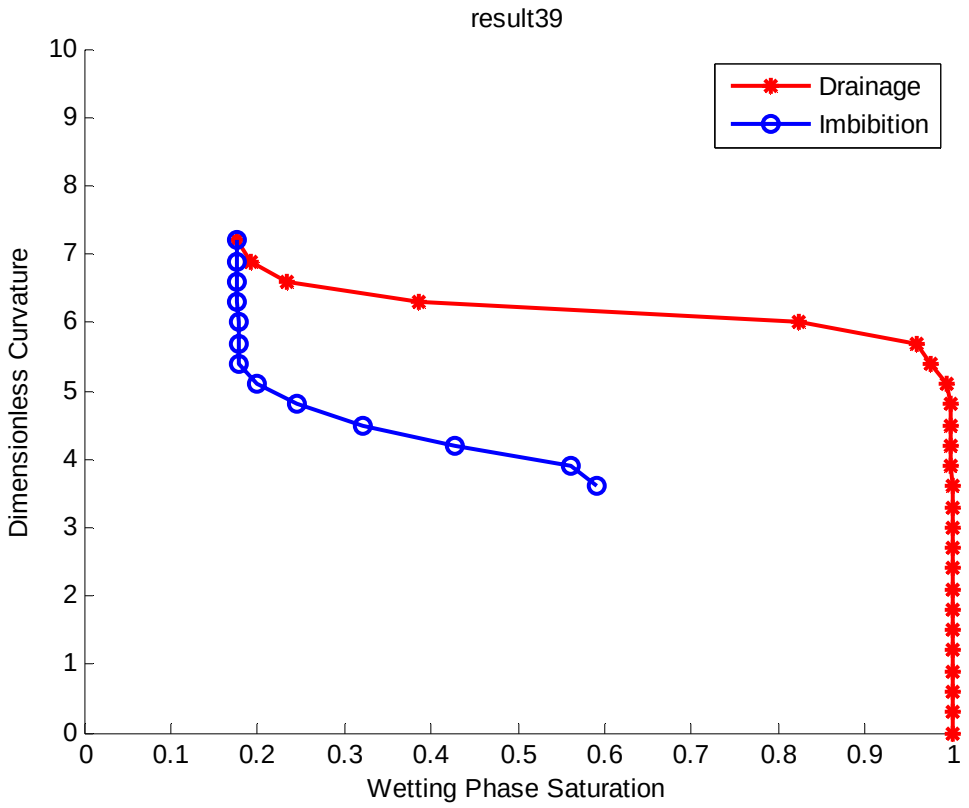
result39
Drainage
Imbibition
Dimensionless Curvature
Wetting Phase Saturation
0
1
2
3
4
5
6
7
8
9
10
0
0.1
0.2
0.3
0.4
0.5
0.6
0.7
0.8
0.9
1

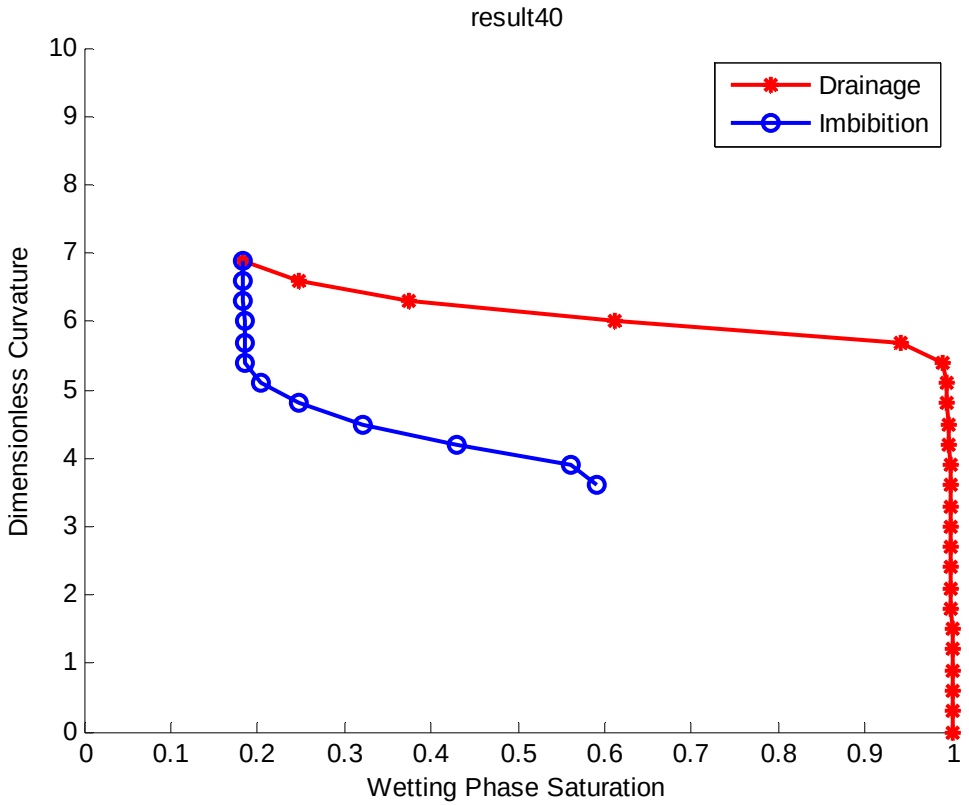
result40
Drainage
Imbibition
Dimensionless Curvature
Wetting Phase Saturation
0
1
2
3
4
5
6
7
8
9
10
0
0.1
0.2
0.3
0.4
0.5
0.6
0.7
0.8
0.9
1

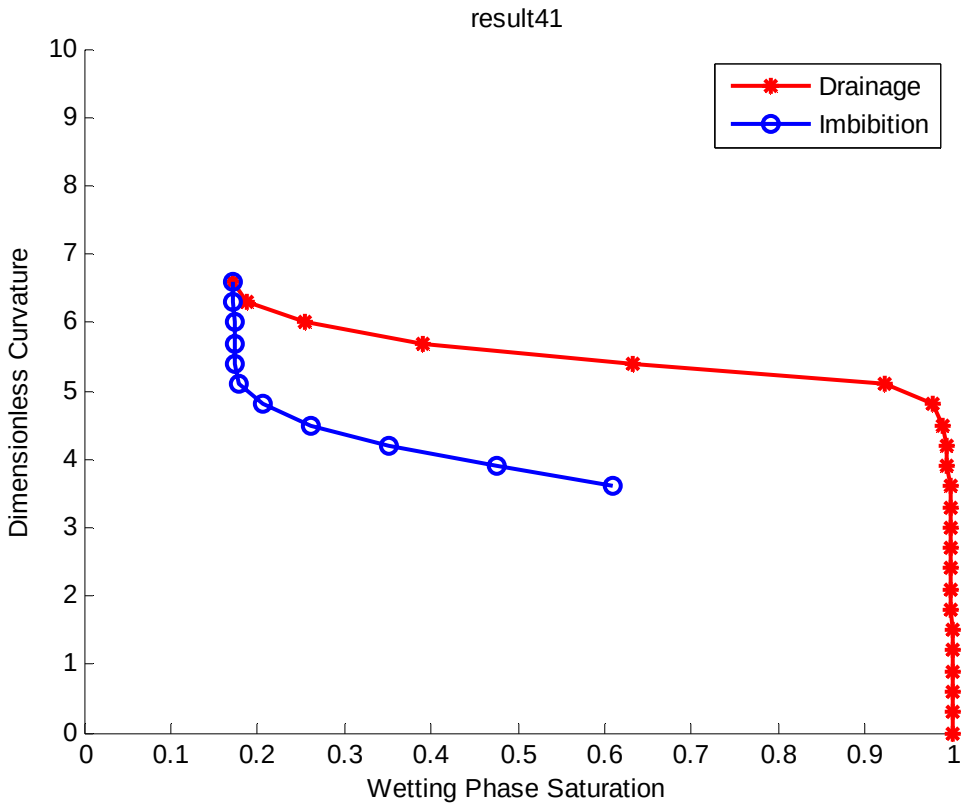
result41
Drainage
Imbibition
Dimensionless Curvature
Wetting Phase Saturation
0
1
2
3
4
5
6
7
8
9
10
0
0.1
0.2
0.3
0.4
0.5
0.6
0.7
0.8
0.9
1

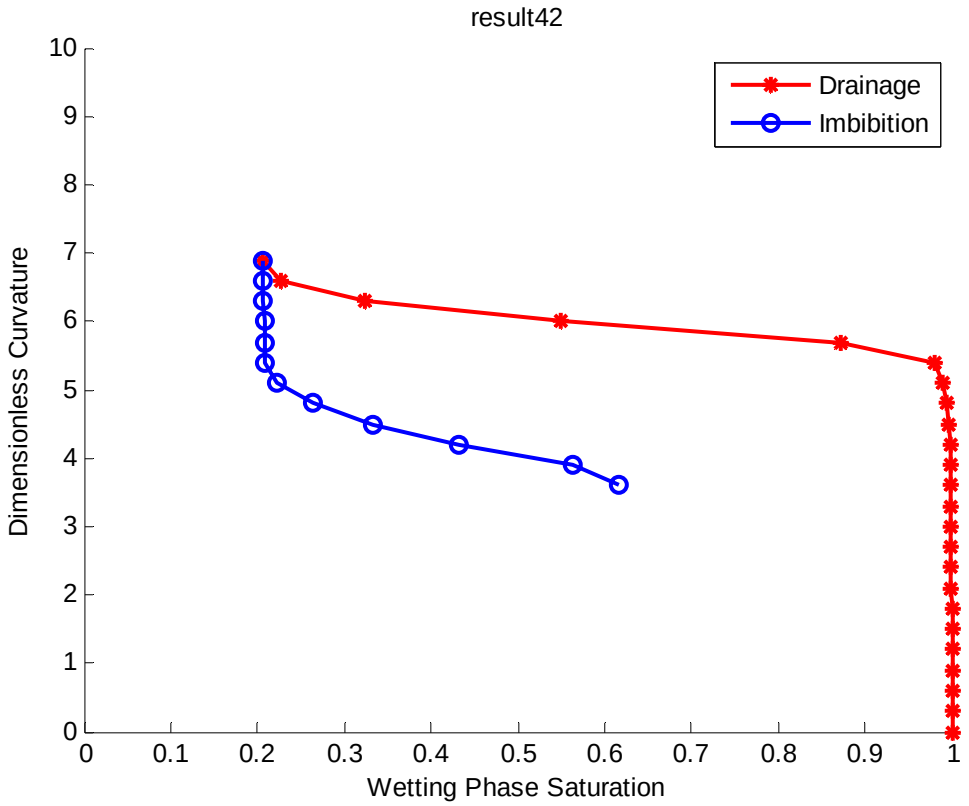
result42
Drainage
Imbibition
Dimensionless Curvature
Wetting Phase Saturation
0
1
2
3
4
5
6
7
8
9
10
0
0.1
0.2
0.3
0.4
0.5
0.6
0.7
0.8
0.9
1

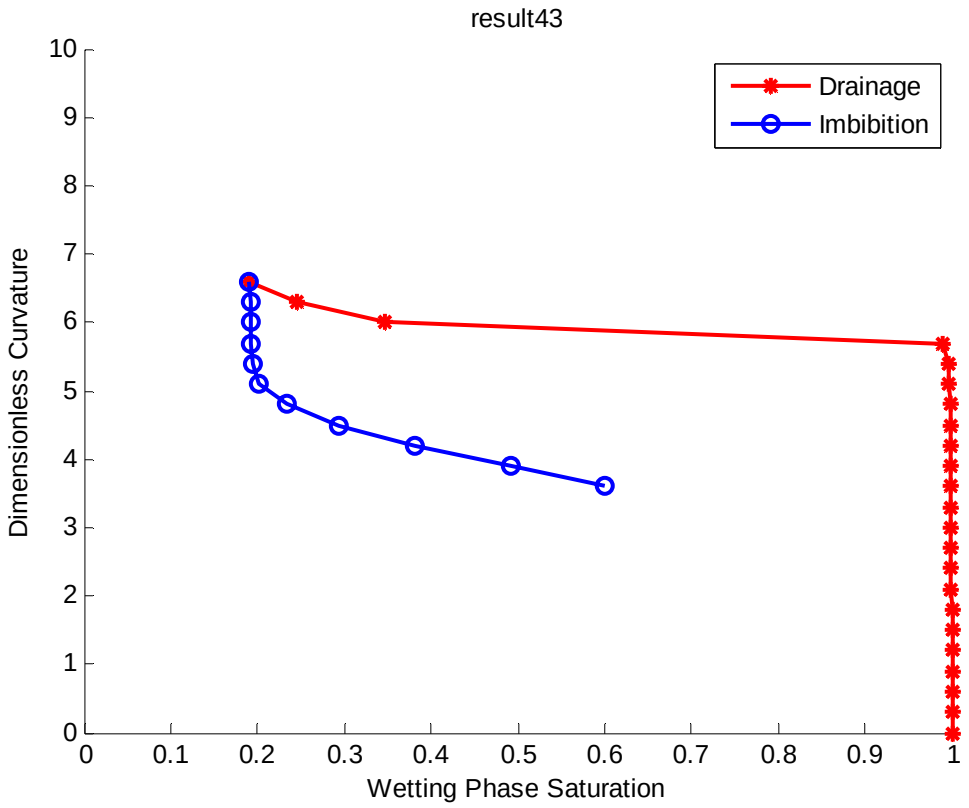
result43
Drainage
Imbibition
Dimensionless Curvature
Wetting Phase Saturation
0
1
2
3
4
5
6
7
8
9
10
0
0.1
0.2
0.3
0.4
0.5
0.6
0.7
0.8
0.9
1

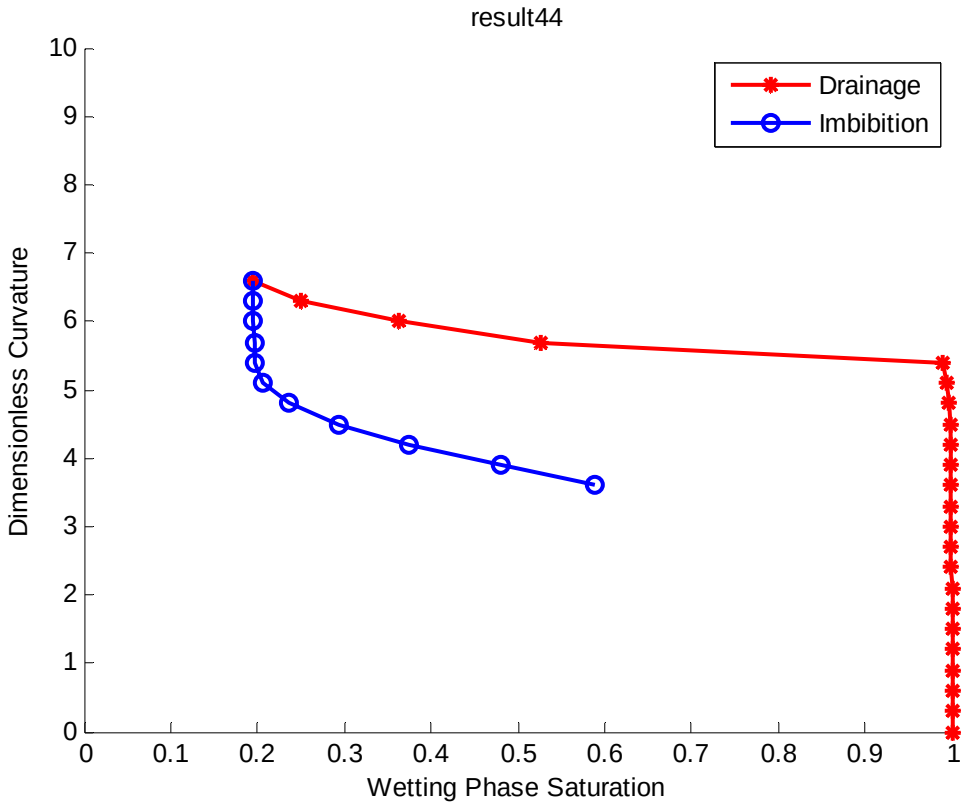
result44
Drainage
Imbibition
Dimensionless Curvature
Wetting Phase Saturation
0
1
2
3
4
5
6
7
8
9
10
0
0.1
0.2
0.3
0.4
0.5
0.6
0.7
0.8
0.9
1

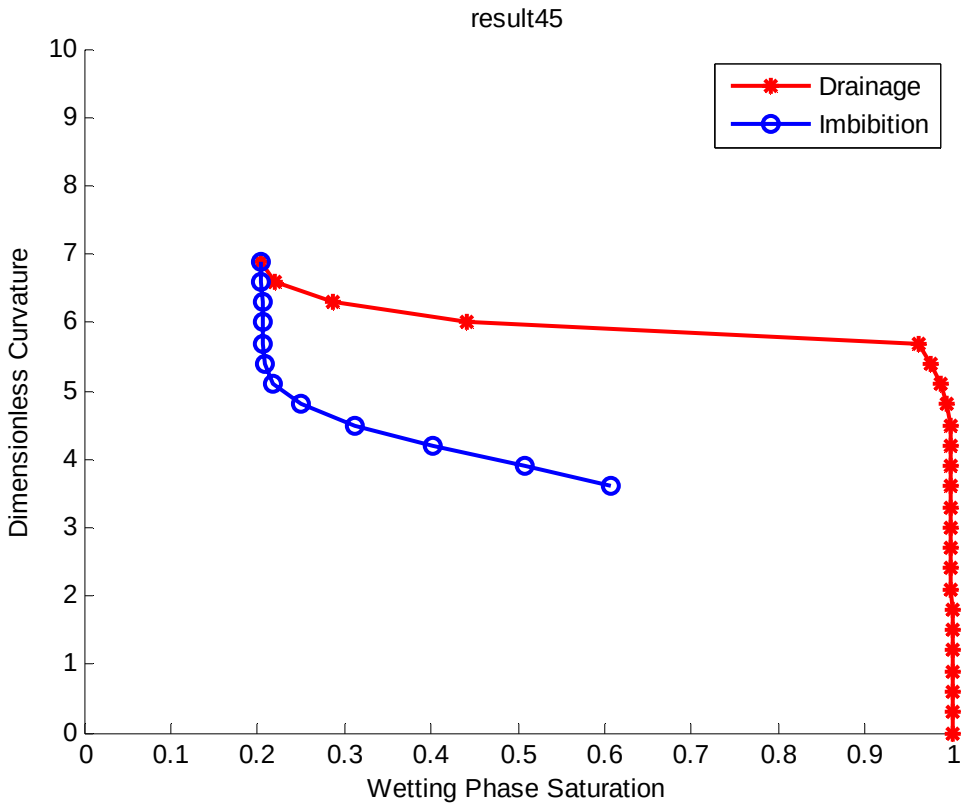
result45
Drainage
Imbibition
Dimensionless Curvature
Wetting Phase Saturation
0
1
2
3
4
5
6
7
8
9
10
0
0.1
0.2
0.3
0.4
0.5
0.6
0.7
0.8
0.9
1

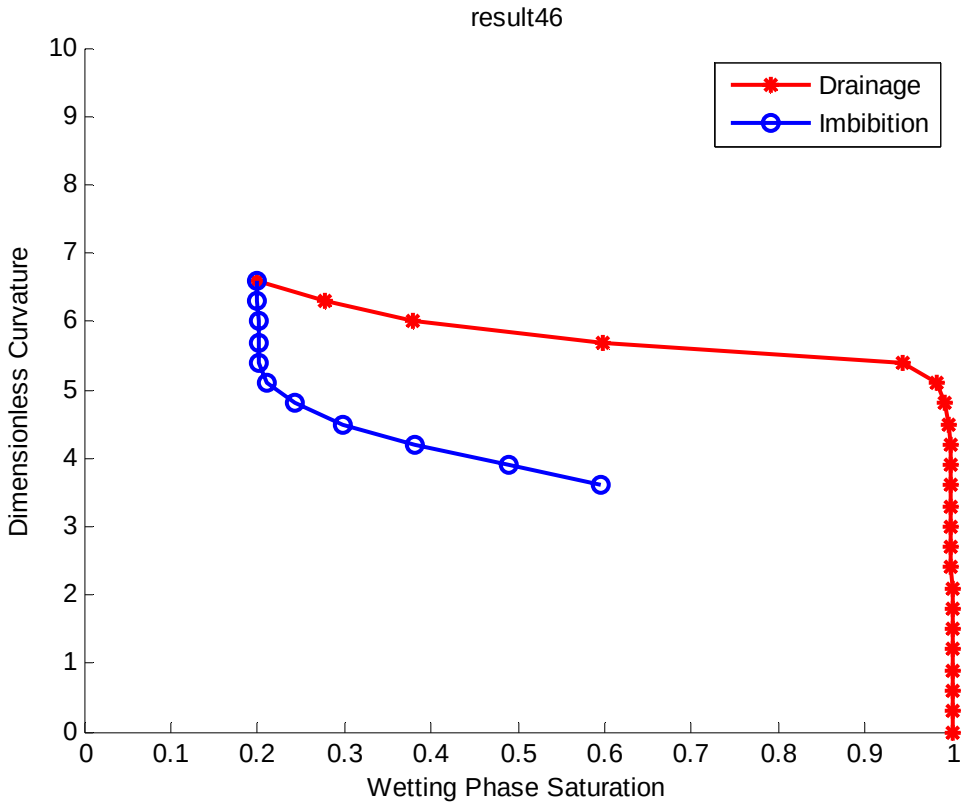
result46
Drainage
Imbibition
Dimensionless Curvature
Wetting Phase Saturation
0
1
2
3
4
5
6
7
8
9
10
0
0.1
0.2
0.3
0.4
0.5
0.6
0.7
0.8
0.9
1

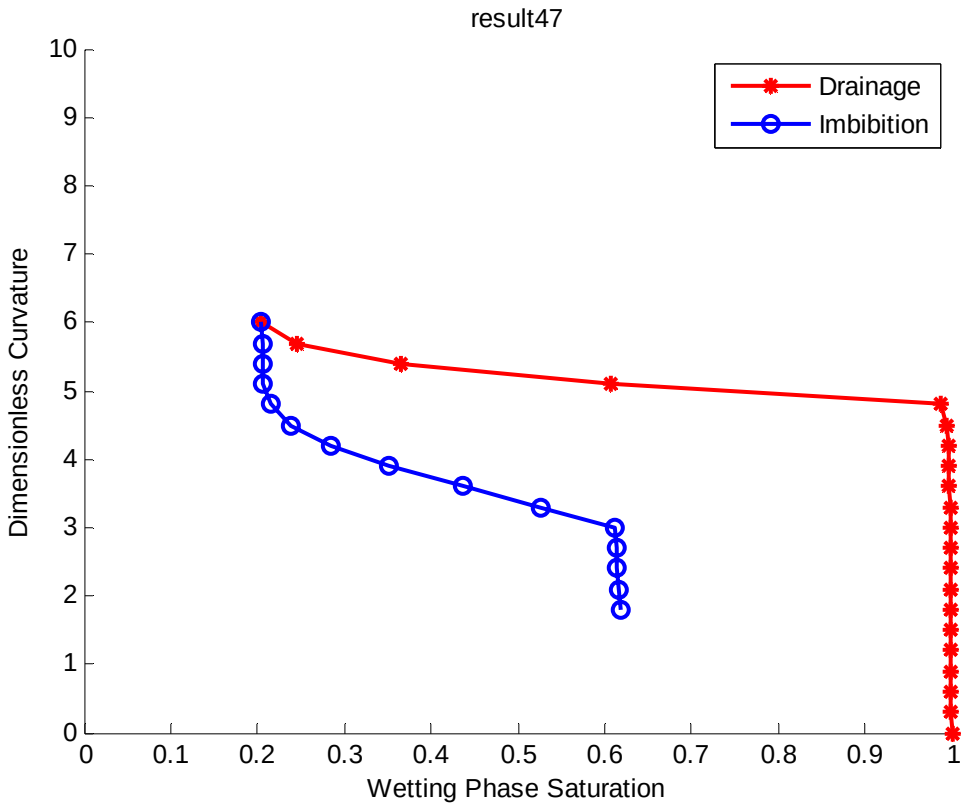
result47
Drainage
Imbibition
Dimensionless Curvature
Wetting Phase Saturation
0
1
2
3
4
5
6
7
8
9
10
0
0.1
0.2
0.3
0.4
0.5
0.6
0.7
0.8
0.9
1

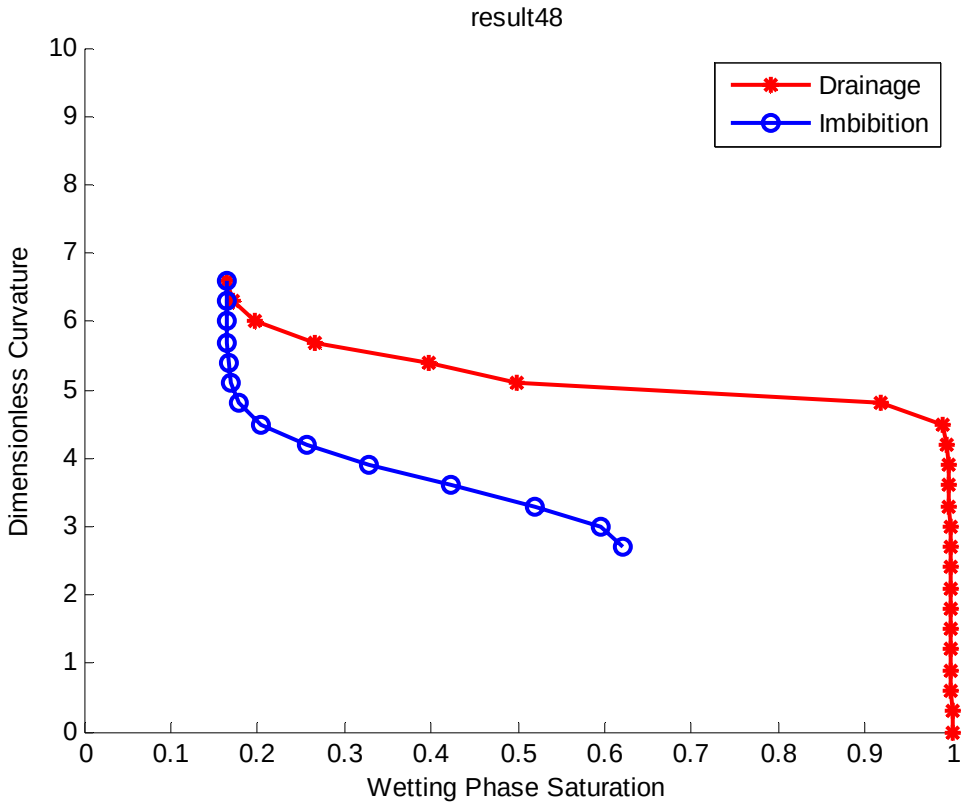
result48
Drainage
Imbibition
Dimensionless Curvature
Wetting Phase Saturation
0
1
2
3
4
5
6
7
8
9
10
0
0.1
0.2
0.3
0.4
0.5
0.6
0.7
0.8
0.9
1

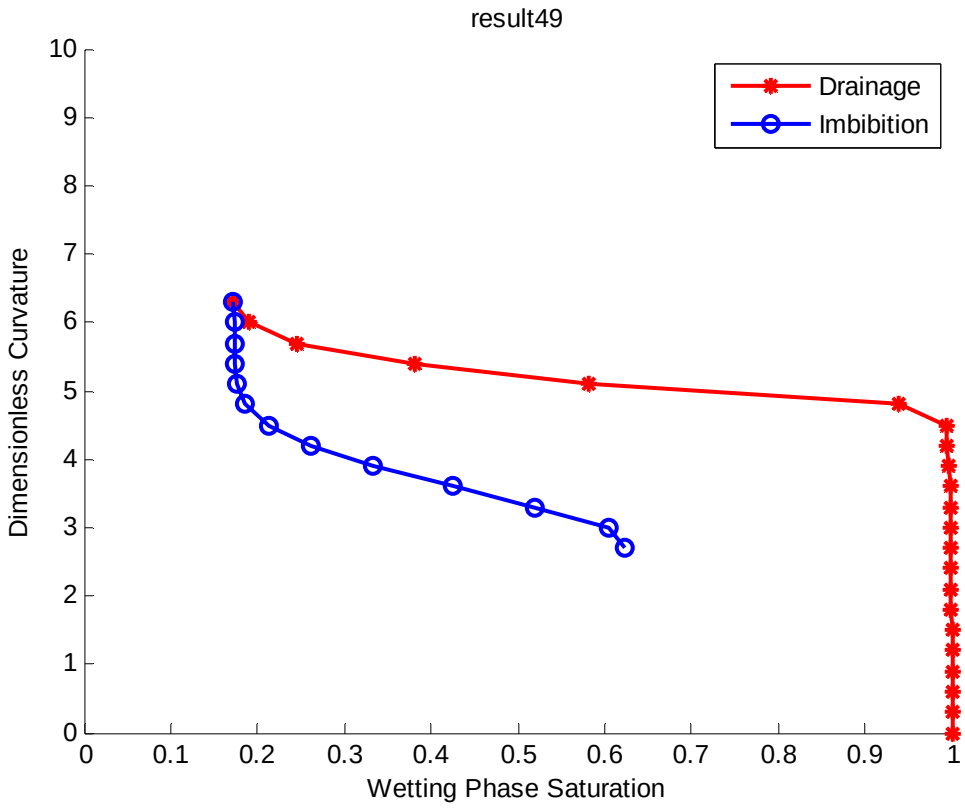
result49
Drainage
Imbibition
Dimensionless Curvature
Wetting Phase Saturation
0
1
2
3
4
5
6
7
8
9
10
0
0.1
0.2
0.3
0.4
0.5
0.6
0.7
0.8
0.9
1

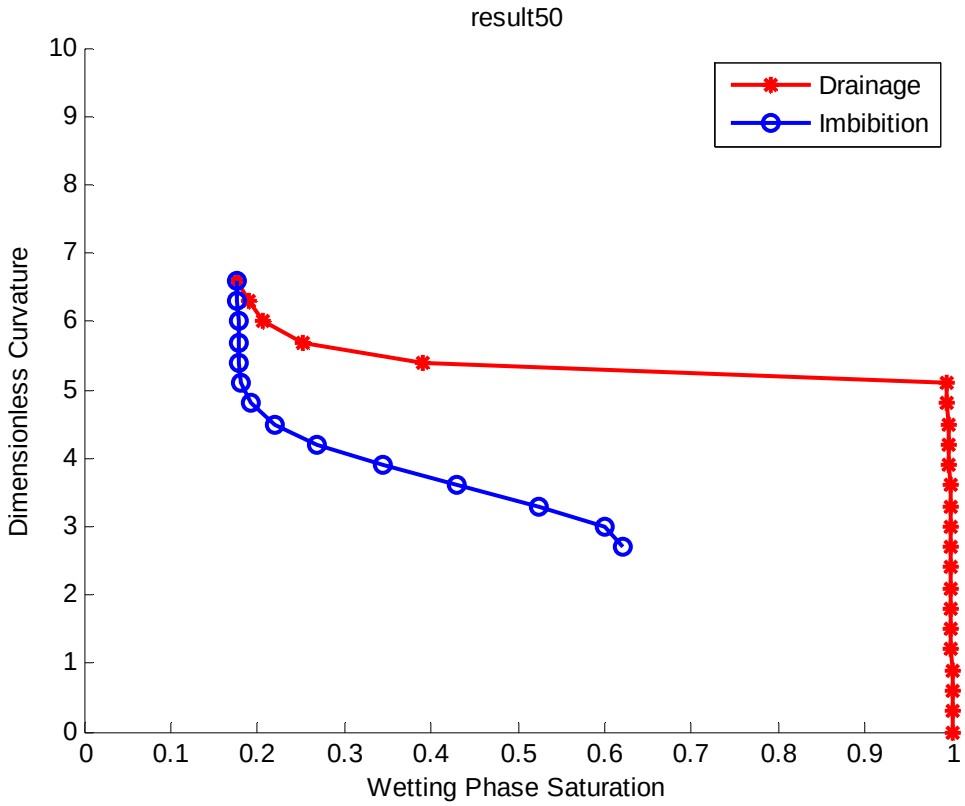
result50
Drainage
Imbibition
Dimensionless Curvature
Wetting Phase Saturation
0
1
2
3
4
5
6
7
8
9
10
0
0.1
0.2
0.3
0.4
0.5
0.6
0.7
0.8
0.9
1

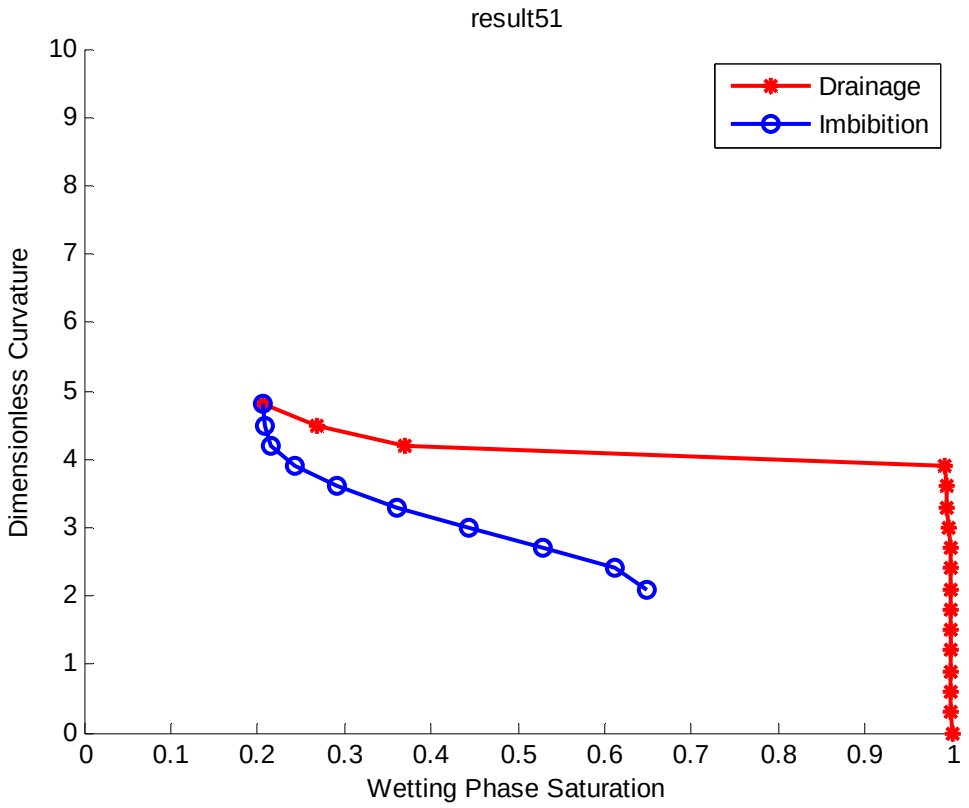
result51
Drainage
Imbibition
Dimensionless Curvature
Wetting Phase Saturation
0
1
2
3
4
5
6
7
8
9
10
0
0.1
0.2
0.3
0.4
0.5
0.6
0.7
0.8
0.9
1

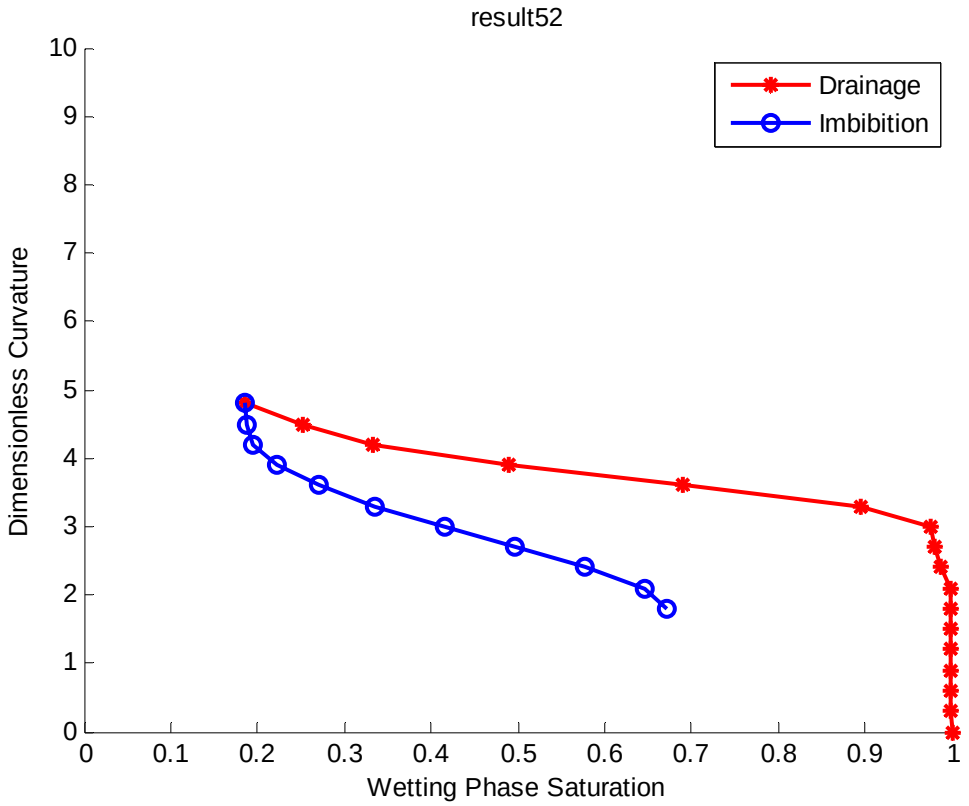
result52
Drainage
Imbibition
Dimensionless Curvature
Wetting Phase Saturation
0
1
2
3
4
5
6
7
8
9
10
0
0.1
0.2
0.3
0.4
0.5
0.6
0.7
0.8
0.9
1

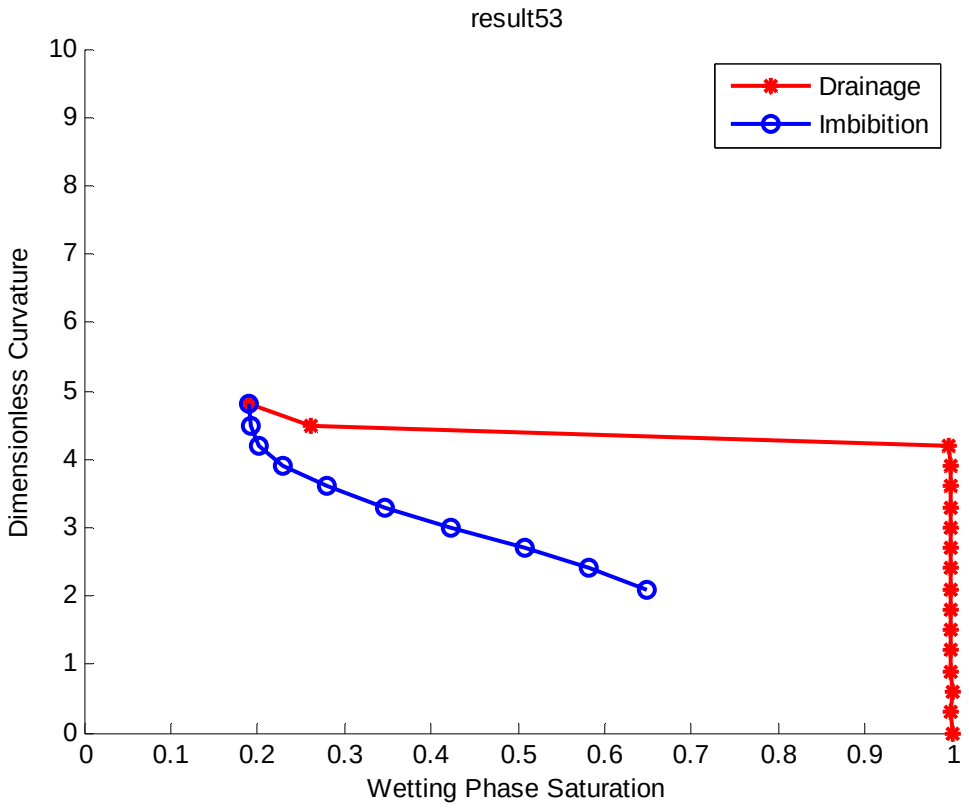
result53
Drainage
Imbibition
Dimensionless Curvature
Wetting Phase Saturation
0
1
2
3
4
5
6
7
8
9
10
0
0.1
0.2
0.3
0.4
0.5
0.6
0.7
0.8
0.9
1

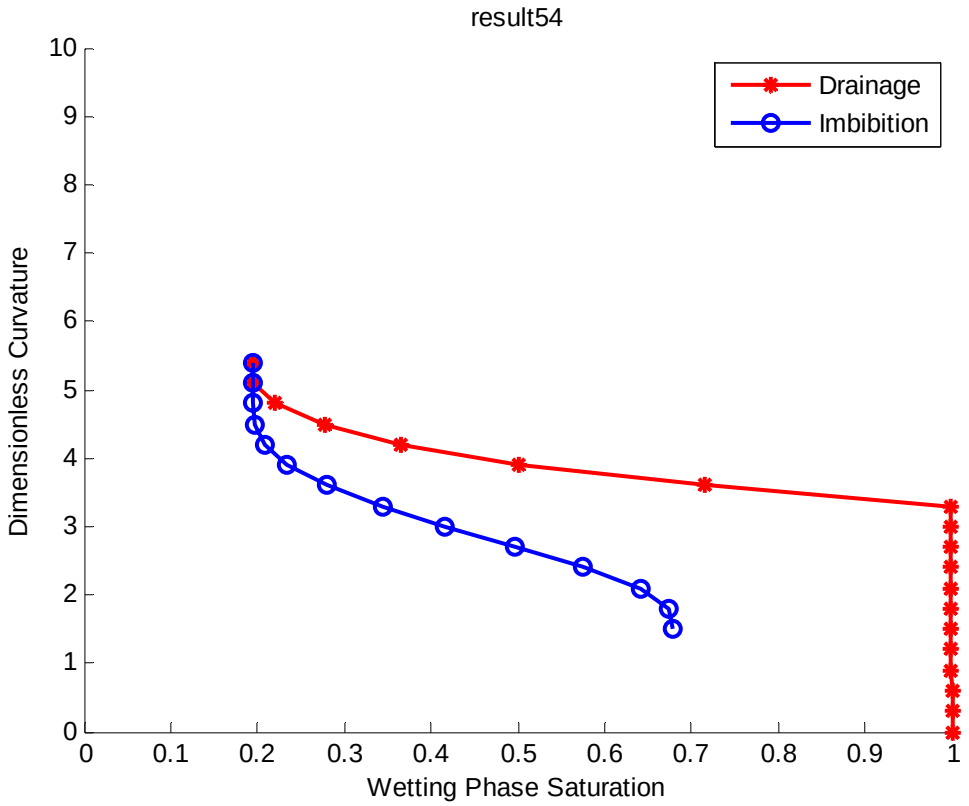
result54
Drainage
Imbibition
Dimensionless Curvature
Wetting Phase Saturation
0
1
2
3
4
5
6
7
8
9
10
0
0.1
0.2
0.3
0.4
0.5
0.6
0.7
0.8
0.9
1

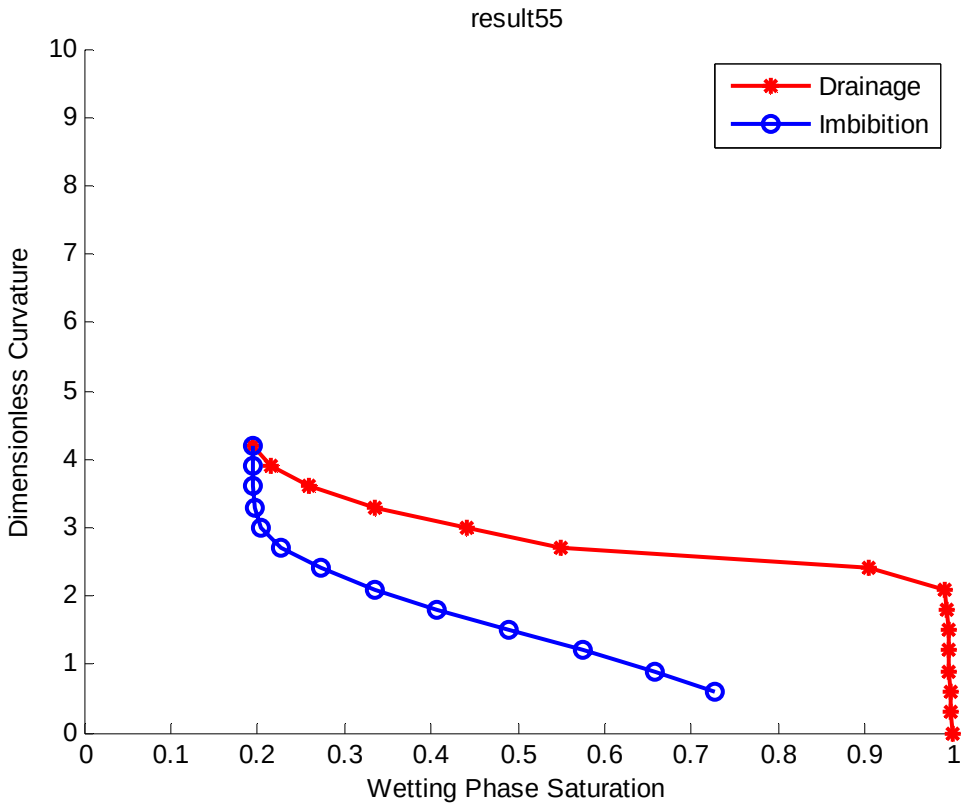
result55
Drainage
Imbibition
Dimensionless Curvature
Wetting Phase Saturation
0
1
2
3
4
5
6
7
8
9
10
0
0.1
0.2
0.3
0.4
0.5
0.6
0.7
0.8
0.9
1

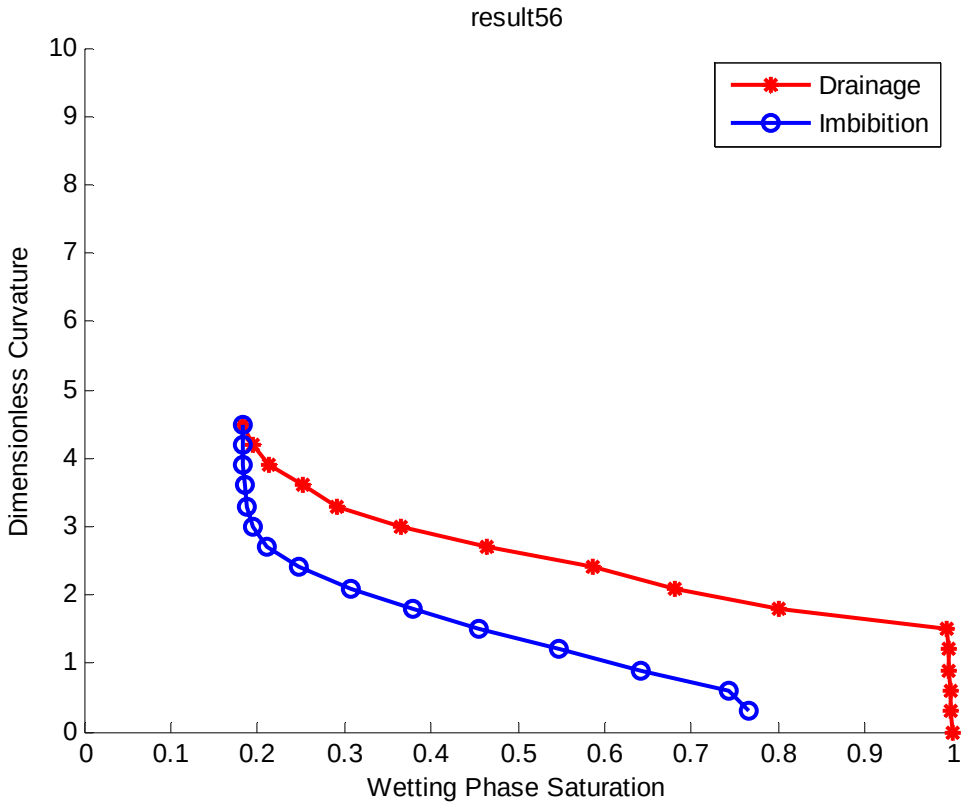
result56
Drainage
Imbibition
Dimensionless Curvature
Wetting Phase Saturation
0
1
2
3
4
5
6
7
8
9
10
0
0.1
0.2
0.3
0.4
0.5
0.6
0.7
0.8
0.9
1

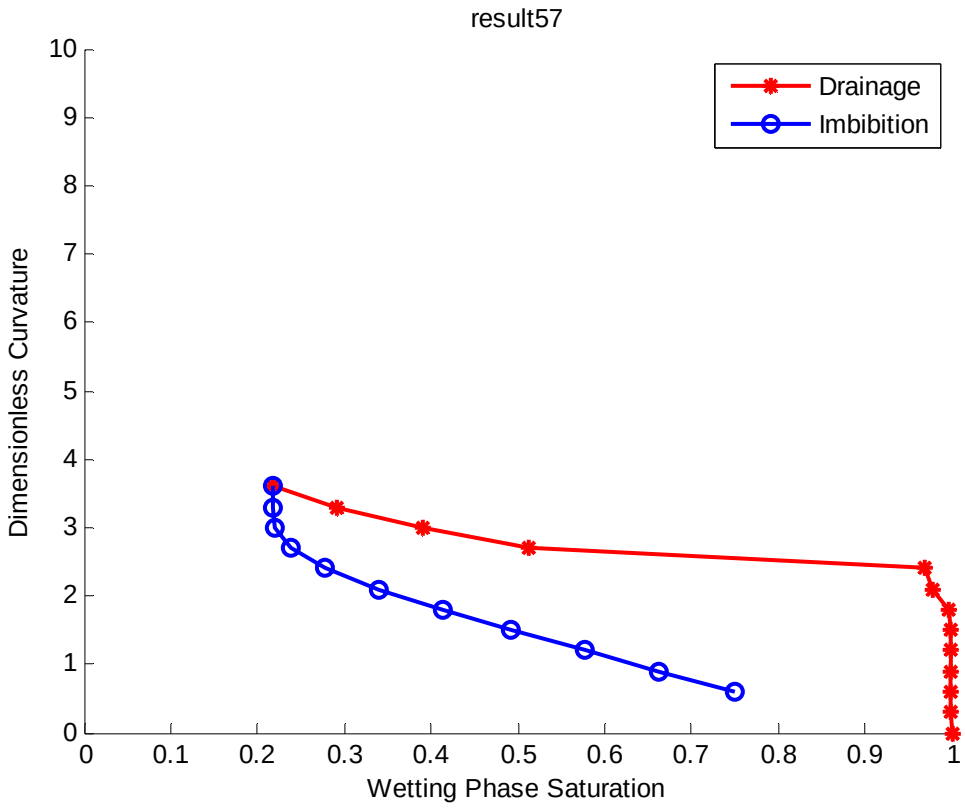
result57
Drainage
Imbibition
Dimensionless Curvature
Wetting Phase Saturation
0
1
2
3
4
5
6
7
8
9
10
0
0.1
0.2
0.3
0.4
0.5
0.6
0.7
0.8
0.9
1

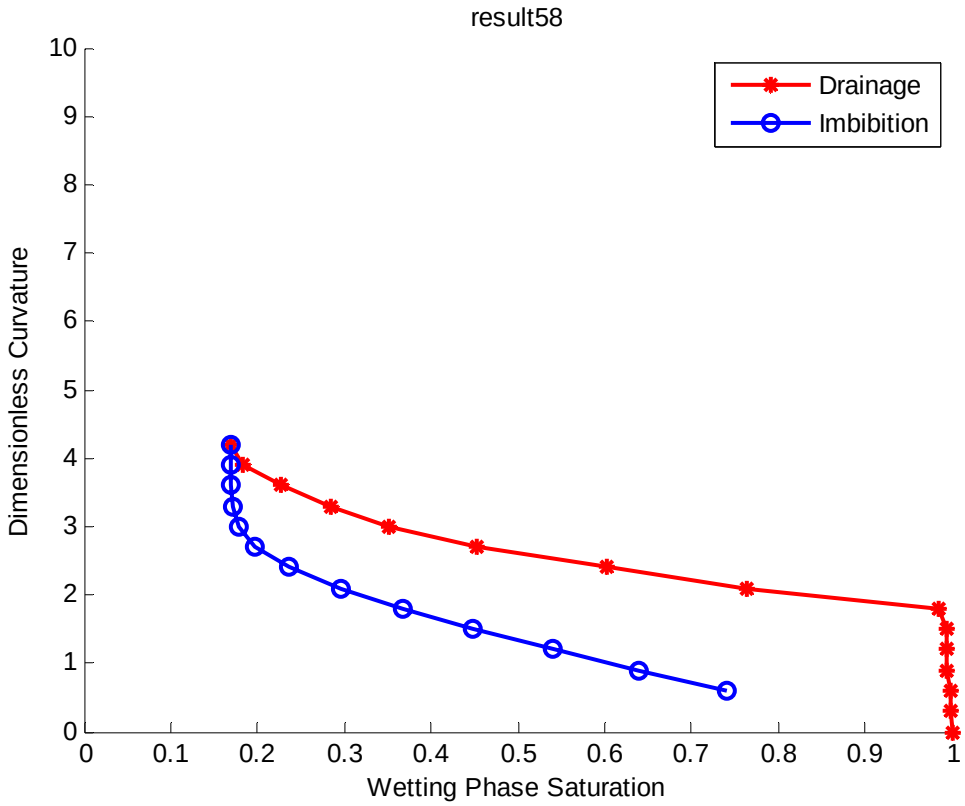
result58
Drainage
Imbibition
Dimensionless Curvature
Wetting Phase Saturation
0
1
2
3
4
5
6
7
8
9
10
0
0.1
0.2
0.3
0.4
0.5
0.6
0.7
0.8
0.9
1

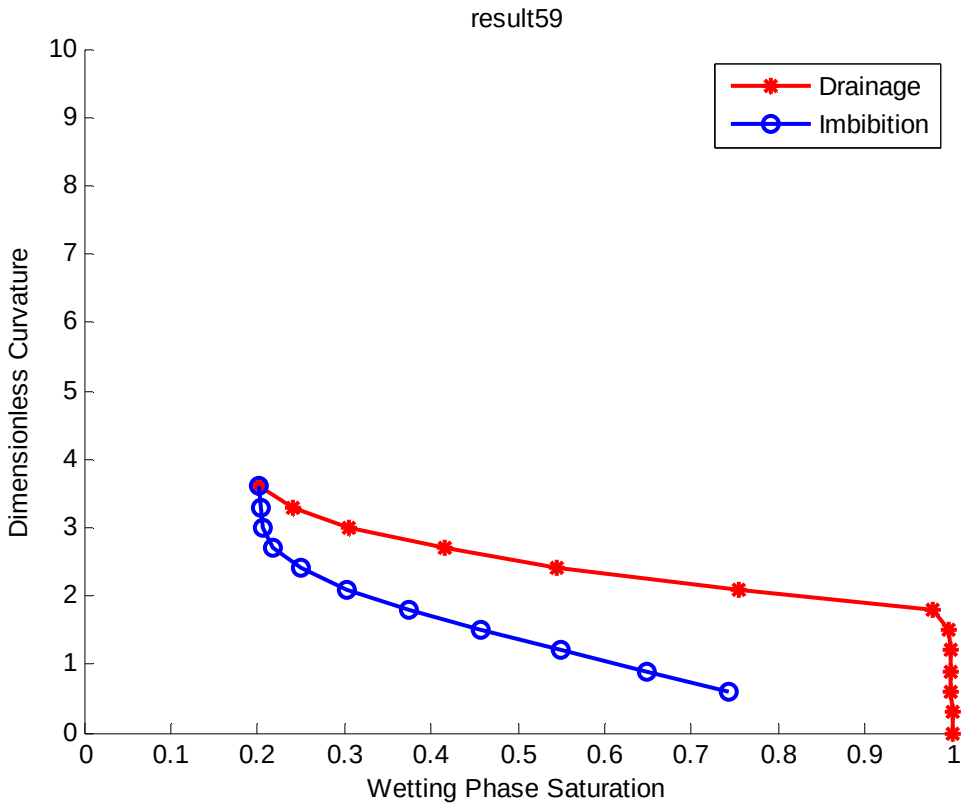
result59
Drainage
Imbibition
Dimensionless Curvature
Wetting Phase Saturation
0
1
2
3
4
5
6
7
8
9
10
0
0.1
0.2
0.3
0.4
0.5
0.6
0.7
0.8
0.9
1

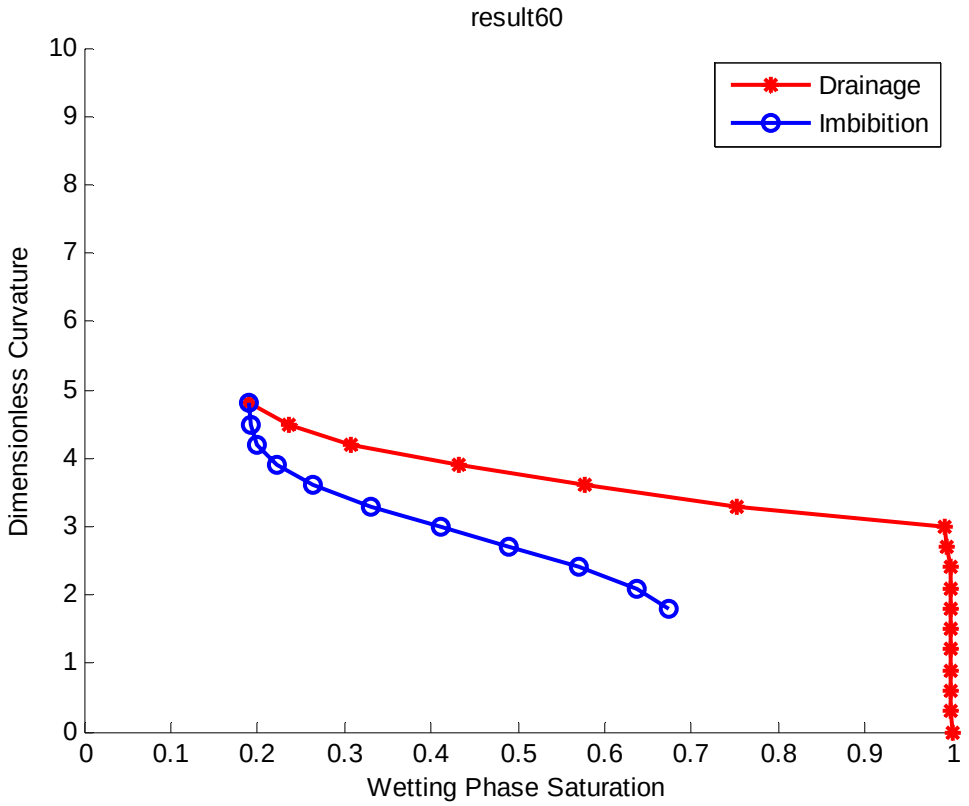
result60
Drainage
Imbibition
Dimensionless Curvature
Wetting Phase Saturation
0
1
2
3
4
5
6
7
8
9
10
0
0.1
0.2
0.3
0.4
0.5
0.6
0.7
0.8
0.9
1

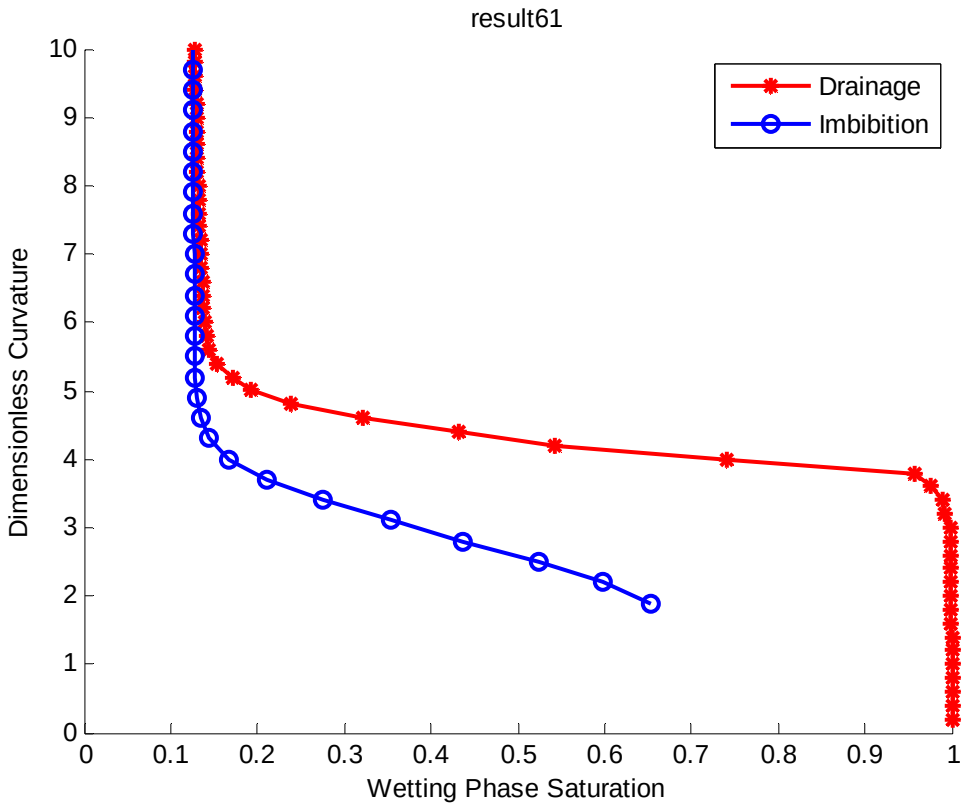
result61
Drainage
Imbibition
Dimensionless Curvature
Wetting Phase Saturation
0
1
2
3
4
5
6
7
8
9
10
0
0.1
0.2
0.3
0.4
0.5
0.6
0.7
0.8
0.9
1

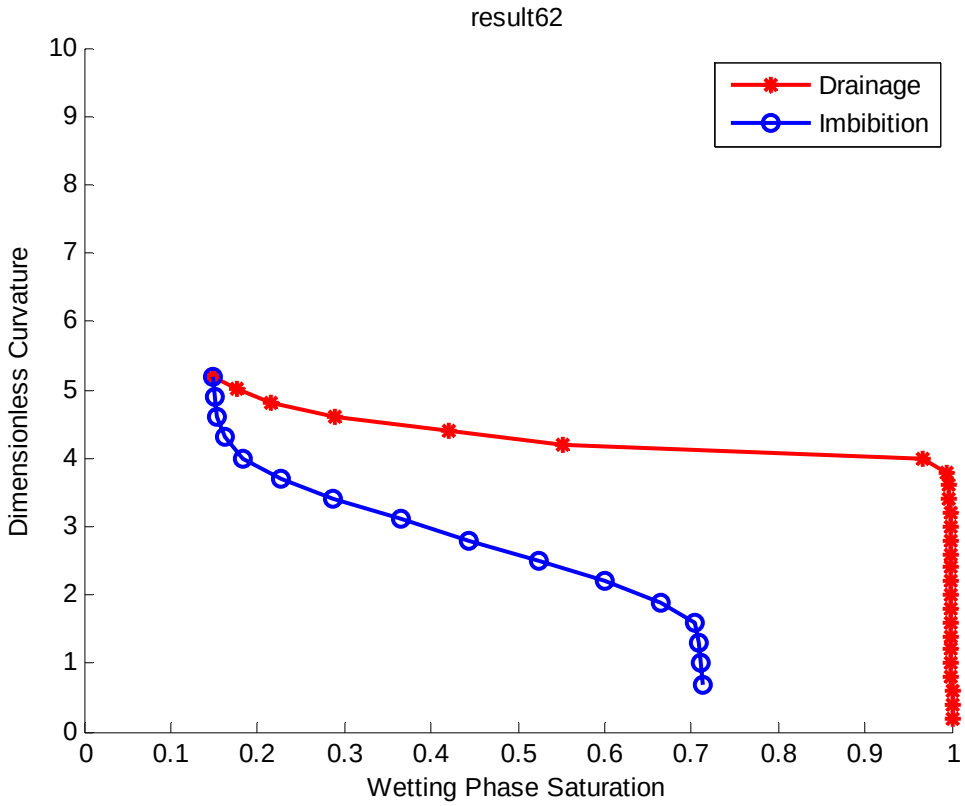
result62
Drainage
Imbibition
Dimensionless Curvature
Wetting Phase Saturation
0
1
2
3
4
5
6
7
8
9
10
0
0.1
0.2
0.3
0.4
0.5
0.6
0.7
0.8
0.9
1

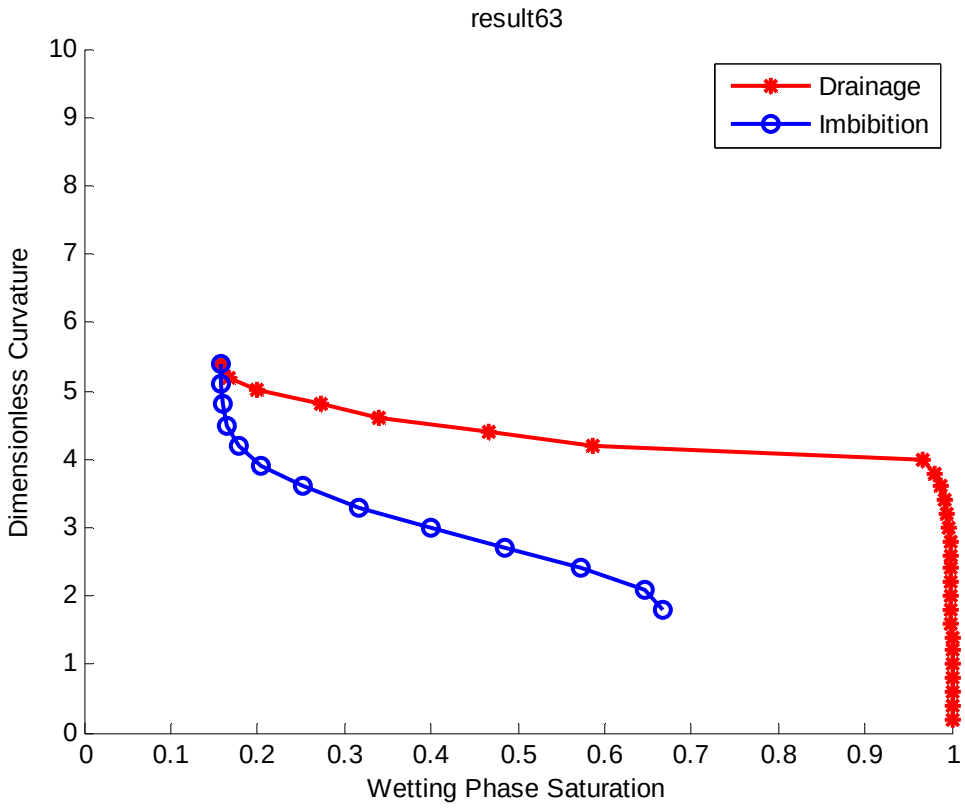
result63
Drainage
Imbibition
Dimensionless Curvature
Wetting Phase Saturation
0
1
2
3
4
5
6
7
8
9
10
0
0.1
0.2
0.3
0.4
0.5
0.6
0.7
0.8
0.9
1

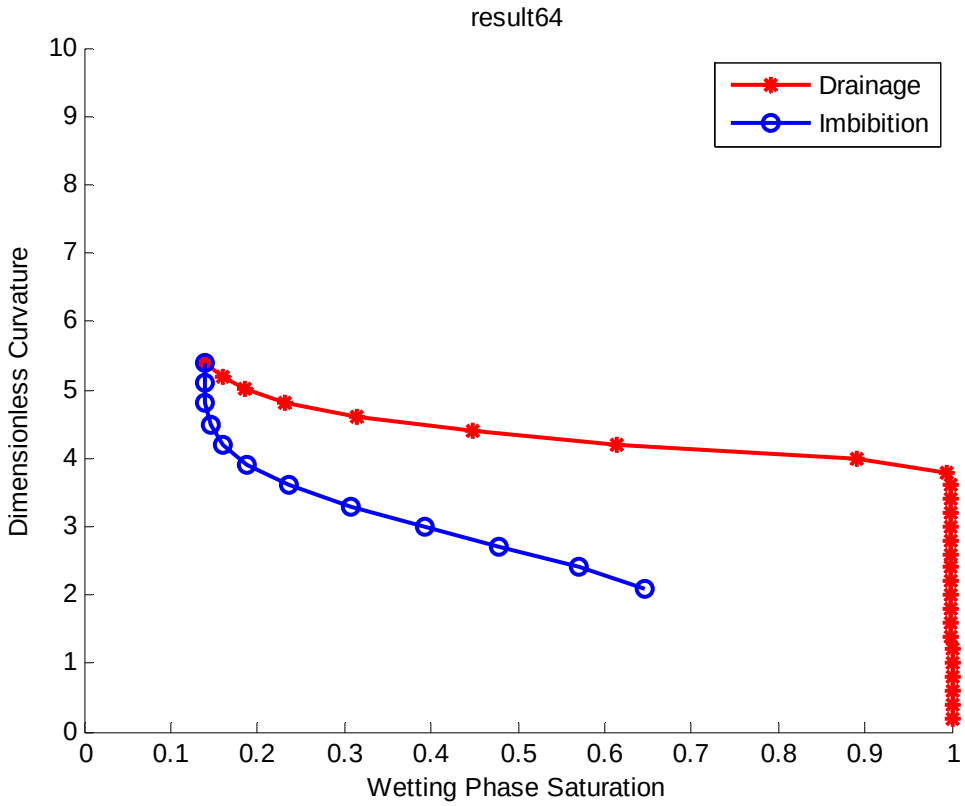
result64
Drainage
Imbibition
Dimensionless Curvature
Wetting Phase Saturation
0
1
2
3
4
5
6
7
8
9
10
0
0.1
0.2
0.3
0.4
0.5
0.6
0.7
0.8
0.9
1

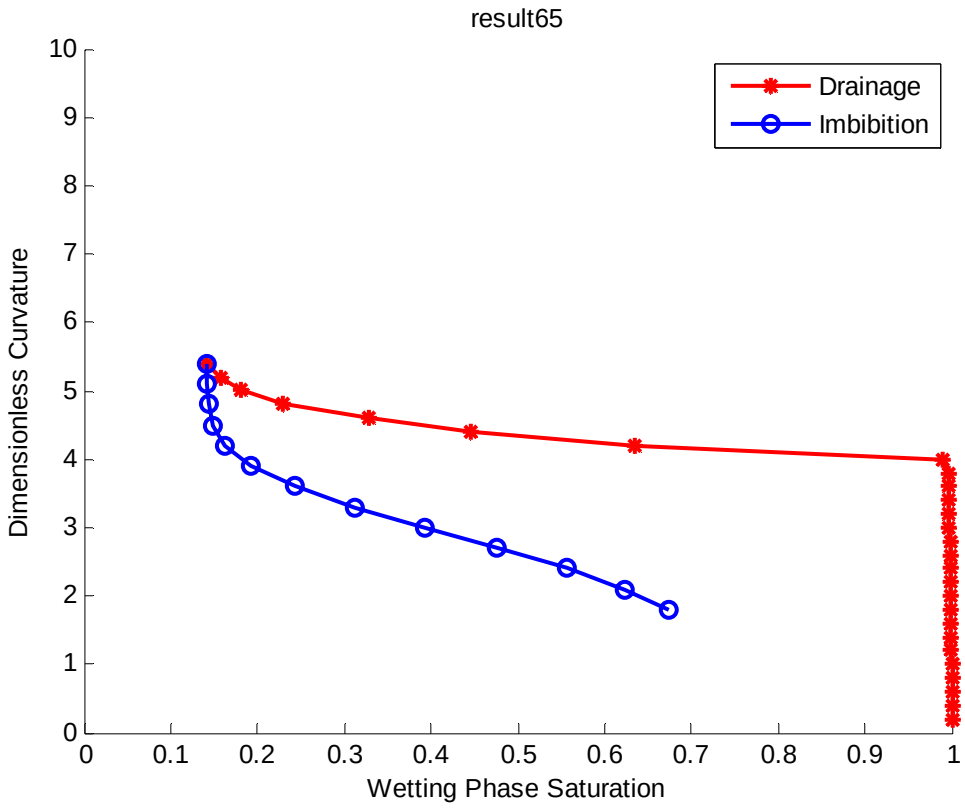
result65
Drainage
Imbibition
Dimensionless Curvature
Wetting Phase Saturation
0
1
2
3
4
5
6
7
8
9
10
0
0.1
0.2
0.3
0.4
0.5
0.6
0.7
0.8
0.9
1

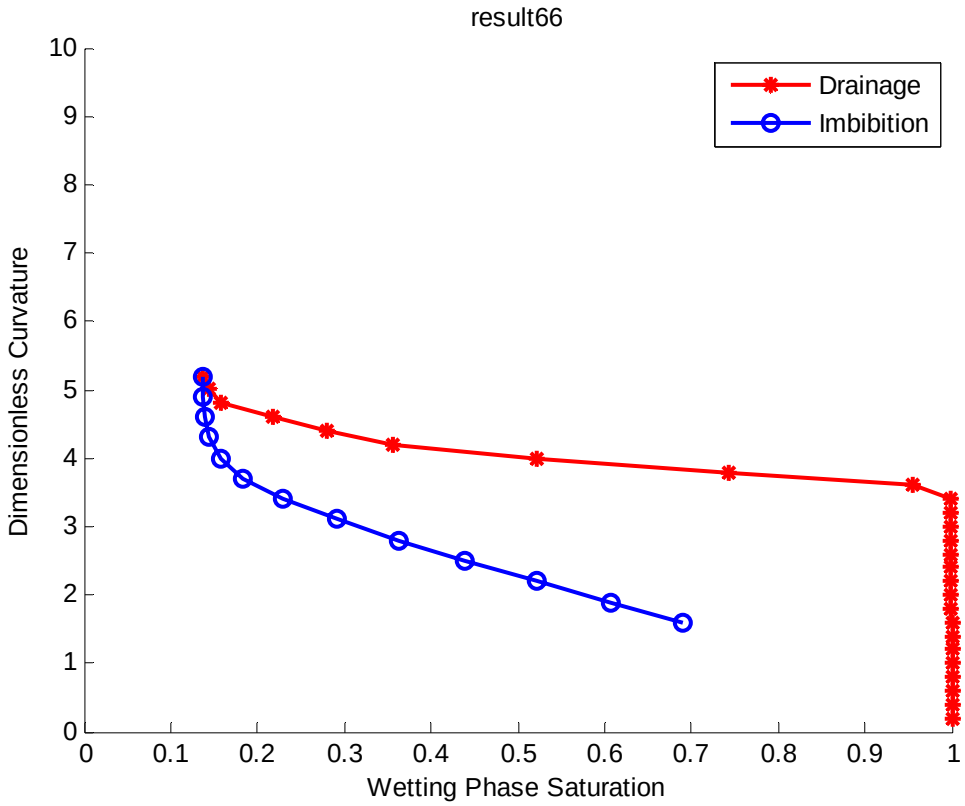
result66
Drainage
Imbibition
Dimensionless Curvature
Wetting Phase Saturation
0
1
2
3
4
5
6
7
8
9
10
0
0.1
0.2
0.3
0.4
0.5
0.6
0.7
0.8
0.9
1

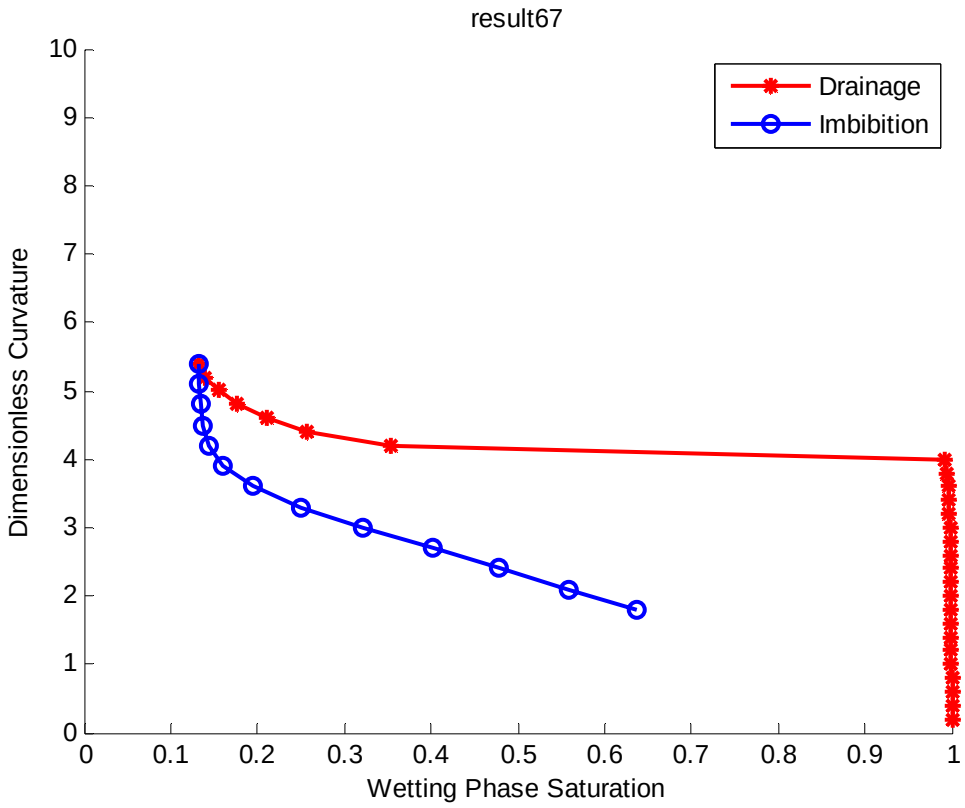
result67
Drainage
Imbibition
Dimensionless Curvature
Wetting Phase Saturation
0
1
2
3
4
5
6
7
8
9
10
0
0.1
0.2
0.3
0.4
0.5
0.6
0.7
0.8
0.9
1

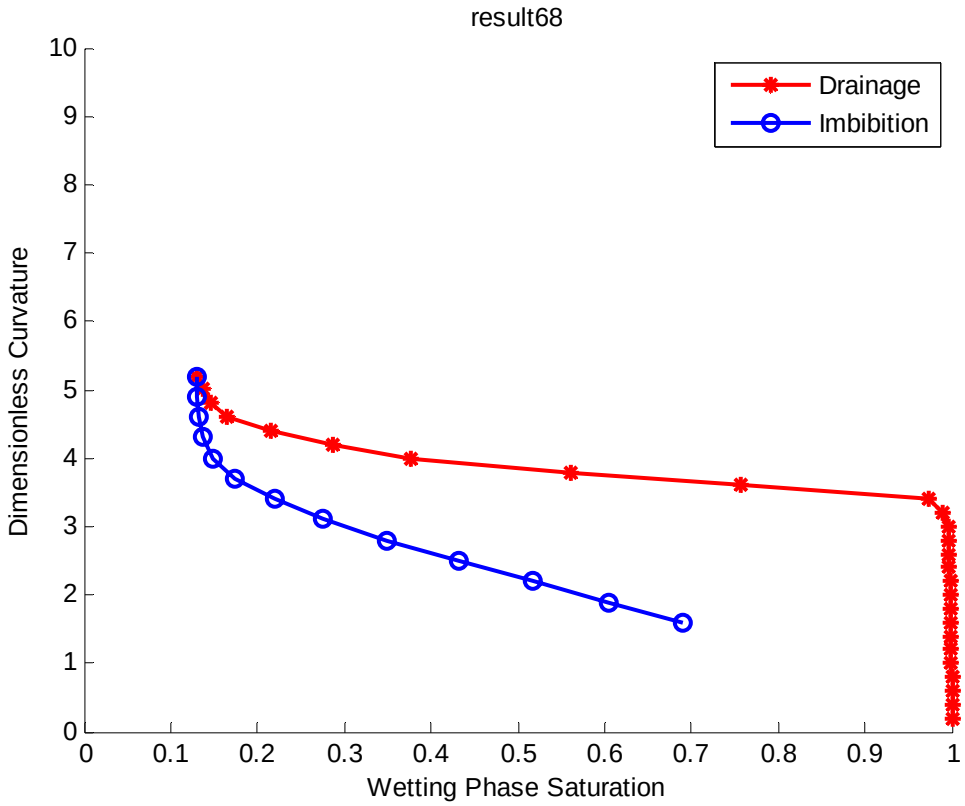
result68
Drainage
Imbibition
Dimensionless Curvature
Wetting Phase Saturation
0
1
2
3
4
5
6
7
8
9
10
0
0.1
0.2
0.3
0.4
0.5
0.6
0.7
0.8
0.9
1

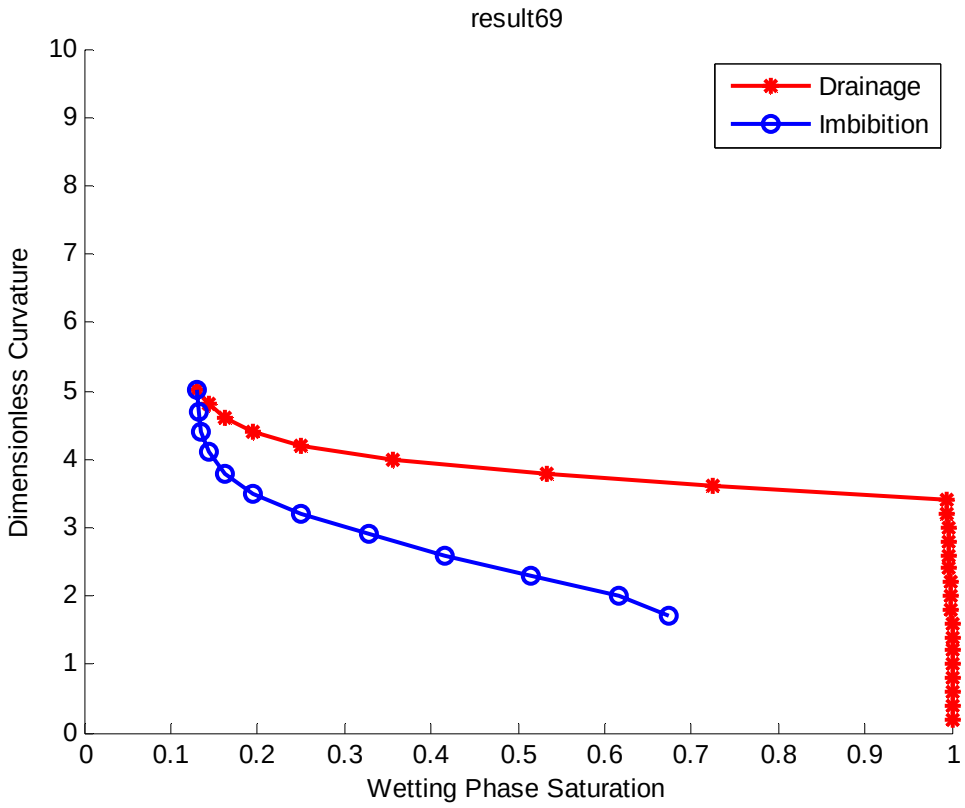
result69
Drainage
Imbibition
Dimensionless Curvature
Wetting Phase Saturation
0
1
2
3
4
5
6
7
8
9
10
0
0.1
0.2
0.3
0.4
0.5
0.6
0.7
0.8
0.9
1

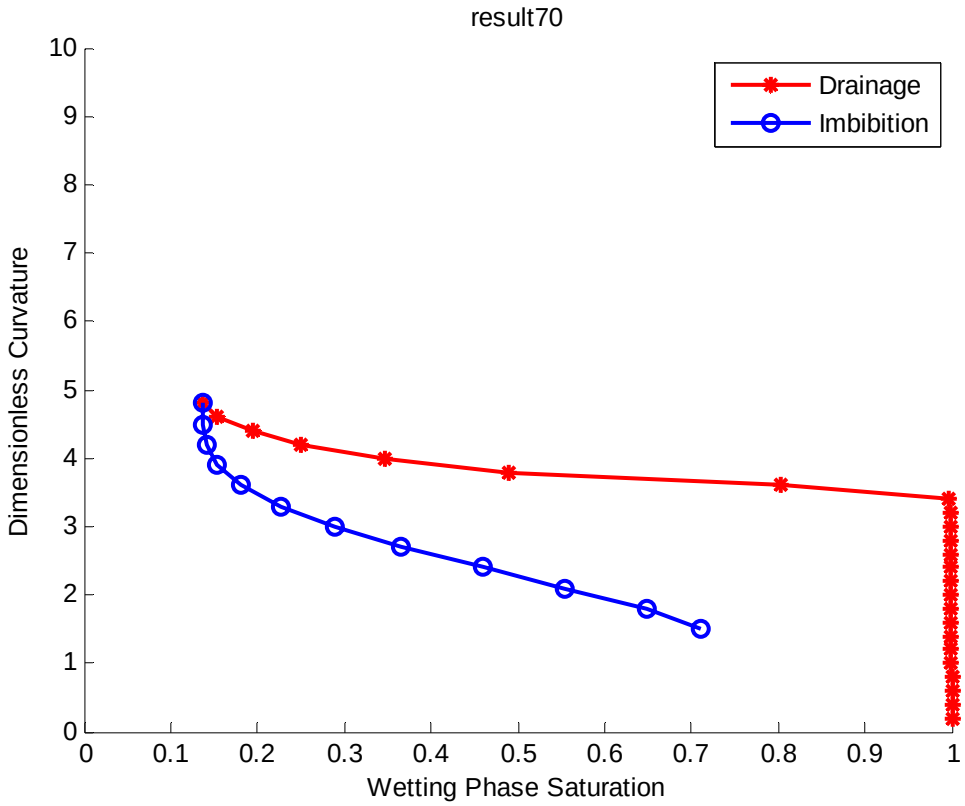
result70
Drainage
Imbibition
Dimensionless Curvature
Wetting Phase Saturation
0
1
2
3
4
5
6
7
8
9
10
0
0.1
0.2
0.3
0.4
0.5
0.6
0.7
0.8
0.9
1

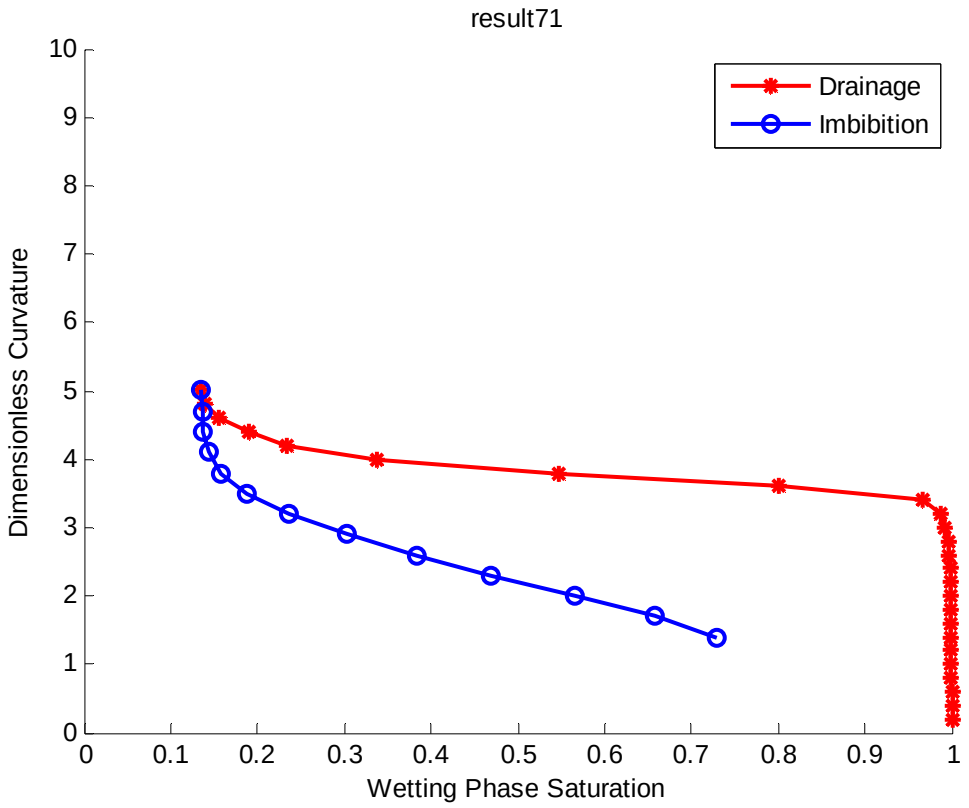
result71
Drainage
Imbibition
Dimensionless Curvature
Wetting Phase Saturation
0
1
2
3
4
5
6
7
8
9
10
0
0.1
0.2
0.3
0.4
0.5
0.6
0.7
0.8
0.9
1

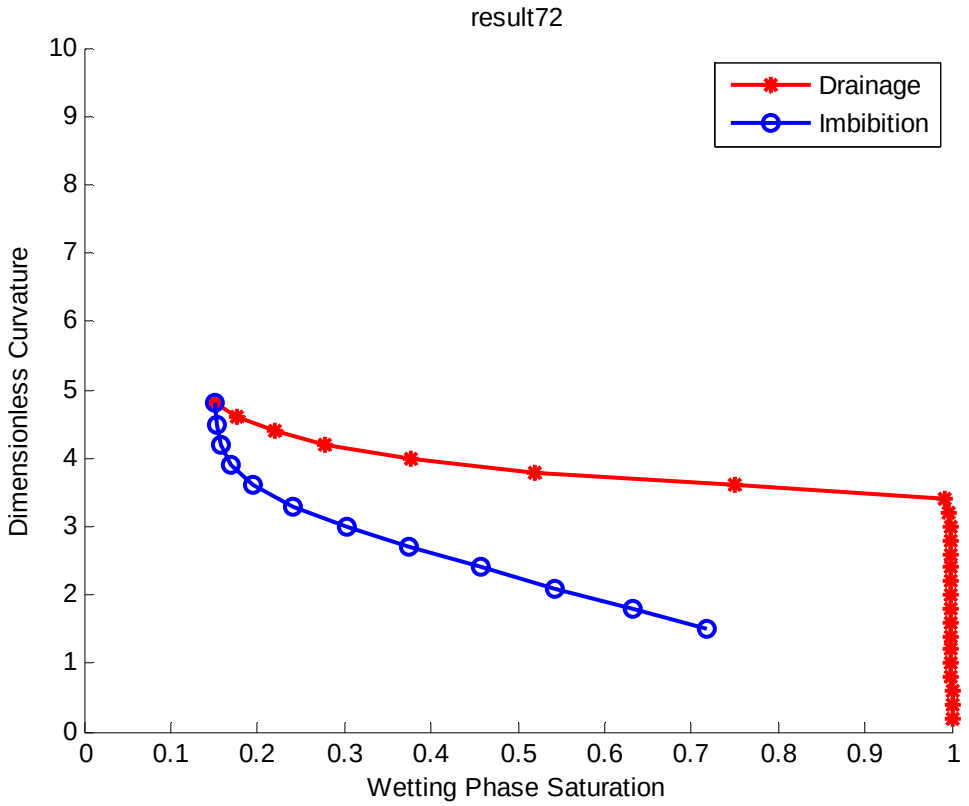
result72
Drainage
Imbibition
Dimensionless Curvature
Wetting Phase Saturation
0
1
2
3
4
5
6
7
8
9
10
0
0.1
0.2
0.3
0.4
0.5
0.6
0.7
0.8
0.9
1

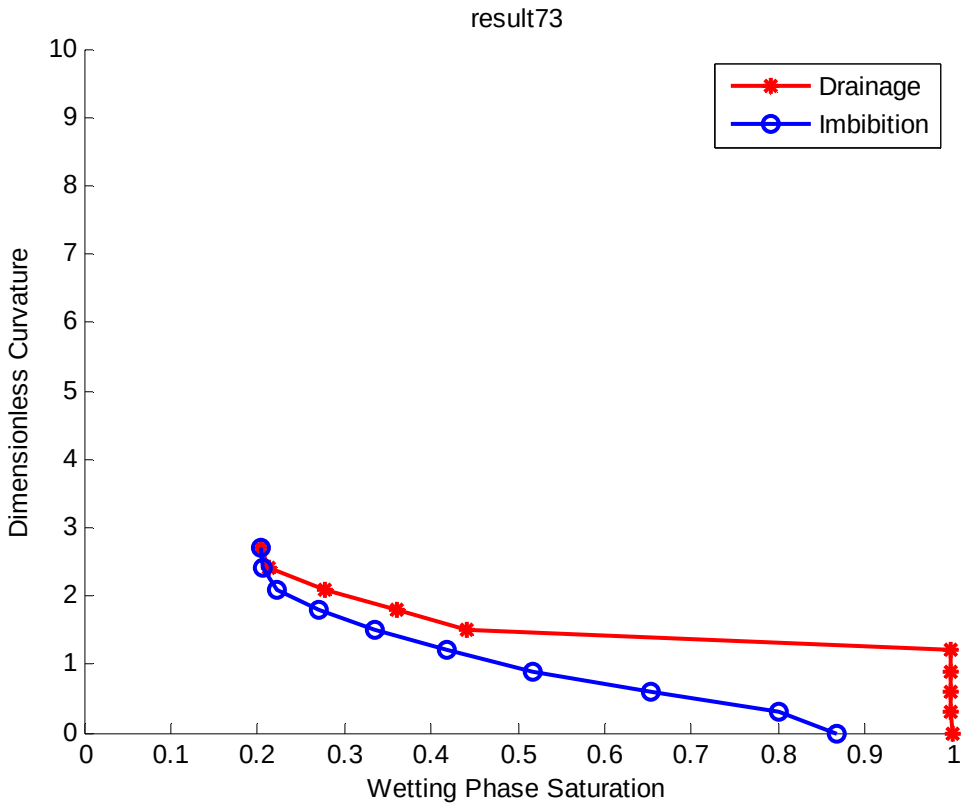
result73
Drainage
Imbibition
Dimensionless Curvature
Wetting Phase Saturation
0
1
2
3
4
5
6
7
8
9
10
0
0.1
0.2
0.3
0.4
0.5
0.6
0.7
0.8
0.9
1

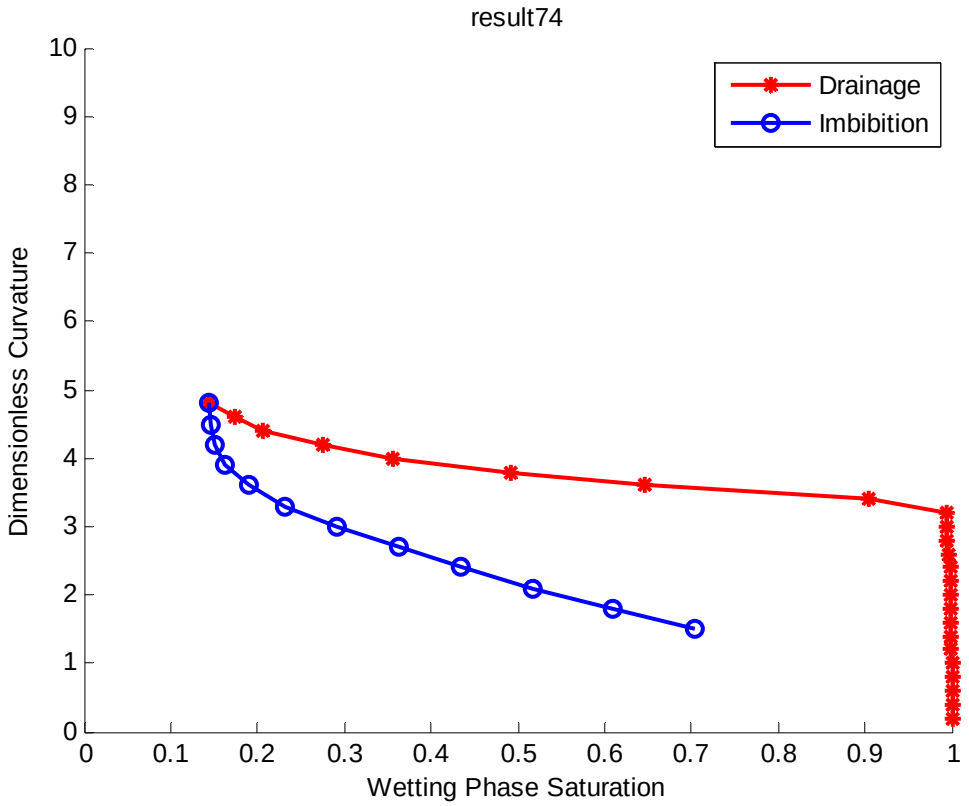
result74
Drainage
Imbibition
Dimensionless Curvature
Wetting Phase Saturation
0
1
2
3
4
5
6
7
8
9
10
0
0.1
0.2
0.3
0.4
0.5
0.6
0.7
0.8
0.9
1

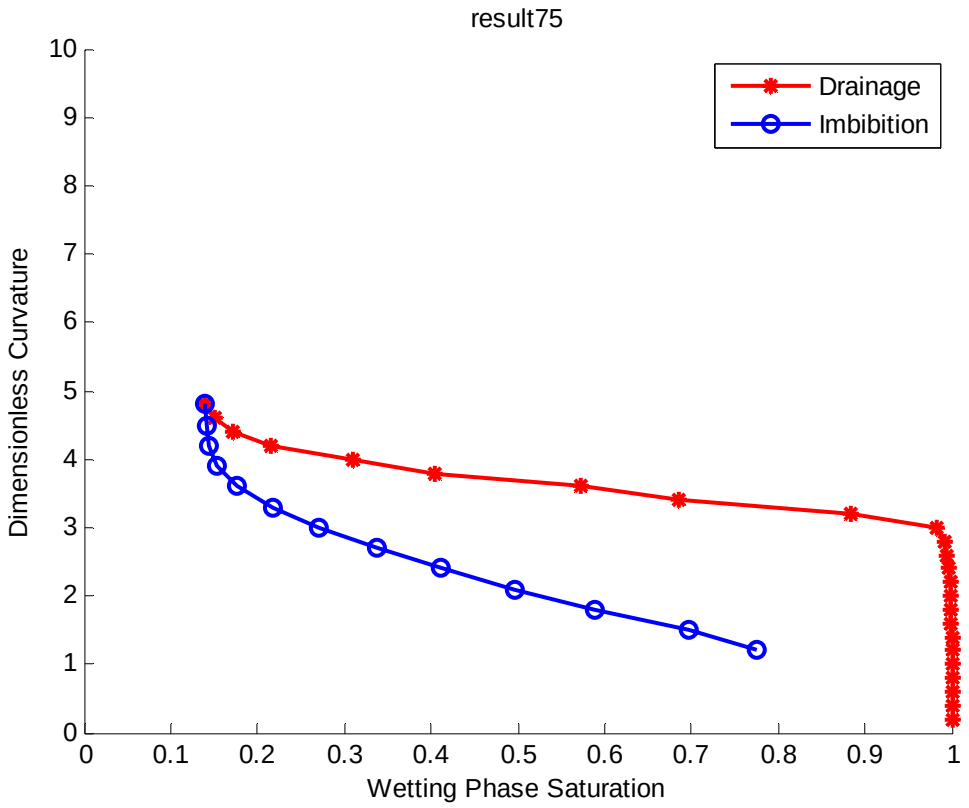
result75
Drainage
Imbibition
Dimensionless Curvature
Wetting Phase Saturation
0
1
2
3
4
5
6
7
8
9
10
0
0.1
0.2
0.3
0.4
0.5
0.6
0.7
0.8
0.9
1

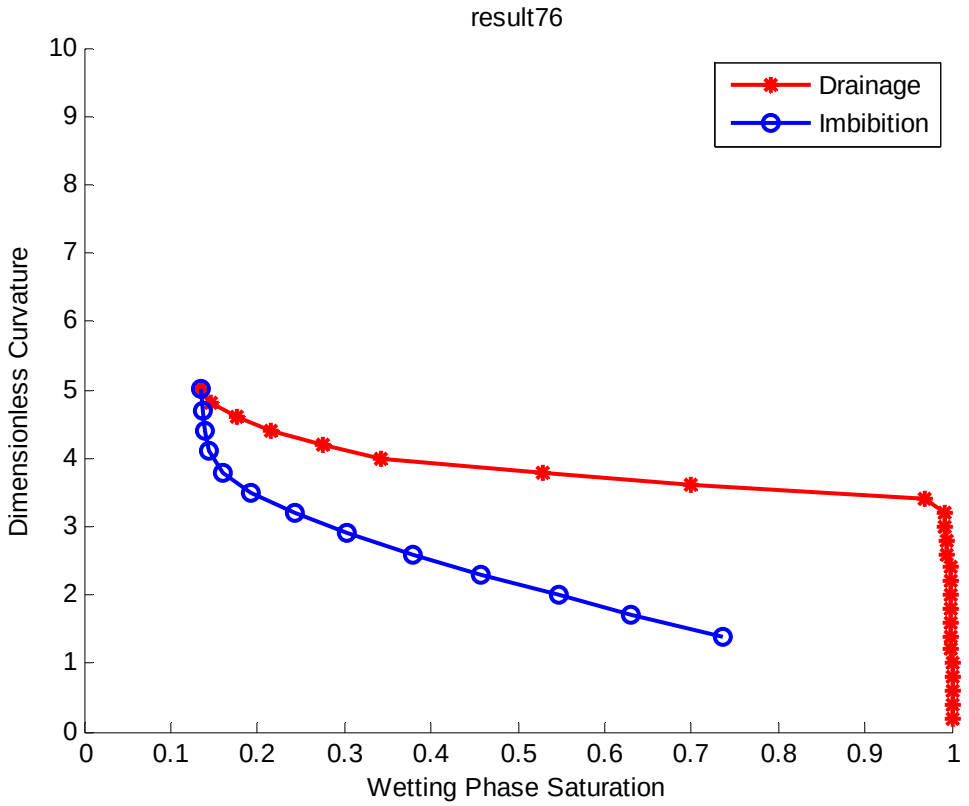
result76
Drainage
Imbibition
Dimensionless Curvature
Wetting Phase Saturation
0
1
2
3
4
5
6
7
8
9
10
0
0.1
0.2
0.3
0.4
0.5
0.6
0.7
0.8
0.9
1

National Energy Technology Laboratory

626 Cochrans Mill Road
P.O. Box 10940
Pittsburgh, PA 15236-0940

3610 Collins Ferry Road
P.O. Box 880
Morgantown, WV 26507-0880

One West Third Street, Suite 1400
Tulsa, OK 74103-3519

1450 Queen Avenue SW
Albany, OR 97321-2198

2175 University Ave. South
Suite 201
Fairbanks, AK 99709

Visit the NETL website at:
www.netl.doe.gov

Customer Service:
1-800-553-7681